April 2018

# Characterization of Scanning Mobility Particle Sizers For Use With Nanoaerosols

Michael R. Henderson
*University of South Florida*, mhenders@health.usf.edu

# Characterization of Scanning Mobility Particle Sizers for Use with Nanoaerosols

by

Michael R. Henderson

A dissertation submitted in partial fulfillment
of the requirements for the degree of
Doctor of Philosophy
Department of Environmental and Occupational Health
with a concentration in Industrial Hygiene
College of Public Health
University of South Florida

Major Professor: Yehia Y. Hammad, Sc.D.
Thomas E. Bernard, Ph.D.
Thomas J. Mason, Ph.D.
Steven P. Mlynarek, Ph.D.

Date of Approval:
April 3, 2018

Keywords: engineered nanomaterials, nanoparticles, direct reading instruments

Dedication

This dissertation is dedicated to my wife, Dana, whose love, support, encouragement, and patience allowed me to fulfill my dream, and to my parents, Henry and Thelma, for all of your support and love.

Acknowledgments

I would like to thank Dr. Yehia Hammad for his wisdom, direction, and patience during my doctoral years. I appreciate his flexibility and willingness to work with me through the various schedule changes that I experienced over those years. I also want thank Dr. Steven Mlynarek for the introduction to the program, and his encouragement and valuable advice. I would like to thank Dr. Thomas Bernard and Dr. Thomas Mason for their direction and assistance, especially with the statistics. Finally, I would like to thank the National Institute for Occupational Safety and Health for supporting this project, and their belief in the future of safety and health.

Table of Contents


List of Tables iii

List of Figures iv

List of Acronyms, Abbreviations, and Symbols vi

Abstract vii

Chapter One - Introduction 1
- Purpose of Study 1
- Research Hypothesis 2
- Importance of Direct Reading Instruments in Industrial Hygiene 2
- Introduction of Engineered Nanoparticles 3
- Study Objectives 4

Chapter Two - Literature Review 5
- Health Effects 5
- Exposure Controls and Guidelines 10
- Particle Generation 15
- Particle Measurement Parameters 19
- Particle Measurement Instruments 23

Chapter Three - Experimental Methods 28
- Design and Operation of Sampling Chamber 28
- Testing of Air Leakage into the Chamber 32
- Sampling Chamber Aerosol Distribution Testing 33
- Test System Development 35
- Relative Humidity Testing 38
- Test System Monitoring Equipment 39
- Testing Procedure 42
- Electron Microscopy 46
- Regression Analysis 47

Chapter Four – Results 48
- Instrument Measurements for Sodium Chloride Nanoparticle Aerosol - Trial 1 Test Runs 48
- Regression Analysis 69
- Instrument Measurements for Polystyrene Latex Nanoparticle Aerosol~ Trial 2 Test Runs 71
- Regression Analysis 95

Chapter Five – Discussion and Conclusion 97
- Instrument Response to Sodium Chloride Aerosols 97

Instrument Response to Polystyrene Latex Aerosols 99
Comparison of SMPS for NaCl and PSL Monitoring 100
Sampling Chamber and Aerosol Performance 101
Conclusions 103

References 105

List of Tables


| | | |
|---|---|---|
| Table 1: | Trial Group 1 Target Particle Sizes and Dilutions | 48 |
| Table 2: | Frequency and Percent of Salt Crystals Observed by Electron Microscopy and Instruments 1-3, Based on Size Interval | 50 |
| Table 3: | Data points derived from figures 1-8 and their distributional differences with respect to the analytical technique | 70 |
| Table 4: | Trial Group 2 Target Particle Sizes and Dilutions | 71 |
| Table 5: | Frequency and Percent of Polystyrene Latex (PSL) nanoparticles Observed by Instruments 1-3, Based on Size Interval | 72 |
| Table 6: | Data points derived from figures 11-22 and their distributional differences with respect to the analytical technique | 96 |

List of Figures


| | | |
|---|---|---|
| Figure 1: | Photograph of aerosol generation system and test chamber | 30 |
| Figure 2: | Photograph of sample inlets and sample filters on rack | 44 |
| Figure 3: | Distribution of NaCl nanoparticle generated aerosol for Test 1, 57 nm generated aerosol, 2,500 dilution | 53 |
| Figure 4: | Distribution of NaCl nanoparticle generated aerosol for Test 2, 57 nm generated aerosol, 2,500 dilution | 55 |
| Figure 5: | Distribution of NaCl nanoparticle generated aerosol for Test 3, 92 nm generated aerosol, 1,250 dilution | 57 |
| Figure 6: | Distribution of NaCl nanoparticle generated aerosol for Test 4, 92 nm generated aerosol, 625 dilution | 60 |
| Figure 7: | Distribution of NaCl nanoparticle generated aerosol for Test 5, 147 nm generated aerosol, 139 dilution | 62 |
| Figure 8 | Distribution of NaCl nanoparticle generated aerosol for Test 6, 147 nm generated aerosol, 139 dilution | 64 |
| Figure 9: | Distribution of NaCl nanoparticle generated aerosol for Test 7, 220 nm generated aerosol, 104 dilution | 67 |
| Figure 10: | Distribution of NaCl nanoparticle generated aerosol for Test 8, 220 nm generated aerosol, 104 dilution | 69 |
| Figure 11: | Distribution of PSL nanoparticle generated aerosol for Test 2-1, 57 nm generated aerosol, 1,250 dilution | 75 |
| Figure 12: | Distribution of PSL nanoparticle generated aerosol for Test 2-2, 57 nm generated aerosol, 1,250 dilution | 77 |
| Figure 13: | Distribution of PSL nanoparticle generated aerosol for Test 2-3, 57 nm generated aerosol, 12,500 dilution | 79 |
| Figure 14: | Distribution of PSL nanoparticle generated aerosol for Test 2-4, 92 nm generated aerosol, 2,778 dilution | 80 |
| Figure 15 | Distribution of PSL nanoparticle generated aerosol for Test 2-5, 92 nm generated aerosol, 312 dilution | 82 |

Figure 16: Distribution of PSL nanoparticle generated aerosol for Test 2-6, 147 nm generated aerosol, 234 dilution 84

Figure 17: Distribution of PSL nanoparticle generated aerosol for Test 2-7, 147 nm generated aerosol, 347 dilution 86

Figure 18 Distribution of PSL nanoparticle generated aerosol for Test 2-8, 147 nm generated aerosol, 694 dilution 88

Figure 19: Distribution of PSL nanoparticle generated aerosol for Test 2-9, 220 nm generated aerosol, 208 dilution 89

Figure 20: Distribution of PSL nanoparticle generated aerosol for Test 2-10, 220 nm generated aerosol, 208 dilution 91

Figure 21 Distribution of PSL nanoparticle generated aerosol for Test 2-11, 220 nm generated aerosol, 139 dilution 93

Figure 22 Distribution of PSL nanoparticle generated aerosol for Test 2-12, 220 nm generated aerosol, 139 dilution 95

List of Acronyms, Abbreviations, and Symbols

| | |
|---|---|
| CC | Cubic Centimeter |
| CMD | Count Median Diameter |
| CNF | Carbon Nanofibers |
| CNS | Central Nervous System |
| CPC | Condensation Particle Counter |
| CNT | Carbon Nanotubes |
| $CM^3$ | Cubic Centimeter |
| DMA | Differential Mobility Analyzer |
| DNA | Deoxyribonucleic Acid |
| ELPI | Electrical Low Pressure Impactor |
| EM | Electron Microscopy |
| ENM | Engineered Nanomaterial |
| FPP | Fiber Pathogenicity Paradigm |
| GI | Gastrointestinal |
| GSD | Geometric Standard Deviation |
| HEPA | High Efficiency Particulate Air |
| L/Min | Liters Per Minute |
| LNP | Log Normal Probability |
| MM | Millimeter |
| MMD | Mass Median Diameters |
| MOUDI | Micro-Orifice Uniform Deposit Impactor |
| MWCNT | Multiwall Carbon Nanotubes |
| NaCl | Sodium Chloride/Salt |
| n-MOUDI | nano-MOUDI |
| OPC | Optical Particle Counter |
| PCTE | Polycarbonate Track Etch |
| PM | Particle Mass |
| PNC | Particle Number Concentration |
| PSIG | Pounds Per Square Inch Gage |
| PSL | Polystyrene Latex |
| RH | Relative Humidity |
| ROS | Reactive Oxygen Species |
| SEM | Scanning Electron Microscopy |
| SMPA | Scanning Mobility Particle Sizer |
| SWCNT | Single Wall Carbon Nanotubes |
| STEM | Scanning Transmission Electron Microscopy |
| T | Temperature |
| TEM | Transmission Electron Microscopy |
| TEOM | Tapered Element Oscillating Microbalance |
| $TiO_2$ | Titanium Dioxide |

Abstract

The purpose of this study was to evaluate the performance of scanning mobility particle sizers in the characterization of nanoaerosols. A sampling chamber was constructed from aluminum and tempered glass, had a volume of 4.6 cubic feet, and was designed for the introduction of aerosols and dilution air, maintenance of aerosol concentration, and continuous exhaust of chamber air. Penetration and aerosol distribution tests were conducted within the chamber. An aerosol generation and measurement system comprised of nitrogen gas, BGI 3 jet Collison Nebulizer, diffusion dryer, aerosol charge neutralizer, mixing chamber, critical orifice, hygrometer, condensation particle counter, scanning mobility particle sizer, air sampling pump, air sampling cassettes, and a vacuum pump was assembled. A BGI 3 jet Collison Nebulizer was used to generate the nanoparticle aerosols. The two types of nanoparticle aerosols utilized in the experiment were salt (NaCl) and polystyrene latex (PSL) spheres. Relative humidity and temperature measurements were obtained within the chamber. Real-time, direct-reading particle measurement instruments including a condensation particle counter (CPC) (TSI, Model 3007), and three scanning mobility particle sizer (SMPS) instruments (Particle Measuring Systems, Nano-ID NPS500; TSI, NanoScan SMPS Nanoparticle Sizer Model 3910) were used for particle measurements. For each test run, two air samples were collected on membrane filters for electron microscopy (EM) analysis. Eight trials were conducted using NaCl nanoaerosols, and twelve trials were conducted using PSL spheres. The selected particle sizes for the experiments were 57 nm, 92 nm, 147 nm, and 220 nm.

For the NaCl nanoaerosol suspensions, the SMPS lines of fit were log-normally distributed and predominantly parallel. The geometric standard deviation (GSD) of these distributions was approximately 1.7, which confirms that the distributions were approximately

the same. In these experiments, instrument 3 identified a higher percentage of NaCl particles within the size range intervals of the selected NaCl size parameter, and the count median diameters (CMDs) for the instrument 3 measurements were closer to the selected NaCl size parameter more often than the other instruments. This suggests that instrument 3 was more responsive than the other instruments to the selected size range and the selected NaCl size parameters. The electron microscopy (EM) lines of fit for the NaCl experiments were predominantly parallel with the SMPS lines of fit, suggesting that the log-normally distributions are similar. The GSD of EM distributions was approximately 1.8, which confirms that the distributions were approximately the same as the SMPS distributions. Results from the regression plots demonstrated that the main effects and interaction were statistically significant with a $p<0.0001$. The coefficient of determination, $R^2$, for the regression lines was 0.87. The post-hoc Tukey HSD results identified a significant difference between the instrument 3 dataset, and the datasets for instruments 1 and 2.

For the PSL nanoaerosol suspensions, the SMPS lines of fit were log-normally distributed and predominantly parallel. The GSD of these distributions was approximately 1.3, which confirms that the distributions were approximately the same. In these experiments, instrument 2 identified a higher percentage of PSL particles within the size range intervals of the selected PSL size parameter, and instrument 2 CMDs were closer to the selected PSL size parameter more often than the other instruments. This suggests that instrument 2 was more responsive than the other instruments to the selected size range and the selected PSL size parameters. Results from the regression plots demonstrated that the main effects and interaction were statistically significant with a $p<0.01$. The coefficient of determination, $R^2$, for the regression lines was 0.44. The post-hoc Tukey HSD test identified a significant difference between the instrument 3 dataset and the instrument 1 dataset. Potential sources of variability include solution water background contamination, surfactants in the PSL solution, and agglomeration.

The performance of all the scanning mobility particle sizers compared in these experiments was acceptable for research and field applications, but caution should be taken when comparing the measurements of SMPS, especially SMPS from different manufacturers.

# Chapter One

# Introduction

## *Purpose of This Study*

The purpose of this study was to characterize scanning mobility particle sizers for use with nanoparticles. The study was conducted in a laboratory located in the College of Public Health, University of South Florida. The characterization will provide the answers to the following questions:

1. What is the instrument response, in terms of concentration, for three scanning mobility particle sizers (SMPS) to generated sodium chloride nanoparticle aerosols?
2. What is the instrument response, in terms of concentration, for three SMPS to generated polystyrene latex (PSL) nanoparticle aerosols?
3. Are there any differences among the SMPS instruments in the measured particle group mean counts?
4. Are there differences in the instrument response for SMPS instruments of similar make and model?
5. Are there differences in the instrument response for SMPS instruments from different manufacturers?

As a result of this study, SMPS characterization information will be available to industrial hygienists and other professionals to enable them to make informed decisions on the use of SMPS in the field.

### *Research Hypothesis*

The null hypothesis ($H_0$) of this study is that there is no difference among instruments for the NaCl or PSL particle size group mean counts. The alternative hypothesis ($H_1$) is that at least one of the instrument measured particle group mean counts differently than another instrument.

### *Importance of Direct Reading Instruments in Industrial Hygiene*

A goal of industrial hygienists is to control occupational health hazards that may occur as a result of or during work (Olishifski, 1988). In other words, industrial hygienists strive to limit worker exposures to materials that can cause a harmful effect on them. Prior to the development of atmospheric direct reading instruments, samples were obtained on or near workers to determine their exposure. The samples were sent to a laboratory for analysis, but the results were typically not available until five or more days after the work task was sampled. Often, the sampled work tasks were completed prior to receipt of the sample results. For repetitive tasks, the sample results could be used to develop procedures or controls that provided protection for future worker exposures. Unfortunately, conditions typically change in a work area and the sample concentrations obtained for a specific task may be different than those experience by the worker during the next task. Changing parameters, including weather conditions, process changes and conditions, worker positioning, and other factors affect the exposure that workers experience performing the task. A solution was needed to provide a quicker response to worker airborne exposure concentrations while conducting the work task.

With the development of instruments that provided real time presentation of ambient contaminant concentrations, industrial hygienists and other professionals were able to evaluate the ambient working conditions of the employees, assess the risk that the environment provided, and assess the effectiveness of the existing controls. One of the first real time devices, used by miners, was a canary. The animal was used to monitor oxygen levels in the

mine and to notify the miners if the oxygen levels were too low to support life. Industry has progressed since that time, developing instruments that are reliable and accurate for several of the contaminants that workers face on a routine basis. Industrial hygienists and others use these instruments daily, on worksites around the globe, to assist in controlling occupational health hazards.

### *Introduction of Engineered Nanomaterials*

Recent scientific progression and developments have resulted in the use of engineered nanomaterials (ENM) in the workplace. A nano-object is defined as a material with one, two, or three external dimensions in the size range of 1-100 nm (Department of Human and Health Services, 2009). Engineered nanoparticles are designed and intentionally produced with specific properties or compositions, including shape, size, chemistry, and surface properties. These materials are being used in many industries, including medicine, electronic manufacturing, cosmetics, pharmaceuticals, and building material manufacturing. Positive results have been obtained in these areas through the use of engineered nanomaterials. Research is being conducted to identify new methods to utilize existing engineered nanomaterials and to develop new materials to apply to these industries. The trends indicate an increase in the research and use of these materials for the future.

New technologies present new challenges for the industrial hygiene professional. Traditional control methods of elimination, substitution, engineering, administrative, and personal protective equipment (PPE) cannot be applied in the same manner to traditional aerosols. The physico-chemical dynamics of engineered nanoparticles are unlike similar materials of larger diameter. The advantages that these engineered nanoparticles provide to the medical, pharmaceutical, and manufacturing sectors are the same properties that make them a challenge to control. Existing control methods should be evaluated to determine their

effectiveness for aerosols in this reduced diameter size range. Measurement of control performance is being conducted using cassette sampling and direct reading devices.

### *Study Objectives*

This study will evaluate the response of scanning mobility particle sizer (SMPS) instruments to generated aerosols of NaCl and polystyrene latex nanoparticles. The null hypothesis is that there is no difference among the SMPS instruments for the NaCl or PSL particle size group mean counts. The alternative hypothesis is that at least one of the SMPS instrument measured particle group mean counts differently than another instrument. A test chamber, aerosol generation system, and aerosol measurement system will be designed, tested and evaluated. Measurements will be collected with three scanning mobility particle sizer instruments. Two of the instruments will be the same make and manufacturer, and the third scanning mobility particle sizer instrument will be from a different manufacturer. Regression analysis of the datasets will be conducted to evaluate the null hypothesis.

# Chapter Two

# Literature Review

## *Health Effects*

Engineered nanomaterial (ENM) manufacturing and downstream use of ENM products is increasing annually, despite the lack of research data concerning the potential adverse health effects associated with the ENMs in these products. Research funding applied to the development and use of various engineered nanoparticle compositions, coatings, and effective sizes has far outpaced the funding provided for research of potential hazards associated with these newly developed ENMs. Although research studies conducted to determine potential health effects of ENMs are limited, these studies have identified adverse health effects related to ENM exposure. The health effects are typically dependent on several variable associated with the ENMs, including the properties, shape, size, surface coating, and structure of ENMs.

Properties of ENMs differ from molecules, individual atoms, and bulk matter (Yokel et al. 2011). The different physico-chemical properties of ENMs can cause an elevated rate of pulmonary deposition and translocation from the lungs to systemic sites. These physico-chemical properties may also result in an elevated inflammation potential. Additionally, the shape, size, solubility, surface reactivity, surface coating, binding to receptors, and agglomeration differ from larger sized particles. These properties result in a faster uptake and greater biological activity for ENMs than the uptake and activity of larger sized particles of similar materials, and may also influence the toxicity of ENMs. For example, an agglomeration of ENMs, loosely bound together by relatively weak forces, results in an external surface area similar to the sum of the individual ENMs surface areas. This increased surface area affects the

uptake, and can increase the effects of the ENMs. The increased surface area of ENMs are responsible for increased health effects in a biological system. Orberdorster et al. (2005) discussed the various effects of ENMs on the human body derived largely from the increased surface area that is available on nanoparticles when compared to similar masses of particles of larger diameters. This increased surface activity associated with smaller particles can be beneficial, detrimental, or a combination of both. For example, increased surface areas of smaller particles are beneficial for therapeutic drug delivery because they provide similar results as larger particles of the same compound, while requiring less total mass of the compound. A reduction in the mass of the therapeutic drug provides a lower treatment cost, and lowers the risks of negative side effects. Unfortunately, this increased surface activity may also result in overexposure to a therapeutic drug. This can occur if the effective dose has not been determined, or unforeseen reactions occur with the drug due to the limited knowledge of the ENM properties in a biological system.

The routes of exposure to ENMs include the respiratory tract, the gastrointestinal (GI) tract, skin, and eyes; however, the primary route of exposure is through the respiratory tract. Particle deposition characteristics in the respiratory tract determine the potential toxicology of the nanoparticle aerosols. The five methods of particle deposition include inertial impaction, sedimentation, diffusion, interception, and electrostatic precipitation. Particle deposition, based on aerodynamic particle size, occurs primarily through inertial impaction, sedimentation, and diffusion (Williams et al. 2011). Due to their size, diffusion is the primary route of deposition for nanoparticles in the lungs, however, particle diameter size can affect whether the nanoparticle is deposited in the nasopharygeal, tracheobrobchial, or alveolar region. Generally, larger aerodynamically sized particles are deposited in the upper airways, and as particle diameters decrease to submicron size, the total lung deposition also decreased. However, as particle sizes decreased to nanoparticle sizes, the total lung deposition increased back to levels similar to deposition levels observed with larger particle sizes in the head airways. In the respiratory

tract, the traditional clearance mechanisms are substantially different for nanoparticles. Depending on where they settle, nanoparticles may avoid the normal clearance methods by quickly translocating to the pulmonary interstitial space. Once translocated to the pulmonary interstitial space, the particles can move into the blood circulation, lymphatic system, and nervous system. After entering the blood circulation and lymphatic system, nanoparticles can be transported throughout the body. Nanoparticle uptake through nerve endings can also travel through the nerves to the central nervous system (CNS) or deeper brain structures. Exposure to the GI tract can occur through swallowing the particles cleared through the mucociliary tract, or through ingestion from hand to mouth activities. Oral exposure may result in translocation to the gastrointestinal tract, followed by translocation to the lymphatic system or the circulatory system. Uptake through the skin, although often not considered the primary route for nanoparticle exposure, can provide an important route under certain circumstances. Due to the abundance of blood and tissue macrophages, lymph vessels, nerves endings, and dendritic cells, the skin may become an active transportation route if the skin surface is flexed, broken, or its' protective mechanisms are diminished. Dermal exposure may result in translocation of the ENMs to the lymphatic system, with further translocation to the circulatory system (blood) and then the organs. Ocular exposure may lead to translocation of the ENPs to the nasal cavity and brain, or it may translocate from the nasal cavity to the circulatory system and the organs. The translocation of ENMs and the related health effects are often related to the ENM properties and structure.

Several health impact studies have been conducted for carbon nanotubes (CNT) due to concerns over their properties and structure. One of the initial concerns was that the fibrous forms of CNT may have similar properties to asbestos fibers, and may elicit similar biological results as asbestos. CNT that have a straight fibrous, high-aspect shape may act like asbestos fibers, causing effects such as frustrated phagocytosis and the related pathogenicity. Frustrated phagocytosis has been observed with both asbestos and certain CNTs. Fiber

pathogenicity paradigm (FPP) relates to a fiber toxicity structure involving length, diameter, and biopersistence. In the FPP paradigm, particle geometry is more important than composition. Fiber diameter is closely associated with the physical diameter of a particle. Smaller diameter particles have smaller physical diameters, and fiber diameters equal to or less than 1 µm are respirable and may be deposited beyond the ciliated airway. For fibers deposited beyond the ciliated airway, the body will use clearance mechanisms such as phagocytosis. Phagocytosis is a slower clearance process, resulting in a longer residence time and longer exposure time. Long fibers deposited beyond the ciliated airway have a longer retention half-life than short fibers deposited in similar locations. CNTs produced inflammation, oxidative stress, genotoxicity, toxicity, and fibrosis in medium term studies conducted by Donaldson et al. 2013. Some of these effects are time-dependent, requiring the passage of a certain amount of time for the effects to occur. Asbestos exposures have produced similar health effects and are also time-dependent. Another study involving the introduction of different shaped CNT samples into the lungs of mice resulted in an inflammation response and progressive thickening of the alveolar septa (Murphy et al. 2013). These effects were only observed with the long CNT, and not the short and tangled CNT. In this study, pleural cavity inflammation and lesions along the diaphragm and chest wall were observed six weeks after the initial exposure, but were not present one week after the initial exposure. Genotoxicity assessments have shown that CNT can cause damage in vivo and in vitro, however, not all CNT have asbestos like properties or physiological effects. The findings from Berlo et al. (2012) were not consistent over the entire spectrum of CNT. Several studies have not identified CNT induced damages. There have been similarities, however, between asbestos related genotoxicity and CNT related genotoxicity. CNT can induce reactive oxygen species (ROS) formation, contribute to oxidative deoxyribonucleic acid (DNA) damage induction, cause antioxidant depletion, and impair the functionality of the mitotic apparatus.

Health impact studies have also been conducted for multiwall carbon nanotubes (MWCNT) due to concerns over their properties and structure. In some animal experiments, MWCNT were as carcinogenic as asbestos fibers to mesothelial cells (Toyokuni et al. 2013). The pathogenic mechanism of the MWCNT were also similar to asbestos. Other MWCNTs, however, were not found to be carcinogenic. The carcinogenicity inflammatory response, and cytotoxicity may be dependent upon a number of factors including, surface modifications, diameter, length, and rigidity of the MWCNT. For single wall carbon nanotubes (SWCNT), genotoxicity was observed in some studies, but carcinogenic activity has not been observed. Exposures to nanoparticles in the 2 nm to 5 nm size range may result in minimal health affects for acute exposures, and short-term health effects with a quick recovery for subacute exposure. Titanium Dioxide ($TiO_2$) was administered to mice in an inhalation study (Grassian et al. 2007). The $TiO_2$ nanoparticles ranged from 2 nm to 5 nm in size. The mice were exposed to the $TiO_2$ acutely (4 hours), and subacutely (4 hours per day for 10 days). The health effects observed with the acutely exposed mice were minimal lung toxicity or inflammation. The health effects observed for the subacutely exposed mice included higher counts of total cells and alveolar macrophages at week-one and week-two post exposure. These mice recovered from these health effects by week-three post exposure.

Finally, translocation of certain nanoparticles may result in various forms of heart pathology. Human aortic endothelia cells were incubated with three different metal oxide nanoparticles for one to eight hours by Gojova et al. (2007). Uptake of the nanoparticles was observed in the cells, and two types of the metal oxide nanoparticles elicited a pronounced inflammatory response. Since heart pathology is often a result of endothelial inflammation, the study showed that the epithelial cells can uptake the tested metal oxide nanoparticles, and that inflammatory response may occur, depending on the metal oxide.

*Exposure Controls and Guidelines*

Exposure controls and guidelines for the production, use, and disposal of engineered nanomaterials (ENMs) are dependent upon risk assessments specific to the predetermined ENM. In the past, risk characterization was considered the final step of a risk assessment process that involved hazard identification, dose-response evaluation, and exposure assessments (Williams et al. 2010). This traditional risk assessment methodology is often applied improperly to ENMs. Traditional risk assessment evaluates dose-response relationships between chemicals and receptors to determine acceptable exposure concentrations. For ENMs, particle shape, size, surface area, and coating are properties that may be more relevant to determining potential exposure health effects than dose-response. Consequently, general controls and guidelines traditionally used for chemicals similar to the ENMs, are not as effective for ENMs due to the variety of ENM structures, properties, and variations.

The various atomic structures, and inorganic and organic surface coatings affect the surface chemistry and behavior of ENMs in the environments where they are present. The environments where the ENMs pass through (air or water), translocate through (lymphatic system, circulatory system, digestive tract, etc.) or reside (lungs, brain, liver, etc.), may change the surface chemistry of an ENM and its behavioral properties. Due to the variety of these initial and potentially evolving behaviors, it is difficult to classify groups of ENMs that will behave similarly with respect to transport mechanisms, toxicity, deposition locations, and risk. Evaluating each ENM individually, in regards to its specific production, use, and disposal, provides the most accurate information for control and guideline development. However, the lack of research data for existing ENMs, the rapid development of new ENMs, and a lack of funding for appropriate research has limited the evaluation of individual ENMs. The National Research Council (2012) has proposed an approach to provide a scientific review of the potential risks in a timely manner, without the burden of conducting separate reviews of

individual ENMs. They suggested that the value-chain and life cycle of the ENMs, ENM-containing products, and generated wastes be evaluated. The evaluation should focus on identifying how ENM properties affect key process that assist in identifying potential hazards and exposures. Based on this evaluation, current knowledge on ENM risks, the plausibility of the risk occurring, and the potential severity of the outcome should be applied to the risk exposure.

Risk exposure, based on particle size, is often used to develop exposure controls and guidelines for nanoparticle exposure. This is challenging, due to the nature of nanoparticles to agglomerate with generated nanoparticles from the same source, and with background particles. Within minutes of entering an environment with background particles present, nanoparticles will agglomerate with these background particles, increasing the nanoparticle size and disguising the anticipated nanoparticle size fraction. Since the chemical properties of the nanoparticles are still present, even when agglomerated with background particles, exposure controls and guidelines cannot be based solely on the absence or presence of nanoparticle size(s) associated with monitored operations. Given that the size of nanoparticles observed with real-time instruments during aerosol monitoring may not adequately represent the nanoparticle aerosol generated by an operation, other properties of the nanoparticles may be used to characterize the nanoparticle aerosol and develop exposure controls and guidelines. McGarry et al. (2013) evaluated six nanotechnology operations for particle number concentration (PNC), particle mass (PM) concentration, and count median diameter (CMD). The processes included emissions of carbon nanotubes (CNTs) and fibrous and non-fibrous particles. The peak and 30-minute average numbers and mass concentration values were analyzed for particles ranging from 20 nm to 1,000 nm, and from 300 nm to 3,000 nm. The study found that peak PNC for 20 nm to 1,000 nm sized particles were up to three orders of magnitude larger than the local background particle concentrations. Peak PNC for 300 nm to 3,000 nm sized particles were up to one order of magnitude larger than the local background

particle concentrations. Based on these results with the observed operations, McGarry et al. (2013) suggested that real time readings exceeding the local background particle concentrations by a magnitude of three should require the implementation of emission or exposure controls.

In addition to establishing acceptable nanoparticle aerosol concentration limits, the development of effective guidelines and controls are dependent upon the acceptance and implementation of these controls by the applicable manufacturing segment. Engeman et al. (2013) observed that exposure controls and developed guidelines for the manufacturing and use of nanoparticle infused materials are not consistent among manufacturers in the United States. Although some of the companies used published government guidance documents in their standard operating procedures, practices that specifically addressed nanoparticle exposure control were generally not in place. Instead, companies typically used chemical hygiene practices in their control procedures. Companies have used chemical hygiene practices successfully for years, and are more familiar with chemical hygiene practices. Additionally, there is currently more support documentation for these types of controls than for nanoparticle controls. They observed that health and safety controls and practices for the downstream related exposures to nanomaterials, i.e. maintenance, were practiced less frequently than most other health and safety practices that were not related to nanomaterials. This inconsistency in exposure control is even greater between larger and smaller manufacturers/users of nanoparticles and nanoparticle related products. Large manufacturers often have a greater number of employees working with nanomaterials, but there is often a larger proportion of workers involved in nanomaterials production and use in smaller facilities. Due to resource restraints, smaller companies have difficulty in implementing appropriate controls. More controls, including controls related to nanoparticle hazards, are needed to be developed and used by manufacturers.

To facilitate the development of potential exposure controls and guidelines across the manufacturing spectrum, Abbott et al. (2010) proposed the development of an exposure metric matrix. The metric matrix could be used to organize previously obtained exposure data. The metrics of this matrix would include exposure pathways (inhalation, ingestion, ocular, and dermal), and nanoparticle characteristics, including charge, size distribution, particle number, and mass. The exposure matrix would compare the exposure pathways with the nanoparticle characteristics to identify any relationships between them. Specifically, this type of matrix would identify the characteristics of the nanoparticles that should be monitored to prevent identified biological responses. This information would be useful for instrument manufacturers in the development of monitoring instruments designed for the identification of these nanoparticle characteristics. This matrix would also assist U.S. companies to identify and monitor those nanoparticle characteristics that are relevant to their operations.

U.S. companies operating globally are utilizing international standards and guidance documents for a variety of other areas including pharmaceutical, food, and chemistry. Currently, there are several international standards and guidelines for nanotechnology. Some of the developers of these standards include the World Health Organization (WHO), International Organization for Standardization (ISO), and the Organization for Economic Cooperation and Development (OECD). Until the U.S. develops and implements national worker protection standards for working with nanoparticles, Murashov et al. (2013) recommend that international standards could be reviewed and nationalized within the U.S. Other recommendations include using the OSHA General Duty Clause to provide a workplace free of recognized hazards, and adopting international standards as U.S. government guidance documents.

The development of exposure controls and guidelines is only the first step in controlling worker exposures. Implementation and validation of these measures are required to ensure they are effective for the site-specific manufacturing process. Methner et al. (2012) conducted

an evaluation of a facility performing preparation, grinding, and cutting activities with a nanocomposite material. They found that even though several engineering and personal protective equipment (PPE) controls were present, personal exposure sampling results identified the presence of substantial amounts of the nanomaterial in the breathing zone. The sample results confirmed the need to conduct sampling to validate effectiveness of the engineering controls. Additionally, personnel were observed bypassing the personal protective equipment (PPE) controls by wearing inadequate PPE or incorrect PPE. Based on the sample results and visual observations, this facility required a reevaluation of the engineering controls and PPE. Additional training was also recommended for site personnel regarding the proper use of the engineering controls and PPE. Daily monitoring with real-time instruments and periodic confirmation air sampling were recommended to monitor the effectiveness of the control methods.

Personal protective equipment will be used to protect workers from potential exposure until engineering exposure controls are accepted and implemented within the ENM manufacturing industry. Inhalation is considered a primary route for employee exposure, and respiratory protection is regularly used as a control method. Due to the additional weight, inhalation resistance, maintenance requirements, employee resistance, and costs, employers often select a filtering facepiece respirator (FFR) over a half-face or full-face respirator with canister/cartridge filters. A comparison between N95 FFR, N100 FFR, and P100 canister/cartridge used with full-face respirators was conducted, using the National Institute for Occupational Safety and Health (NIOSH) respirator certification test method (Rengasamy et al. 2013). This method tested the respirator types with different sized monodispersed and polydispersed Sodium Chloride (NaCl) aerosols. For monodisperse nanoparticles, the most penetrating particle size (MPPS) was 40 nm for N95 and N100 FRRs. The P100 canister/cartridge full-face respirator had a MPPS of $\geq$ 150 nm. Based on the NIOSH test method, the P100 canister/cartridge full-face respirator exhibited a lower penetration for various

sized nanoparticles than the N100 FFR. For FFRs, the face seal is more important than penetration for larger nanoparticle sizes. Study results noted that particle sizes of 50 nm and 100 nm particle sizes were more penetrating than either 8 nm or 400 nm sized particles, with 50 nm particles penetrating more than any of the others. For 400 nm particles, leakage through the face seal was the predominant source of leakage into the facepiece, not penetration of the filter. The Rengasamy et al. (2013) study and other similar studies using the NIOSH respirator certification test method have shown that full face respirators equipped with canister/cartridges have a higher MPPS, and offer better protection from a larger size range of nanoparticles than FFR. However, due to the negative factors associated with full face respirators, many companies continue to offer FFR to their employees when working with nanoparticles.

### *Particle Generation*

Various methods are used to generate nanoparticle aerosols for inhalation assessments. Typically, aerosols are generated from liquid suspensions containing dissolved or suspended solids, or from dry, bulk powders. The more prevalent methods for aerosol generation include nebulizers, electrospray generators, fluidized beds, acoustic, brush feed, and dust feeders (Polk et al. 2016). The selection of an aerosol generator for an inhalation assessment study is dependent upon the material to be aerosolized, the desired test concentration and particle size, and the length of the experiment.

Schmoll et al. (2009) evaluated the effectiveness of five different methods of generating nanoparticle aerosols from bulk powder. The methods evaluated included dry aerosol generators and wet aerosol generators. The dry aerosol generators included a small-scale powder dispenser, acoustic dry aerosol generator/elutriator, and fluidized bed aerosol generator. The wet aerosol generators evaluated were an electrospray aerosol generator, and a Collison nebulizer. Five nanoparticle powders were selected to test the aerosol generators. The five powders used for the assessment were 21 nm titanium dioxide, 5 nm titanium dioxide,

20 nm silicon dioxide, 1-2 nm single walled carbon nanotube, and 2-5 nm silver with a 2-3 nm polymer coating. The purpose of the study was to test the aerosol generators to determine their ability to produce an “acceptable” aerosol. The authors defined an “acceptable” aerosol as having the following characteristics: Providing a consistent concentration over several hours; providing a homogenous composition free from contaminants; and generating a size distribution that is unimodal with both a small geometric mean diameter (<200 nm), and a small geometric standard deviation (<2.5). The authors did not predetermine an acceptable concentration level, but required the aerosol generators to provide a consistent concentration with minimal fluctuation. Upon completing the study, they stated that several of the tested instruments were able to meet some of the “acceptable” aerosol criteria, but the Collison nebulizer was more effective at meeting these criteria. The Collison nebulizer produced a consistent aerosol concentration over time for the 21 nm titanium dioxide, 20 nm silicon dioxide, and 1-2 nm single walled carbon nanotube particles with a 1-4% fluctuation from the average. The nebulizer produced concentrations with average counts ranging from 10,000 per $cm^3$ to more than 30,000 per $cm^3$. Although the Collison nebulizer performed more effectively than the other tested generators, there were still areas of concern. The Collison experienced issues with size distribution due to contaminated carrier water. The authors used ultrapure water but determined that the water was contaminated with impurities. They stated that these background impurities can cause a nebulized nanoparticle aerosol to be bimodal in distribution, unless a concentrated solution is used. Based on another concern about agglomeration, sonication of the nanoparticle solution was conducted. Sonication of the suspension, prior to nebulizing, was evaluated to determine if it would reduce the agglomeration of particles occurring in the experiments. When compared to the nanoparticle solutions that were not sonicated, sonication of the solutions did not provide an observable change in the distribution or geometric mean of the generated aerosol.

Shimada et al. (2009) used a liquid aerosol generation set-up that included a pressurized nebulizer, drying section, stainless steel exposure chamber, electrostatic precipitator, particle spectrometer, and a condensation particle counter (CPC). They were evaluating a nanoparticle generation method that used a spray drying technique in which a nebulizer was used to atomize nanoparticle suspensions, and the resulting droplets were dried to produce nanoparticles. They determined that the pressurized nebulizer was effective in generating high concentrations of aerosol particles with good monodispersion. They observed that generated aerosol particle concentrations were affected by nebulizer air flow rates and suspension concentrations. Air flow rates of 10 L/min produced a low concentration of particles with a flat, broad peak. They determined that this air flow rate was not fast enough to produce droplets from the liquid thread. Airflow rates of 20 L/min generated significantly higher particle concentrations than the 10 L/min airflow rate, with a peak diameter at 60 nm. The highest peak concentration was observed at an air flow rate of 30 L/min, and the second highest peak concentration was observed with a flow rate of 40 L/min. At a flow rate of 40 L/min, the peak concentration increased but the peak diameter decreased slightly. They stated that in a two fluid nozzle, higher flow rates lead to smaller droplets, which subsequently leads to smaller particle sizes. Increasing the flow rate to 50 L/min resulted in a decreased peak concentration that fell between the peak concentrations observed at 20 L/min and 40 L/min flow rates. They also evaluated the effects of suspension concentrations on the size distributions of the aerosol nanoparticles. The suspension concentrations that they evaluated were 0.0625 mg/ml, 0.125 mg/ml, 0.25 mg/ml, and 0.5 mg/ml. They stated that the peak diameters of the aerosol particles decreased as the suspension concentrations decreased. Additionally, increasing suspension concentrations resulted in higher peak and total number concentrations of the aerosol nanoparticles. In summary, lower suspension concentrations resulted in predominantly smaller diameter particles and a smaller total number of particles.

Nebulizers are used to generate nanoparticles aerosols for drug delivery in pulmonary therapeutic treatments. Dailey et al. (2003) used various types of aerosol generation including a jet nebulizer, an ultrasonic nebulizer, and a piezoelectric crystal nebulizer to evaluate the influence of the nebulization process on biodegradable polymer nanoparticle suspensions. They produced the nanoparticle suspensions from four polymers that had different characteristics. The generated nanoparticle sizes were 103.7 nm, 93.1 nm, 115.9 nm, and 101.4 nm. For this study, they evaluated the characteristics of the nebulized aerosol, the influence of nebulization methods on the nanoparticle characteristics, and particle agglomeration that occurred during the various methods. They stated that the aerosol droplet size was not affected by the biodegradable nanoparticles, however, the nanoparticle characteristics and the aerosol generation technique influences the nanoparticle aggregation that occurs during aerosolization. Specifically for the air-jet nebulizer (Pari LC Star), they stated that it produced a mass median aerodynamic diameter (MMAD) aerosol droplet size of 4 μm, which was within the respirable fraction size and could deliver the nanoparticles within the droplet to the lungs. Additionally, the air-jet nebulizer produced an aerosol with a narrower size distribution than the other aerosol generation methods used. Unfortunately, the primary disadvantage of the air-jet nebulizer was the particle agglomeration of the nanoparticles.

Noel, A et al. (2012) evaluated the agglomeration of nanoaerosols generated with wet and dry generation methods. The purpose of the study was to determine if agglomeration was more prevalent with the wet generation methods or dry generation methods. A six jet Collison device, with a Delavan siphon spray nebulizer, was selected as the wet generation method. For the dry generation method, the authors selected the Palas RBG-1000 dust feeder and the TSI Fluidized Bed. The nanoparticle aerosol generation was conducted for a six hour period. During the experiment, the Collison device produced stable mass concentrations with smaller sized agglomerates (less than 100 nm). The Palas RBG-1000 dust feeder and the TSI Fluidized Bed generators produced mass concentrations with larger sized agglomerates

(greater than 100 nm). In this study, stable aerosols were generated with both the dry and wet generation techniques, however, they observed smaller nanoparticle agglomerates with the wet-generation method.

Some nebulization techniques are not effective at producing nanoparticle aerosols. Beck-Broichsitter et al. (2013) used air-jet and vibrating-membrane nebulizers to generate a biodegradable nanoparticle aerosol from a sodium chloride (NaCl) solution. Dynamic light scattering was used by the researchers to determine particle size, and size distributions of the biodegradable nanoparticles. The morphology of the nanoparticle suspension droplets was determined using a transmission electron microscope (TEM) to analyze the collected air sample filters. They determined that air-jet nebulization was not an effective method to produce a stable aerosol concentrations of biodegradable nanoparticles. Additionally, they determined that the air-jet nebulizing method used in their research produced particle agglomeration. They also noted that the nebulizer reservoir retained a majority of the suspended particles. It was determined that the use of a vibrating membrane to nebulize biodegradable nanoparticles did not produce agglomeration or the concentration issues identified with the air-jet nebulizing method.

### *Particle Measurement Parameters*

Exposure to nanoparticles may occur through the entire lifecycle of the engineered nanomaterial (ENM) product. Worker exposures can occur during the ENMs manufacturing, during use of manufactured ENMs to produce other products, while maintaining and cleaning the ENM manufacturing/production equipment and air filtration devices, and by the end users of the ENMs. Similar to other potential contaminants in the workplace, real time measurements of ENM concentrations are often used to determine employee exposures or the effectiveness of engineering controls. Unfortunately, a current issue in the ENM industry is the absence of fully established or agreed upon ENM exposure measurement parameters among manufacturers or

users of the products (Abbott et al. 2010). There is also uncertainty regarding which property of ENMs (mass, particle number, surface area, chemical composition) is responsible for adverse health effects (Solomon et al. 2012). Since the relationship between particle concentration parameters and risk of illness or disease have not been clearly determined, there is no consensus on the appropriate sampling method or metric to use to determine aerosol nanoparticle aerosol concentrations. However, since employee protective measures, including engineering controls and personal protective equipment, are frequently evaluated and selected based on real-time exposure monitoring results, acceptable ENM measurement parameters should be established for use by manufacturers and end users (Seipenbusch et al 2008).

There are six metrics often used to evaluate nanoparticle concentrations and exposure potential. These measurement parameters include mass-direct (total and/or elemental), mass-indirect (calculation), number-direct, number-indirect, surface area-direct, and surface area-indirect (NIOSH Publication No. 2009-125). Mass-direct involves the collection of the nanoparticles, and subsequent gravimetric and/or chemical analysis of the collected nanomaterials. Mass-indirect metrics are based on a calculation from collected sample information including particle charge, aerodynamic diameter, and mobility diameter. Number-direct metrics involve counting a representative number of the generated aerosol nanoparticles. This can be conducted by enlarging the particles through condensation and using high intensity lasers to count the enlarged particles, determining particle mobility diameters, or by direct analysis using electron microscopy. For the number-indirect metric, particles are electrically charged, passed through a Cascade impactor, and are classified according to their physical diameter (Amarai et al 2015). The fifth particle measurement metric is surface area-direct. In this metric, particles receive a charge by passing through an ionizer. The aerosol charge is measured, and the particle surface area is calculated from the amount of charge/ions observed on the particles. The final metric is surface area-indirect. Particle mobility diameter,

aerodynamic diameter, and a comparison of these parameters are used to estimate surface area.

When comparing mass to particle number concentration (PNC), most of the mass is found in the particle size range of 0.1 µm to 10 µm, while most of the particles are observed in the size range below 0.1 µm (100 nm). Since many of these <100 nm sized particles deviate from unit density and are not spherical, the equivalent diameters of these irregular particles are usually reported. The particle equivalent diameter properties are used by various instruments to measure the particles. Differential mobility analyzers (DMA) and scanning mobility particle sizers (SMPS) measure mobility diameter by sizing the particles through the use of an electric field. Impactors and cyclones measure aerodynamic diameter through the use of inertia to separate particle sizes (Solomon et al. 2012).

McGarry et al. (2013) evaluated the particle measurement parameters of PNC, particle mass (PM) concentration, count median diameter (CMD), alveolar deposited surface area, elemental composition, and morphology. They stated that using mass to determine nanoparticle aerosol concentrations is inadequate for particle sizes < 100 nm, due to the surface area to mass ratio. PNC, surface area and activity, and fiber aspect ratio and length are better exposure metrics than mass. The limited data available for determining the relationship between exposure and illness/disease has made determining a single measurement metric difficult. They were also concerned with concentrating on nanoparticles with a physical diameter less than 100 nm for risk hazard assessment. Nanoparticles have a tendency to agglomerate, especially in this size range. A nanoparticle identified by real-time measurement equipment is rarely the same size as it was when it was generated or initially released into the work or testing environment. Agglomeration of the nanoparticles with themselves or background particles will often result in a decrease in nanoparticle numbers, and an increase in the nanoparticle size fractions. Changes in both of these parameters are dependent upon particle size and particle concentration of the background aerosol, and nanoparticle aerosol

number concentrations. Based on the difficulty of obtaining and using equipment to identify particles in the nanoparticle range, and the propensity of nanoparticles to agglomerate into larger diameter articles, they decided to use a portable CPC with a particle range that includes particles ranging from 0.02 µm to 1.0 µm, an optical particle counter (OPC) with a particle range of 0.3 µm to 10 µm, and a photometer fitted with a 2.5 µm impactor. For their research, they used real-time particle number and mass concentration data to evaluate excursion guidance criteria. They recommended using particle number and mass concentration data to determine if an ENM process is a significant emitter of particles to the local environment. They stated that portable instruments, including a CPC (measurement range of <100nm), an OPC (particle measurement range of submicrometer to 10 µm), and a photometer (particle measurement range that overlaps the OPC and CPC measurement ranges) should be used simultaneously to measure the particle aerosols. These instruments are adequate to measure the presence of ENM emissions associated with a manufacturing process, based on a knowledge of the background levels of particle concentration, and a comparison of the instrument data.

Determining the nanoaerosols concentrations associated with a process may also be possible through the use of modeling techniques and particle number concentrations (PNCs). Kumar et al. (2009) compared measured and modeled PNCs, ranging from 10 nm to 300 nm, at different heights between buildings in a city environment. The primary source of the nanoaerosols for the study were vehicle emissions. The PNCs were modelled using an Operational Street Pollution Model, a modified Box model, and a Computational Fluid Dynamics code. When the computer model size inputs were carefully chosen, a correlation was identified between measured PNCs and modeled PNCs, particularly in the areas between ground level and 2 meters above ground level. The correlation between the measured and modeled PNCs became weaker as the distance increased above 2 meters. This modeling technique could be useful in an occupational setting. If the air flow changes, personnel traffic, and PNCs are identified in a production area, then the use of modeling to determine anticipated exposure

levels of PNCs for a similar area may be applicable in determining potential worker breathing zone exposures.

### *Particle Measurement Instruments*

Direct-reading instruments are used in various industries to assess ambient atmospheres, evaluate engineering controls, and estimate worker exposures to airborne contaminants. Unlike traditional sampling methods which require sample collection and submission to a laboratory to determine ambient levels of contaminants, these instruments provide nearly real-time contaminant concentrations in the work area. The real-time capability of the instruments allows them to be used in the development of an "aerosol map" for a manufacturing area. Aerosol mapping entails measuring the contaminant concentrations in a workplace with a direct-reading instrument, and documenting the findings on a facility drawing (Peters et al. 2005). The results from the mapping activity are used to determine background contaminant levels, identify potential contaminant emission sources, and develop administrative and engineering controls. Based on the aerosol mapping results, traditional sampling methods with laboratory analysis can be conducted to confirm the contaminant concentrations identified by the mapping process. After implementation of the selected workplace controls, aerosol mapping can be repeated to document the effectiveness of the controls. In ENM manufacturing operations, the use of particle measurement direct-reading instruments to conduct aerosol mapping is useful for determining background ENM air concentrations, when leaks of fugitive ENM emissions are present in the workplace, and where the ENM emissions are occurring (Evans et al. 2010). They can also be used to estimate worker exposures. The National Institute for Occupational Safety and Health (NIOSH) conducted an exposure assessment for carbon nanofibers (CNF) during the cutting, grinding and sanding of products containing CNFs (Methner et al. 2012). Real-time particle measurement instruments and filter based samples were used to collect measurements in the areas where these activities were conducted.

Personal exposure monitoring, with filter samples, were conducted on a representative number of the personnel conducting the work. The direct reading instrument measurements identified specific work tasks and areas with elevated aerosol readings. Some of the monitored areas with elevated aerosol readings had engineering controls in place. The results from the filter based air samples confirmed that CNFs were being released during some of the material handling activities. The direct reading instruments measurements, combined with the personal exposure filter samples, identified specific work tasks that had elevated aerosol readings and confirmed the ineffectiveness or improper use of controls in some of these production areas.

For traditional manufacturing operations, worker exposure is often determined over an eight hour period. In the ENM manufacturing industry, the potential for nanoparticle exposures often occur during short, task driven manufacturing or cleaning activities (McGarry et al. 2013). Unfortunately, many of the direct-reading instruments commonly used to measure aerosol concentrations are not designed to measure particles less than 100 nm in size. In response to this need, equipment manufacturers developed direct-reading instruments that were sensitive to this size range.

There are various methods used for nanoparticle aerosol measurement, including mass (direct or indirect), particle number (direct or indirect), and surface area (direct or indirect) (Solomon et al. 2012; NIOSH Publication No. 2009-125). Examples of mass-direct instruments include size selective static samplers, tapered element oscillating microbalance (TEOM), and filter collection and elemental analysis. Mass-indirect measurement methods include the micro-orifice uniform deposit impactor (MOUDI), the nano-MOUDI (n-MOUDI), electrical low pressure impactor (ELPII), and differential mobility analyzer (DMA). A DMA is a real-time size selective instrument that detects number concentrations and provides aerosol size distribution (NIOSH Publication No. 2009-125). DMAs may detect particles ranging from 3 nm to 800 nm. Particle number direct measurement methods include condensation particle counter (CPC), optical particle counter (OPC), DMA, SMPS, and electron microscopy. A CPC is

a real-time instrument that measures number concentrations within its particle size detection limits, often ranging from 10 nm to over 1,000 nm. The CPC operates through the condensation of vapor, usually alcohol or water, onto nanoparticles in the sampled aerosol. The condensation causes the particles to grow in size until they can be observed by an optical counter. CPCs are one of the most widely used instruments for detecting and counting nanoparticles aerosols. They require a nanoparticle pre-separator to count particles in the nanoscale range, and are typically used for particle physical diameters below 100 nm. An OPC also measures real-time number concentrations within its particle detection limits, typically detecting and counting nanoparticle aerosols greater than 50 nm. The OPC utilizes a light source, typically a laser diode, to illuminate a selected sample of air. A photodetector then measures the light scattered off the particles by reflection, refraction, and deflection. Based on the intensity of the flash, particles can be counted and sized at the same time. SMPS and DMA are real time mobility diameter size-selective particle counting instruments. These instruments can provide number based size distributions. For particle size distribution measurements, a differential mobility analyzer (DMA) is used to classify particles, based on their electrical mobility. A DMA requires a detector, which may include a CPC, or a CPC and SMPS combination. SMPS are used for long-term monitoring of atmospheric particle size distributions, particularly in the submicrometer diameter range (Wiedensohler et al. 2012). For SMPS, the aerosol stream is passed through an impactor or cyclone to remove the larger diameter particles. The remaining particles are brought to a bipolar charge equilibrium with a bipolar charger, prior to entering the DMA. When the particles enter a DMA, they are separated by their electrical mobility. The electrical mobility is dependent upon the size of the particle. Particles meeting the pre-determined electrical mobility range proceed through a classifier and a condensation particle counter. A long DMA can detect particles in the size range of 10 nm to 1000 nm. A nano-SMPS, using a nano-DMA, can measure particles from 3 nm to 150 nm. The high inlet flow and short inlet passage in the nano-DMA reduces aerosol residence time, and lowers the particle loss (Chen et al. 1998).

Comparing measurements from SMPS is difficult due to the lack of accepted standards and guidelines, particularly for measurement mode, instrument set-up, quality control, and the evaluation of data[8]. Although technical standards are developed to address the minimum requirements of mobility size spectrometry used for long term aerosol measurements, not all manufacturers have followed these recommendations. Some of these recommendations addressed continuous monitoring flow rates, and relative humidity, temperature and pressure of the sample and sheath air in the differential mobility analyzer. Wiedensohler et al. (2012) compared several custom built mobility particle size spectrometers to determine the uncertainties between the instruments. They found that particle number size distributions ranging from 20 nm to 200 nm, under controlled conditions, were within an uncertainty range of plus or minus 10%. Particle number size distributions above 200 nm exhibited an uncertainty range of plus or minus 30%. Identically designed reference mobility spectrometers, operated under carefully controlled settings, agreed within a plus or minus 4% of the peak particle number concentration. These reference instruments were inconsistent with the total particle number concentration. Ham et al (2016) conducted a comparison of real time nanoparticle monitoring instruments in a workplace. Although correlation was observed between the instruments, caution was recommended when comparing measurements between similar instruments, specifically SMPS from different manufacturers. The study observed an approximately 20% difference in readings between the two SMPS instruments. Electron microscopy (EM) does not provide real-time aerosol measurement. It is used to analyze prepared air filter samples and can provide size-specific aerosol number concentrations. The EM uses high energy beams to scan the sample surface. The energy beams react with the particles on the surface of the sample to produce signals. These signals are used to produce detailed images of the sample's surface. Micrographs, taken with the EM, can be analyzed to provide size specific aerosol number concentrations. Particle number indirect measuring instruments include ELPI and MOUDI (NIOSH Publication No. 2009-125). These instruments

can provide real-time physical diameter size selective detection of active surface area concentrations. Surface area-direct measurements can be obtained with a diffusion charger, epihaniometer, ELPI, MOUDI, and electron microscope (Shin et al. 2007). Surface area-indirect measurements can be obtained with a DMA, SMPS, and DMA and ELPI used in parallel (NIOSH Publication No. 2009-125). Transmission electron microscopy (TEM) and scanning transmission electron microscopy (STEM) provide an effective method for characterizing nanoparticles. Due to its available diffraction, spectroscopy, and imaging techniques, STEM is an effective microscope for characterizing the physicochemical properties of nanoparticles (Liu et al. 2005). However, the use of a TEM and STEM requires a highly trained operator and requires large amount of time to do correctly (Lagos et al. 2015). Additionally, interpretation of the images can also be difficult for operators with less experience.

Scanning electron microscopy (SEM) is the most widely used electron beam based instrument. The effective operations of a SEM does not require the same level of training as TEM or STEM. Interpretation of the SEM micrographs are easier than TEMs, and the SEM is able to process slides more quickly that TEM or STEM. An SEM may be restricted when analyzing nanoparticles with diameters below 20 nm, due to resolution loss associated with size reduction and small signal difficult nanoparticle imaging (Lagos et al. 2015). Some of the disadvantages of SEM include the time required to analyze enough particles for statistical significance, and the interpretation of 3 sizes and shapes from 2 dimensional images (Giechaskiel et al. 2014).

# Chapter Three

# Methodology

## *Design and Operation of Sampling Chamber*

All experimental procedures were conducted in a test chamber that was designed and developed at the University of South Florida for the evaluation of real time direct reading instruments in an environment of stable nanoparticle aerosol concentration. Chamber design prerequisites included the following: size parameters; access ports; pressure monitoring devices; prevention of contamination by particle penetration from the laboratory air; delivering controlled amounts of air flow rates; even distribution of the concentration of the generated test aerosols; and convenient access to the inside of the chamber. The volume of test chamber was selected to be large enough to allow for an adequate volume the generated nanoparticle aerosol and installation of test equipment, without the consumption of excessive amounts of the test aerosols such as sodium chloride, polystyrene latex spheres and nitrogen gas used for aerosol generation. The volume of the chamber also influenced the amount of required HEPA filtered dilution air as well as purging the chamber prior to, and after each run in order to remove residual nanoparticles used in previous runs of the experiments. Based on the review of these parameters and requirements a 20” x 20” x 20” chamber (4.6 cubic feet) was selected for the experiments.

The chamber was fabricated from 0.125” aluminum plates for the top, front (door), and back. Tempered glass panels 0.25” thick were used for the bottom and two sides of the chamber. Aluminum and glass plates were held together by a welded aluminum frame. The aluminum door was attached to the frame with eight bolts, metal washers and wing-nuts. A

Neoprene foam gasket was used to seal the door. The glass panels were sealed and secured to the aluminum frame using silicone rubber. The aluminum frame allowed for grounding of the chamber components to minimize build-up of static electricity during operation of the chamber.

Access ports drilled in the top, back and door of the chamber allowed for the introduction and removal of purging gases, introduction and removal of generated nanoparticles and installation of a Magnahelic pressure gauge for monitoring the pressure inside the chamber. The rest of the ports were utilized for connections to aerosol sampling devices, installation of a hygrometer, and tubing for the collection of aerosol samples on membrane filter cassettes.

The regular activities and procedures for operation of the chamber, such as introduction of aerosols and dilution air, maintenance of aerosol concentration, and continuous exhaust of chamber air created negative pressure in the chamber. Since the chamber was designed to be operated within a pre-designated and limited pressure range, monitoring the chamber pressure changes was required to maintain safe operation and testing conditions. The installation of the Magnahelic pressure gauge in the chamber's door was essential for determining when designated pressures were reached, and to alert of any changes in that pressure. Controlling the leakage and possible penetration of room air was another critical aspect of the chamber design. Since the purpose of the chamber was to create and maintain a stable well defined nanoparticle aerosol, it was important that the chamber design would not allow penetration of ambient air into the chamber, or the leakage of generated nanoparticle aerosol out of the chamber. Therefore, testing to eliminate any possible penetration of ambient air was conducted to insure the success of the experiment as described below.

The flow rate of nitrogen gas used for the generation of nanoparticle aerosols and filtered dilution air into the chamber were carefully monitored to allow for adequate mixing and appropriate residence time within the chamber without overwhelming the aerosol measuring instruments. The residence time of the generated aerosol and filtered air assists in maintaining the even distribution of the aerosols throughout the chamber. This was achieved using

perforated aluminum sheets that served as diffusion devices. An exhaust manifold was designed to provide appropriate aerosol residence time within the chamber. It also assured the development of even distribution of aerosol concentration and as well as the even spread of HEPA filtered dilution air without air short circuits. Access to the inside of the chamber was also required to adjust diffusion units, install ingress and egress ports, install sampling media, and provide general maintenance.

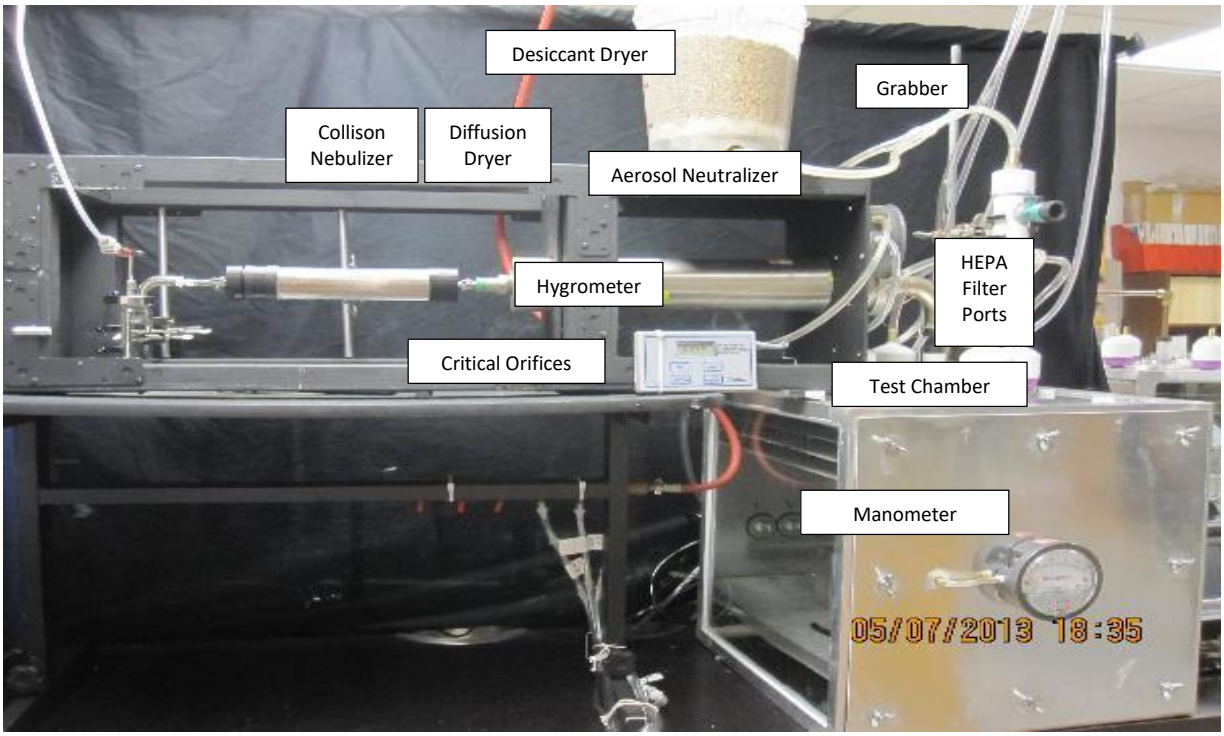


Figure 1: Photograph of aerosol generation system and test chamber

Several holes were drilled into the back, top, and front aluminum plates of the chamber. The holes were required as access ports to allow for installation of air connection fittings, instrumentation probes, and the pressure gauge. The aluminum top plate was used to install four welded 1" threaded tubes approximately 5" from the corners for filtered air ports. HEPA filter cartridges (North P100, Part # 7580P100) were installed into the four threaded ports. A 1 3/8" aerosol inlet tube was also welded in the center of the top plate. Four copper 90$^{O}$ elbows were attached to the four HEPA filter ports. The four elbows were directed toward center of the chamber facing the aerosol inlet stream. The filtered air moving through the copper elbows

provided good mixing of the dilution air and the generated aerosol. This turbulent mixing of dilution air and inflow of the aerosol allowed for a more even air flow through the diffusion baffles and into the test chamber.

Thirteen access ports were drilled in the back of the chamber. Brass, barb nosed connections were installed in five of the access ports. Four of these ports, located approximately 2.5” above the bottom of the chamber, were used as instrument exhaust returns. Quick-Disconnect fittings were installed in seven of the rear access ports. These ports were used for sampling and were located across the middle of the back wall. SMPS inlets were connected with conductive tubing to port numbers 2, 3 and 4. Inside of the test chamber, the SMPS inlet tubes were connected to a brass “T” connection to ensure that they all sampled from the same area within the chamber. A hygrometer / thermometer probe (Traceable Hygrometer Thermometer Dew Point, Fisher Scientific) was installed in the last access port, located adjacent to the instrument exhaust return ports at the bottom of the rear wall. One of the four ports, located closer to the bottom of the chamber, was connected to the exhaust manifold. The copper exhaust manifold was installed at the bottom of the chamber to assist in pulling the generated aerosol and HEPA filtered air down though the test chamber in an even flow pattern. Thus, collection and exhaust of the aerosol occurred near the bottom of the chamber. To induce even air exhaust, 25 holes were drilled along the manifold.

The diffusion baffles were comprised of five aluminum screen panels, cut to slightly smaller dimensions than the inside dimensions of the chamber. The purpose of the diffusion baffles was to control the flow of the generated aerosol and HEPA filtered air, resulting in an even distribution of the aerosol concentration through the chamber and prevent air short circuit. Three diffusion baffles were installed at the top of the chamber, and two diffusion baffles were installed at the bottom of the chamber. The first top baffle was installed approximately 2” from the chamber ceiling, and the remaining baffles were installed 1“apart below the top baffle. Shelving brackets were used at the bottom of the chamber to allow for the installation of the

bottom two diffusion baffles. The lowest bottom baffle was installed approximately 3” above the bottom of the chamber, to allow for installation of the exhaust manifold. The second bottom baffle was installed approximately 1” above the lowest baffle.

### *Testing of Air Leakage into the Chamber*

Pressure testing was conducted to identify leakage points at the welded aluminum seams and the caulked glass panels. Prior to conducting any testing, the chamber was cleaned with a degreasing soap and water to remove any oils and metal shavings generated from the fabrication process. After the chamber was cleaned, then the door was installed and sealed with the threaded bolts and wing-nuts, and all of the chamber access points were sealed except for the exhaust outlet port. The Magnahelic gauge was calibrated using a “U” tube water manometer. A pump was attached with tubing to the exhaust port, and the chamber was placed under 6 inches of water positive pressure. A solution of soap and water was applied to the exterior of the test chamber to identify any penetration points in the chamber walls, ceiling, or floor seams. Soap bubbles formed at various locations around the seams of the chamber, identifying the leakage points. All identified Leakage points were sealed using silicone caulk. This procedure was repeated on the chamber door. Air leaks were identified at the door bolt locations, so silicon grease was applied to the threads of the bolts and the wing nuts were tightened to reduce this leakage around the bolts. The number of wing nut turns required to reduce air leakage was recorded and applied for future experiment test runs. Neoprene foam gasket was used for the door. The Neoprene gasket was found to be effective for preventing ambient air leakage.

Upon completion of the leak test of the chamber seams and door, access port connections, installed valves, sample collection and instrument collection ports were tested for leakage and sealed. The threaded tubes, installed in the top of the chamber for the HEPA filters, were also tested and sealed using Teflon tape and “O” rings. After completing the leak

test of the chamber, access port connections and valves, the chamber was leak tested using negative pressure. For this test, the chamber was placed under a negative pressure of approximately five inches of water, and the rate of pressure change inside the chamber was recorded. Time increments were measured for each ½" move between the initial reading of negative 5 inches water pressure and the final pressure reading of negative ½" pressure. A graph was developed to compare the time versus pressure loss. Minor adjustments were made to the chamber until the leakage rate was within acceptable leakage accordance to published leakage acceptance criteria[18].

*Sampling Chamber Aerosol Distribution Testing*

A visual evaluation of the air flow patterns and aerosol distribution within the chamber was conducted using smoke. Ten separate trials were conducted using generated smoke. An assessment was conducted of the air drawn into the test chamber through the aerosol inlet port located on top of the chamber. A vacuum air pump was connected to the exhaust access port located at the bottom of the test chamber and a smoke source was placed into a large flask with two holes rubber stopper was placed in the flask opening. Flexible tubing was connected to the smoke flask and the smoke was drawn in the aerosol inlet tube located at the top of the chamber. The smoke source was ignited and allowed to generate a steady stream of smoke into the flask. After the flask was filled with smoke, the smoke was introduced into the test chamber at a flow rate of 6 liters per minute (L/Min). Following introduction of the smoke, the exhaust vacuum pump was turned on at a flow rate of 40 L/min. The smoke inlet flow rate and the vacuum flow rates were set to simulate the experimental flow rates. When the vacuum pump was turned on, and the smoke aerosol was drawn into the chamber through the aerosol inlet port, filtered air was also drawn into the test chamber through the HEPA filter ports located at the top of the chamber. As noted above, a 90 degree copper elbow was installed in each of the HEPA filter ports. The filtered air flowed into the chamber, through the elbows, and was mixed with the incoming smoke stream.

The air and smoke stream were induced to pass through the baffles. The smoke flowed into the chamber and progressed down through the upper diffusion baffles, through the middle of the chamber, and subsequently through the lower diffusion baffles, and was exhausted through the lower exhaust port. The smoke was used to visually identify the air flow patterns and pattern changes that occurred within the chamber as the aerosol passed through the upper diffusion baffles, and into the rest of the chamber. A lamp was mounted adjacent to the chamber, to illuminate the smoke movement within the test chamber. Several test runs were completed to identify the airflow and dispersion patterns, and these test runs were videotaped for review. To facilitate identification of the smoke aerosol pathway through the diffusion baffles and along the sides of the chamber, different colors of smoke sources were used throughout the evaluation. The residue left behind from each uniquely colored smoke assisted in evaluating the air flow patterns and distribution. Additionally, a white cloth, placed on top of the diffusion baffles located at the bottom of the chamber, was also used to register the smoke distribution pattern through the test chamber.

Initial testing identified a generally direct line of the airflow between the aerosol inlet and the exhaust port. The air flow moved directly through the top diffusion baffles, through the chamber, through the lower diffusion baffles, and out through the exhaust vent without a general distribution throughout the chamber. Neither the upper baffles nor the HEPA air inlet elbows were effective in redirecting the incoming air stream to allow for even distribution and increased residence time within the chamber. To redirect the aerosol inlet air flow, a solid deflection plate was installed on the upper baffle system. The 2 1/4" metal deflection plate was installed on the 3$^{rd}$ baffle down from the top, directly below the inlet aerosol port. The deflection plate redirected the flow of the incoming aerosol back up into the upper two diffusion baffles. After installation of the deflection plate, the smoke dispersion and patterns were observed to be more uniform and equally distributed as it passed from the top to the bottom of the test chamber. To further test the aerosol distribution, several 8" x 8" perforated templates were made from cardstock

material. The templates were placed on the upper diffusion baffles and several test runs were conducted to observe the aerosol smoke pattern on the cardstock template. After 4 test runs, the aerosol smoke distribution appeared to be directed toward the front of the test chamber. After closer examination, the aerosol inlet supply fitting was observed to be tilted as it entered the aerosol inlet port. After the supply fitting was corrected, additional test runs were conducted with the cardstock templates. The smoke aerosol distribution was no longer directed toward the front of the chamber. To further facilitate aerosol distribution through the test chamber, and reduce the direct flow of the smoke aerosol between the aerosol inlet and the exhaust manifold, the exhaust manifold placement was tested at different locations in the bottom of the chamber until an even distribution of the smoke was achieved.

### *Test System Development*

Once the chamber penetrations, and the air flow and aerosol dispersion patterns were determined to be acceptable, then the remainder of the nanoparticle aerosol generation, and measurement system was assembled. The system included the following components: nitrogen gas; BGI 3 jet Collison Nebulizer; diffusion dryer; aerosol charge neutralizer; mixing chamber; critical orifice; hygrometer; condensation particle counter; scanning mobility particle sizer; air sampling pump; air sampling cassettes; and a vacuum pump.

The nanoparticle aerosols were generated using a BGI 3 Jet Collison Nebulizer (BGI, Inc., 2001). The Collison Nebulizer is comprised of a “T” stem, which passes through a sealed penetration on the lid of the liquid solution glass jar. The “T” stem is then connected to the 3 jet sonic velocity nozzle. The lid has 2 other penetrations to allow for attachment of the aerosol outlet, and an external fill adapter. The Collison Nebulizer uses a two fluid atomization. The compressed gas is used to aspirate the liquid solution into a sonic velocity gas jet, equipped with 3 jets. The gas jet shears the solution into droplets, which are emitted against the side wall of the liquid solution container. When the droplets strike the side walls of the container, then the

larger size fraction of the droplets drop back into the solution while the smaller size fraction droplets are discharged through the aerosol outlet. Using the BGI Collison Nebulizer with a 3 jet nebulizer and compressed nitrogen gas at flow rate of 6 L/min and a pressure of 20 pounds per square inch gage (psig), produces droplets with median mass diameters (MMD) of 2 microns. At this air flow rate and pressure, the liquid use rate of the nebulizer is 4.5 milliliter/hour. BGI recommends that the "T" stem be immersed no more than 3/8" into the liquid solution. Due to the extended run times of the experiments, the "T" stem was gradually pushed down farther into the solution container, as the test run progressed, to maintain this depth of 3/8". Depending on the length of the sample run, additional sample solution was added to provide the correct solution depth for the 3 jet nozzle. The external fill adapter was installed in the lid, through the designated lid penetration. On extended test runs, the external fill adapter was used to add additional prepared solution into the jar, while the Collison Nebulizer was operating.

After nebulizer generation, the aerosol cloud was sent through a diffusion dryer (ATI, Model 250). The diffusion dryer was used to remove the water humidity generated through the nebulization process. At the inlet of the dryer is a water trap for collecting large water droplets. After the aerosol passes through the water trap, it passes through a removable desiccant cartridge. The desiccant cartridge has an inner layer of fine steel mesh and an outer layer of steel mesh screen. In between the mesh layers, the desiccant cartridge is filled with dry, regenerated silica gel. As the aerosol passes through the desiccant cartridge, the excess moisture is removed by diffusional capture through the inner mesh screen and onto the silica gel. Since the aerosol cloud has minimal contact with the silica gel, there is minimal particle loss from the aerosol. The desiccant cylinder is placed into an oven for three hours at 250$^{O}$F to regenerate the silica gel[19], as needed.

After passing through the diffusion dryer, the aerosol cloud was directed through a radioactive aerosol neutralizer (TSI, Model 3054) prior to entry into the mixing chamber and test chamber. The radioactive neutralizer was used to reduce the effects of the electrostatic

charge produced during the nebulization process. In the TSI aerosol cylindrical neutralizer, inert Kr-85 gas is sealed inside of a stainless steel tube. A metal outer housing is used to shield the stainless steel tube. The Kr-85 ionizes the atmosphere between the tube and the outer housing into positive and negative ions. The generated aerosol is directed through this ionized atmosphere resulting in charge equilibrium.

After the aerosol cloud passed through the diffusion dryer and radioactive neutralizer, it was discharged into the test chamber aerosol inlet through a brass “T” connector inserted into two drilled rubber stoppers. Prior to discharge into the chamber, a designated volume of the aerosol cloud was removed through the “T” connector by a device termed the “Grabber”. The purpose of the Grabber was to remove a portion of the generated aerosol, while adding HEPA filtered air to maintain a steady aerosol concentration within the chamber, and not overwhelm the measurement capacity limits of the CPC and SMPS monitoring instruments. The Grabber air flow rate was adjusted, depending on the concentration measurements obtained from the CPC and SMPS monitoring instruments, during the sampling runs. After several pre-test runs were conducted, the Grabber was adjusted to an air flow rate that required minimal adjustments when the final testing sample runs were conducted.

Ambient air from the laboratory was introduced into the test chamber through four HEPA filters located at the top of the chamber. The combined air flow rate through the HEPA filters was approximately 40 L/min. The laboratory ambient air was conditioned to remove elevated levels of humidity, because the test parameters of the experiments required that the relative humidity of the air inside the test chamber be lower than ambient air levels. The reduction in moisture content of the air was achieved by pre-treatment through a large desiccant dryer. The dried air was passed through a distribution manifold that mixed the treated air with ambient air, prior to passing through the HEPA filter ports in order to obtain the desired moisture level required within the test chamber.

The two types of nanoparticle aerosols utilized in the experiment were salt (NaCl) and polystyrene latex (PSL). NaCl and PSL solutions were made for use in the Collison Nebulizer based on the test run parameters, the selected aerosol concentration, and selected aerosol nanoparticle size. For the NaCl solutions, a calculation was used to determine the mass of NaCl required to produce the desired nanoparticle aerosol particle size. After this mass was determined, a quantity of NaCl was weighed on a Mettler balance (AE240) and placed in a mixing flask. A pre-designated amount of high grade purified water was measured using a graduated cylinder and poured into the mixing flask with the NaCl. The solution was stirred until the NaCl was dissolved.

For the PSL solutions, the appropriate size PSL stock material was selected to create a solution of the desired nanoparticle size. Four different sizes of PSL, obtained from Polysciences, Inc., and ThermoFisher Scientific were used for the experiments – 57 nm, 92 nm, 147 nm, and 220 nm. The PSL solutions were prepared with pre-determined amounts of ethyl alcohol and high grade pure water to provide a known dilution value for the test run. The selected size of PSL stock material was measured in a graduated cylinder and poured into a mixing flask. The ethyl alcohol and water were also measured in a graduated cylinder and poured into the mixing flask with the PSL spheres.

### *Relative Humidity Testing*

After the system was fully assembled, testing was conducted to ensure that the required relative humidity levels were achieved in the chamber. Constant relative humidity levels were necessary to maintain a stable aerosol concentration. A relative humidity/hygrometer probe was installed into one of the back wall access ports to monitor the humidity levels in during the experiments. The vacuum pump was turned on to a pre-determined flow rate, and the fresh-air mixing manifold was adjusted until the relative humidity measured by the hygrometer in the test

chamber was at an acceptable level. The test was repeated several times, with freshly prepared desiccant, to confirm the fresh-air mixing manifold setting was repeatable.

### *Test System Monitoring Equipment*

The generated aerosol cloud in the test chamber was measured using a condensation particle counter, SMPS instruments, and air sampling with media filters. Measurements of the aerosol cloud in the chamber were obtained using real-time, direct-reading particle measurement instruments including a condensation particle counter (CPC) (TSI, Model 3007), and three scanning mobility particle sizer (SMPS) instruments. Tubing was connected from the inlet port of the instrument to access port on the back wall of the test chamber. The access port was connected to a sampling tube on the inside of the chamber. The sampling tube was placed on a standing rack inside of the chamber, to allow for sampling of the generated aerosol in a central area of the test chamber, between the upper and lower diffusion baffles. The return ports on the CPC and SMPS instruments were connected via tubing to the bottom of the chamber, adjacent to the exhaust manifold. Two of the SMPS were the same model and manufacturer (Particle Measuring Systems, Nano-ID NPS500), and one SMPS was from a different manufacturer (TSI, NanoScan SMPS Nanoparticle Sizer Model 3910). During the early stages of the experiment, SMPS Instrument 1, Particle Measuring Systems (PMS) Nano-ID NPS500, was not functioning properly and was sent back to the manufacturer for repair. While this unit was being evaluated and repaired, the manufacturer sent a second SMPS for use in the interim, SMPS Instrument 2 (PMS, Nano-ID NPS500, loaner). This SMPS was the same model as the one being repaired. During the same period of time, TSI was approached and submitted their instrument, NanoScan SMPS Nanoparticle Sizer Model 3910 (instrument 3) to be evaluated in the experiment. After Instrument 1 was repaired and returned, PMS allowed Instrument 2 to be retained for evaluation during the experiment. When the test runs of the experiments were completed, Instrument 2 was returned to the manufacturer.

The condensation particle counter uses a laser light scattering source and a detector to count the particles. Due to the small aerodynamic diameter of the generated particles, it is difficult for the detector to identify them. The CPC uses the principle of vapor condensation on the aerosol particles to make the particles larger, and easier for the detector to detect. As the aerosol is pulled into the CPC, it is saturated with an alcohol vapor. The particles in the generated aerosol act as nuclei for the alcohol vapor to condense upon. The vapor droplets, with the generated particles as their nucleus, are directed past the laser light source and the individual pulses of light (scattering) are counted. The particle size detection range for the TSI CPC used for this experiment was 10 nanometers to <1 micrometer. The concentration range for the instrument was from 0 to 100,000 particles per cubic centimeter ($cm^3$). Aerosol concentrations greater than 100,000 $cm^3$, may not accurately report aerosol concentration because the detector can only observe a set amount of scattered light pulses at one time. As the aerosol concentration increases, and the light beams are all being used to detect the particles, then dead time occurs. Dead time is the time when aerosol particles pass by the detector without being counted, because the counting capacity of the detector is full.

Two models of SMPS, PMS Nano-ID and TSI Nanoscan, were used in the test chamber to measure nanoparticle aerosol concentrations. The SMPS operates on the principle of a charged particles mobility in an electric field. A radioactive source is used to neutralize particles coming into the instrument so that they have a Fuchs equilibrium charge distribution. The particles are sent through a Differential Mobility Analyzer (DMA) and the aerosol cloud is separated according to the electrical mobility of the particles. Particles with a limited electrical mobility can pass through the output slit of the DMA. The DMA is a cylinder with a negatively charged rod in the center, and a laminar sheath of particle free air running through it. The neutralized particle flow is inserted at the exterior edge of the DMA, and positively charged particles move across the air sheath towards the negatively charged rod. The electrical mobility of the particles determines their rate of travel towards the central rod. The electrical mobility of

the particle determines if the particle will exit with the exhaust flow or pass through the slit at the top of the DMA. Factors that influence the particle sizes that pass through the DMA slit include voltage of the central rod, particle charge, particle size, and flow in the DMA. The SMPS determines the particle size distribution by exponentially scanning the voltage on the center rod. The PMS Nano-ID SMPS contained a SMPS mode and a CPC mode. In the SMPS mode, this model measured particle size distributions ranging from 5 nm to 500 nm. The maximum particle concentration that it could process was 100,000 particles/$cm^3$ in particle counting mode, and 1,000,000 particles/$cm^3$ in the spectrometer mode. The DMA sizing accuracy of the model was +/- 3% mean mobility diameter. For the experiment test runs, the PMS Nano-ID SMPS was operated within the following parameters: measured particle size distributions ranging from 15 nm to 300 nm over 128 channels; two minute sampling scan; and 50 second reverse scan. The two minute sampling time was selected to measure similar aerosol concentrations during the sample period. Aerosol concentrations fluctuated during an entire test run, and the short sample time reduced the impact of these fluctuations on the sample results. Additionally, collecting samples over a shorter time period allowed for the collection of several data points during the test run. The reverse time between samples, when the instrument flushes itself with clean air to remove any residual aerosol particles in preparation for collecting the next sample. The time of 50 seconds was selected to allow the SMPS enough time to conduct this flushing.

The TSI NanoScan SMPS measured particle size distributions ranging from 10 nm to 420 nm, over 13 channels. The maximum particle concentration that it could process was 1,000,000 particles/$cm^3$. For the experiment test runs, the TSI NanoScan SMPS was operated within the following parameters: measured particle size distributions ranging from 10 nm to 420 nm; and one minute sampling scan.

For each test run, two air samples were collected on membrane filters for electron microscopy (EM) analysis. Polycarbonate Track Etch (PCTE) membrane hydrophobic filters 25 millimeter (mm) in diameter with 0.2 micron pore size from Sterlitech (#PCTF0225100). The

sample filters were placed in a 25 mm three-piece polypropylene static conductive cowl filter cassette housing (Nucleopore). The filter holders were attached with conductive tubing into sampling ports number 6 and 7 on the back of the chamber. The sampling ports and conductive tubing were grounded to the exhaust manifold with copper wiring to reduce the build-up of electrostatic charge. On the exterior of the chamber, the sampling ports were connected to sample tubing, calibrated critical orifices, and a vacuum pump. The critical orifices were calibrated to a sampling flow rate of 1.8 L/min. For high concentration test runs, the air samples were collected for approximately 30 minutes. For low concentration test runs, the samples were collected for approximately 105 minutes. The sample run times were based on the calculation of aerosol concentrations and empirical data obtained during trial test runs.

*Testing Procedure*

The testing procedure for NaCl test runs were conducted following these procedures. The BGI 3 jet Collison Nebulizer glassware, lid, and "T" stem were cleaned with methylene chloride and acetone. The nebulizer components were sonicated and then rinsed several times with deionized water. The components were then rinsed with high grade pure water. The 25 mm PCTE filters were placed in the 25 mm 3-piece cassette housings in preparation for NaCl nanoaerosols air sample collection. The two PCTE cassettes were connected to the air sample pump tubing within the test chamber, and placed on the chamber sample rack. The chamber sample rack was located in the center of the chamber and the air samples and sample collection hoses for the CPC, and SMPSs were placed next to it. This placed the sample inlets and sample filters in the center of the chamber. The chamber door was closed and secured with the wing-nut fasteners. The silica desiccant, previously treated in the laboratory oven, was placed in the desiccant dryer, and the dryer was attached to the fresh air mixing manifold (Grabber). The fresh air vacuum pump was turned on to purge out the chamber with several dehumidified, HEPA cleaned air changes. The chamber pressure was maintained at -0.5 inches of water. The fresh air mixing manifold was set to 5.9 L/min, and the vacuum pump was run

until an initial chamber concentration of less than 0.3 particles/cc on the CPC was obtained. Additional chamber aerosol measurements were obtained with the CPC to validate the test chamber background. The test chamber and laboratory RH and temperature measurements were measured throughout the testing process. The fresh air mixing manifold was adjusted to obtain a test chamber RH less than 40%. The nitrogen gas cylinder pressure was inspected to ensure that an adequate amount of gas was available to complete the experimental test run. Nitrogen gas was used to purge the dehumidifier and chamber. A NaCl solution was prepared with 99.5% Sodium Chloride (Acros Organics, Belgium) and high grade pure water (Fisher Scientific, New Jersey). The volume of water, and NaCl reagent added to the solution were dependent upon the desired nanoparticle aerosol diameter. The Collison Nebulizer was started and the fresh-air mixer was adjusted to a 1 L/min. Instrument 1 and Instrument 2 were turned on to allow the instruments to warm-up. When the chamber aerosol concentrations stabilized, then the CPC was run to verify the test chamber background prior to conducting NaCl sampling. NaCl samples were collected over a 30-minute period on the two, 25 mm PCTE filter samples. The samples were collected at a flow rate of approximately 2 L/min. The CPC, Instrument 1, Instrument 2, and Instrument 3 were collecting measurements during the 30-minute sampling period. RH and T readings were obtained from the test chamber and the laboratory. The vacuum exhaust pump was operated for approximately five minutes to purge the test chamber. After the exhaust pump was turned off, the chamber door was opened and the PCTE samples were removed and sealed. Eight test runs were conducted for the NaCl, following the procedure noted above.

The testing procedure for PSL test runs were conducted using the following procedures. The BGI 3 jet Collison Nebulizer glassware, lid, and “T” stem were cleaned with methylene chloride and acetone to remove any residual PSL spheres. The nebulizer components were sonicated and then rinsed several times with deionized water. The components were then rinsed with high grade pure water. In the initial test runs, the components were rinsed with tap

water, sonicated, rinsed with deionized water, and rinsed with high grade pure water. In subsequent test runs, residual PSLs were identified by electron microscopy. It was deduced that the water rinses and sonication were not removing the PSLs, so rinsing the equipment with acetone and methylene chloride was added to the nebulizer preparation procedures. 25 mm PCTE filters were placed in the 25 mm 3-piece cassette housings in preparation for PSL air sample collection. The two PCTE cassettes were connected to the air sample pump tubing within the test chamber, and placed on the chamber sample rack. The chamber sample rack was located in the center of the chamber, and the air samples and sample collection hoses for the CPC, and SMPSs were placed on next to it. This placed the sample inlets and sample filters in the approximate center of the chamber, both vertically and horizontally.


Figure 2: Photograph of sample inlets and sample filters on rack. Note the brass “T” fitting where the SMPS inlets are connected.

The chamber door was closed and secured with the wing-nut fasteners. The silica desiccant, previously treated in the laboratory oven, was placed in the desiccant dryer, and the dryer was attached to the fresh air mixing manifold (Grabber). The fresh air vacuum pump was

turned on to purge out the chamber with several dehumidified, and HEPA cleaned air changes. The chamber pressure was maintained at -0.5 inches of water. The fresh air mixing manifold was set to 5.7 L/min, and the vacuum pump was run until an initial chamber concentration reading of 0.3 pt/cc on the CPC was obtained. Additional chamber aerosol measurements were obtained with the CPC to validate the test chamber background. The test chamber and laboratory RH and T measurements were measured throughout the testing process. The fresh air mixing manifold was adjusted to obtain a test chamber RH reading of <40%. The nitrogen gas cylinder pressure was inspected to ensure that an adequate amount of gas was available to complete the experimental test run. Nitrogen gas was used to purge the dehumidifier and chamber. High grade pure water was run through the collision using nitrogen gas. A PSL solution was prepared with ethyl alcohol and the high grade pure water. The volume of ethyl alcohol, water, and PSL added to the solution were dependent upon the desired dilution of the solution. As an example, 20 microliters of 0.057 micrometer (57 nm) PSL was mixed with 5 ml ethyl alcohol and 20 ml of High grade pure water provide a solution dilution of 1,250. The solution volume was doubled to allow for adequate solution in the Collison Nebulizer over the testing period. The Collison Nebulizer was started and the fresh-air mixer was adjusted to a 1 L/min. Instrument 1 and Instrument 2 were turned on to allow the instruments to warm-up. When the chamber aerosol concentrations stabilized, then the CPC was run to verify the test chamber background prior to conducting PSL sampling. PSL samples were collected over a 30-minute period on the two, 25 mm PCTE filter samples. The samples were collected at a flow rate of 2 L/min. The CPC, Instrument 1, Instrument 2, and Instrument 3 were collecting measurements during the 30-minute sampling period. After 30 minutes, the PSL sample pump, nitrogen gas, and the Collison Nebulizer were turned off. RH and T readings were obtained from the test chamber and the laboratory. The vacuum exhaust pump was operated for approximately five minutes to purge the test chamber. After the exhaust pump was turned off,

the chamber door was opened and the PCTE samples were removed and sealed in preparation for analysis by electron microscopy.

### *Electron Microscopy*

To prepare the air samples for scanning electron microscopy (SEM) analysis, a representative portion of the PCTE filter was removed from each sample, placed in a sputter coating mount, and sputter coated with gold/palladium at 50 milliamps for 75 seconds. The sputter coated filter samples were placed into the SEM for examination, and to obtain micrographs of the aerosol nanoparticles. A JOEL JSM6490 SEM, with a resolution of 3.0 nm, was used to obtain the micrographs. The parameters for the JOEL SEM were: 30 kiloelectronvolts, 12 millimeter working distance, and a spot size of 25. The prepared sample filters were observed at magnification levels of 30,000, 60,000, and 90,000. Micrographs were taken with the SEM at the magnification level of 30,000.

For the NaCl nanoparticles, a minimum number of 20 observations were taken from various areas on each sputter coated slide. A number of micrographs were obtained. An initial micrograph was obtained for a PSL of 220 nm, as a size reference for calibrating the Porton graticule used in sizing the NaCl nanoparticles. The micrographs of the slides were later reviewed and the nanoparticles on the slide were sized and counted. This was conducted by using the Porton graticule scale to measure all of the nanoparticles that were present on each micrograph taken from the individual slides.

For the PSL spheres, a minimum of 20 observations were taken from various areas of the sputter coated slide. A number of micrographs were obtained. The obtained micrographs were reviewed to evaluate if there was a low or high presence of the PSL spheres on the slide, the number of single PSL spheres (singlets), and the amount of agglomeration (doublet, triplet and greater number of PSL spheres agglomerated together).

*Regression Analysis*

The datasets for the NaCl and PSL experiments included date, instrument (nanoID-1, nanoID-2, or NanoScan), geometric mean size based on range of group (bucket), mean count of particles observed in that bucket, and the percent of the total count that the bucket represented. Separate datasets were assembled from the NaCl and PSL experiment data results. Average count versus bucket size plots were prepared for the NaCl and PSL trials.

The null hypothesis is that there is no difference among instruments for the NaCl or PSL particle size group mean counts. The alternative hypothesis is that at least one of the instrument measured particle group mean counts differently than another instrument. The dependent variable was particle counts. The independent variables were the measurement instrument and geometric mean of the bucket size. The alpha level was set at 0.05. The tests were assumed to be independent, the distributions from which the samples were selected were assumed to be normal, and the variance of the distributions in the population were assumed to be equal. To test the hypothesis, the following model was used:

$$\text{Count} = \alpha + \beta_1 \text{ Instrument} + \beta_2 \text{ Log (Bucket)} + \beta_3 \text{ (Instrument} \bullet \text{Log (Bucket))}$$

JMP® Pro (v13) software was used to fit the model to the data.

# Chapter Four

## Results

### *Instrument Measurements of Sodium Chloride Nanoparticle Aerosol - Trial 1 Test Runs*

Tests were conducted using a solution of sodium chloride and purified water to generate crystal particles. The target mass median diameters (MMD) of the particle were 57 nm, 92 nm, 147 nm, and 220 nm. Concentration dilutions ranged from 104 to 2,500. The specific particle diameter sizes and dilution concentrations for each of the eight test runs are presented in Table 1. Instrument 1 refers to the Nano-ID, Instrument 2 refers to the Loaner Nano-ID, and Instrument 3 refers to the TSI Nanoscan. Instruments 1, 2, and 3 were used to obtain measurements during each test run.

Table 1: Trial Group 1 Target Particle Sizes and Dilutions

| Test | Particle Size, nm | Dilution |
|---|---|---|
| 1 | 57 | 2,500 |
| 2 | 57 | 2,500 |
| 3 | 92 | 1,250 |
| 4 | 92 | 625 |
| 5 | 147 | 139 |
| 6 | 147 | 139 |
| 7 | 220 | 104 |
| 8 | 220 | 104 |

Table 2 presents the frequency and percent within each size interval for instruments 1, 2, 3, and the electron microscopy for Trial 1, tests 1-8. Figures 1 – 8 present the comparison between the upper size intervals of the distributions and the cumulative percent for each test. Table 3 presents the diameters at 16%, 50%, and 84%. These diameters, as well as the geometric standard deviations (GSD), were calculated from the lines of fit presented in Figures 1-8. A comparison of the count median diameters (CMDs) for instruments 1, 2, 3, and the electron microscopy are also included in Table 3.

For test 1, the designated sodium chloride aerosol concentration of 57 nm was conducted using a dilution of 2,500. From the EM images, the highest percentage of particles (34%) were observed in the size range interval of 34.1 – 48.1 nm. The lowest range of particles (4.8%) were observed in the size range interval of 96.4 – 136.1 nm. 29.1 percent of particles were observed in the size range interval of 48.2 – 68.1. For instrument 1, the highest percentage of particles (41.2%) were observed in the size range interval of 25.4 – 36.2 nm. The lowest range of particles (4.0%) were observed in the size range interval of 102.9 – 142.1 nm. 18.0 percent of particles were observed in the size range interval of 50.2 – 71.7 nm. For instrument 2, the highest percentage of particles (30.3%) were observed in the size range interval of 25.4 – 36.2 nm. The lowest range of particles (3.2%) were observed in the size range interval of 102.9 – 142.1 nm. 24.9 percent of particles were observed in the size range

Table 2: Frequency and Percent of Salt Crystals Observed by Electron Microscopy and Instruments 1-3, Based on Size Interval

| Test 1, 57 nm | | | | | | | | | | | | | | | |
|---|---|---|---|---|---|---|---|---|---|---|---|---|---|---|---|
| EM | | | | Instrument 1 | | | | Instrument 2 | | | | Instrument 3 | | | |
| Size Interval, nm | | Frequency | Percent | Size Interval, nm | | Frequency | Percent | Size Interval, nm | | Frequency | Percent | Size Interval, nm | | Frequency | Percent |
| 24.2 | 34 | 153 | 14.0 | 25.4 | 36.2 | 1.43E+07 | 41.2 | 25.4 | 36.2 | 2.36E+07 | 30.3 | 23.6 | 31.9 | 3.70E+06 | 10.5 |
| 34.1 | 48.1 | 371 | 34.0 | 36.3 | 50.1 | 9.65E+06 | 27.8 | 36.3 | 50.1 | 2.28E+07 | 29.3 | 31.9 | 41.9 | 5.89E+06 | 16.7 |
| 48.2 | 68.1 | 318 | 29.1 | 50.2 | 71.7 | 6.24E+06 | 18.0 | 50.2 | 71.7 | 1.94E+07 | 24.9 | 41.9 | 74.3 | 1.42E+07 | 40.5 |
| 68.2 | 96.3 | 100 | 9.2 | 71.8 | 103 | 3.15E+06 | 9.1 | 71.8 | 103 | 9.65E+06 | 12.4 | 74.3 | 101 | 5.98E+06 | 17.0 |
| 96.4 | 136 | 52 | 4.8 | 102.9 | 142.1 | 1.40E+06 | 4.0 | 103 | 142 | 2.51E+06 | 3.2 | 101 | 132 | 3.88E+06 | 11.0 |
| | Total | 994 | | | Total | 3.47E+07 | | | Total | 7.79E+07 | | | Total | 3.37E+07 | |
| Test 2, 57 nm | | | | | | | | | | | | | | | |
| EM | | | | Instrument 1 | | | | Instrument 2 | | | | Instrument 3 | | | |
| Size Interval, nm | | Frequency | Percent | Size Interval, nm | | Frequency | Percent | Size Interval, nm | | Frequency | Percent | Size Interval, nm | | Frequency | Percent |
| 24.2 | 34 | 145 | 16.0 | 25.4 | 36.2 | 1.25E+07 | 40.7 | 25.4 | 36.2 | 1.75E+07 | 23.3 | 23.6 | 31.9 | 4.87E+06 | 11.5 |
| 34.1 | 48.1 | 273 | 30.0 | 36.3 | 50.1 | 8.22E+06 | 26.7 | 36.3 | 50.1 | 1.68E+07 | 22.4 | 31.9 | 41.9 | 6.78E+06 | 16.0 |
| 48.2 | 68.1 | 272 | 29.9 | 50.2 | 71.7 | 5.34E+06 | 17.3 | 50.2 | 71.7 | 1.47E+07 | 19.6 | 41.9 | 74.3 | 1.48E+07 | 35.1 |
| 68.2 | 96.3 | 73 | 8.0 | 71.8 | 103 | 2.74E+06 | 8.9 | 71.8 | 103 | 8.05E+06 | 10.7 | 74.3 | 101.0 | 6.11E+06 | 14.4 |
| 96.4 | 136 | 48 | 5.3 | 102.9 | 142 | 1.27E+06 | 4.1 | 103 | 142 | 2.70E+06 | 3.6 | 101.0 | 132.1 | 4.04E+06 | 9.6 |
| | Total | 811 | | | Total | 3.01E+07 | | | Total | 5.98E+07 | | | Total | 3.66E+07 | |
| Test 3, 92 nm | | | | | | | | | | | | | | | |
| EM | | | | Instrument 1 | | | | Instrument 2 | | | | Instrument 3 | | | |
| Size Interval, nm | | Frequency | Percent | Size Interval, nm | | Frequency | Percent | Size Interval, nm | | Frequency | Percent | Size Interval, nm | | Frequency | Percent |
| 34.1 | 48.1 | 357 | 30.7 | 36.3 | 50.1 | 6.78E+06 | 45.3 | 36.3 | 50.1 | 1.62E+07 | 28.7 | 31.9 | 41.9 | 5.81E+06 | 24.3 |
| 48.2 | 68.1 | 326 | 28.1 | 50.2 | 71.7 | 4.28E+06 | 28.6 | 50.2 | 71.7 | 1.38E+07 | 24.5 | 41.9 | 74.3 | 1.03E+07 | 43.1 |
| 68.2 | 96.3 | 106 | 9.1 | 71.8 | 103 | 2.30E+06 | 15.4 | 71.8 | 103 | 7.65E+06 | 13.6 | 74.3 | 101.0 | 3.98E+06 | 16.7 |
| 96.4 | 136 | 62 | 5.3 | 102.9 | 142 | 1.04E+06 | 7.0 | 103 | 142 | 2.15E+06 | 3.8 | 101.0 | 132.1 | 2.58E+06 | 10.8 |
| 136 | 193 | 47 | 4.0 | 142.2 | 204 | 5.59E+05 | 3.7 | 142 | 204 | 4.71E+05 | 0.8 | 132.1 | 179.6 | 1.10E+06 | 4.6 |
| | Total | 898 | | | Total | 1.50E+07 | | | Total | 40255873 | | | Total | 2.38E+07 | |
| Test 4, 92 nm | | | | | | | | | | | | | | | |
| EM | | | | Instrument 1 | | | | Instrument 2 | | | | Instrument 3 | | | |
| Size Interval, nm | | Frequency | Percent | Size Interval, nm | | Frequency | Percent | Size Interval, nm | | Frequency | Percent | Size Interval, nm | | Frequency | Percent |
| 34.1 | 48.1 | 241 | 23.4 | 36.3 | 50.1 | 3.96E+06 | 32.2 | 36.3 | 50.1 | 1.96E+07 | 39.3 | 31.9 | 41.9 | 6.06E+06 | 20.4 |
| 48.2 | 68.1 | 307 | 29.8 | 50.2 | 71.7 | 4.15E+06 | 33.7 | 50.2 | 71.7 | 1.80E+07 | 36.0 | 41.9 | 74.3 | 1.31E+07 | 44.1 |
| 68.2 | 96.3 | 91 | 8.8 | 71.8 | 103 | 2.32E+06 | 18.9 | 71.8 | 103 | 9.39E+06 | 18.8 | 74.3 | 101.0 | 5.55E+06 | 18.7 |
| 96.4 | 136 | 89 | 8.6 | 102.9 | 142 | 1.09E+06 | 8.8 | 103 | 142 | 2.47E+06 | 4.9 | 101.0 | 132.1 | 3.62E+06 | 12.2 |
| 136 | 193 | 46 | 4.5 | 142.2 | 204 | 5.64E+05 | 4.6 | 142 | 204 | 4.85E+05 | 1.0 | 132.1 | 179.6 | 1.34E+06 | 4.5 |
| | Total | 774 | | | Total | 1.21E+07 | | | Total | 5.00E+07 | | | Total | 2.97E+07 | |
| Test 5, 147 nm | | | | | | | | | | | | | | | |
| EM | | | | Instrument 1 | | | | Instrument 2 | | | | Instrument 3 | | | |
| Size Interval, nm | | Frequency | Percent | Size Interval, nm | | Frequency | Percent | Size Interval, nm | | Frequency | Percent | Size Interval, nm | | Frequency | Percent |
| 48.2 | 68.1 | 357 | 27.1 | 50.2 | 71.7 | 4.39E+06 | 49.2 | 50.2 | 71.7 | 1.87E+07 | 64.3 | 41.9 | 74.3 | 1.18E+07 | 53.1 |
| 68.2 | 96.3 | 131 | 9.9 | 71.8 | 103 | 2.47E+06 | 27.7 | 71.8 | 103 | 8.43E+06 | 29.1 | 74.3 | 101.0 | 5.00E+06 | 22.5 |
| 96.4 | 136 | 93 | 7.1 | 102.9 | 142 | 1.15E+06 | 12.8 | 103 | 142 | 1.68E+06 | 5.8 | 101.0 | 132.1 | 3.48E+06 | 15.6 |
| 136 | 193 | 48 | 3.6 | 142.2 | 204 | 6.37E+05 | 7.1 | 142 | 204 | 2.23E+05 | 0.8 | 132.1 | 179.6 | 1.59E+06 | 7.1 |
| 193 | 272 | 29 | 2.2 | 203.8 | 312 | 2.80E+05 | 3.1 | 204 | 312 | 1.55E+04 | 0.1 | 179.6 | 235.0 | 3.67E+05 | 1.6 |
| | Total | 1317 | | | Total | 8.93E+06 | | | Total | 2.90E+07 | | | Total | 2.23E+07 | |

Table 2: Frequency and Percent Based on Size Interval (continued)

| Test 6, 147 nm | | | | | | | | | | | | | | | |
|---|---|---|---|---|---|---|---|---|---|---|---|---|---|---|---|
| EM | | | | Instrument 1 | | | | Instrument 2 | | | | Instrument 3 | | | |
| Size Interval, nm | | Frequency | Percent | Size Interval, nm | | Frequency | Percent | Size Interval, nm | | Frequency | Percent | Size Interval, nm | | Frequency | Percent |
| 48.2 | 68.1 | 312 | 29.7 | 50.2 | 71.7 | 4.53E+06 | 49.9 | 50.2 | 71.7 | 1.91E+07 | 62.6 | 41.9 | 74.3 | 1.59E+07 | 52.8 |
| 68.2 | 96.3 | 111 | 10.6 | 71.8 | 103 | 2.53E+06 | 27.9 | 71.8 | 103 | 9.03E+06 | 29.5 | 74.3 | 101.0 | 5.76E+06 | 19.1 |
| 96.4 | 136 | 69 | 6.6 | 102.9 | 142 | 1.13E+06 | 12.5 | 103 | 142 | 2.07E+06 | 6.8 | 101.0 | 132.1 | 4.53E+06 | 15.0 |
| 136 | 193 | 48 | 4.6 | 142.2 | 204 | 6.09E+05 | 6.7 | 142 | 204 | 3.30E+05 | 1.1 | 132.1 | 179.6 | 2.75E+06 | 9.1 |
| 193 | 272 | 42 | 4.0 | 203.8 | 312 | 2.77E+05 | 3.0 | 204 | 312 | 2.47E+04 | 0.1 | 179.6 | 235.0 | 1.22E+06 | 4.1 |
| | Total | 1051 | | | Total | 9.08E+06 | | | Total | 3.06E+07 | | | Total | 3.02E+07 | |
| Test 7, 220 nm | | | | | | | | | | | | | | | |
| EM | | | | Insrument 1 | | | | Instrument 2 | | | | Instrument 3 | | | |
| Size Interval, nm | | Frequency | Percent | Size Interval, nm | | Frequency | Percent | Size Interval, nm | | Frequency | Percent | Size Interval, nm | | Frequency | Percent |
| 48.2 | 68.1 | 225 | 28.0 | 50.2 | 71.7 | 5.21E+06 | 53.5 | 50.2 | 71.7 | 1.38E+07 | 54.8 | 41.9 | 74.3 | 1.17E+07 | 54.6 |
| 68.2 | 96.3 | 80 | 10.0 | 71.8 | 103 | 2.57E+06 | 26.4 | 71.8 | 103 | 7.66E+06 | 30.5 | 74.3 | 101.0 | 4.89E+06 | 22.8 |
| 96.4 | 136 | 37 | 4.6 | 102.9 | 142 | 1.14E+06 | 11.7 | 103 | 142 | 2.70E+06 | 10.7 | 101.0 | 132.1 | 3.26E+06 | 15.2 |
| 136 | 193 | 32 | 4.0 | 142.2 | 204 | 5.92E+05 | 6.1 | 142 | 204 | 8.26E+05 | 3.3 | 132.1 | 179.6 | 1.40E+06 | 6.5 |
| 193 | 272 | 13 | 1.6 | 203.8 | 312 | 2.35E+05 | 2.4 | 204 | 312 | 1.76E+05 | 0.7 | 179.6 | 235.0 | 1.84E+05 | 0.9 |
| | Total | 804 | | | Total | 9.75E+06 | | | Total | 2.52E+07 | | | Total | 2.15E+07 | |
| Test 8, 220 nm | | | | | | | | | | | | | | | |
| EM | | | | Instrument 1 | | | | Instrument 2 | | | | Instrument 3 | | | |
| Size Interval, nm | | Frequency | Percent | Size Interval, nr | | Frequency | Percent | Size Interval, nm | | Frequency | Percent | Size Interval, nm | | Frequency | Percent |
| 48.2 | 68.1 | 315 | 32.0 | 50.2 | 71.7 | 3.82E+06 | 50.7 | 50.2 | 71.7 | 1.72E+07 | 61.3 | 41.9 | 74.3 | 1.06E+07 | 48.0 |
| 68.2 | 96.3 | 109 | 11.1 | 71.8 | 103 | 2.08E+06 | 27.6 | 71.8 | 103 | 8.43E+06 | 30.1 | 74.3 | 101.0 | 4.82E+06 | 21.8 |
| 96.4 | 136 | 81 | 8.2 | 102.9 | 142 | 9.50E+05 | 12.6 | 103 | 142 | 2.02E+06 | 7.2 | 101.0 | 132.1 | 3.58E+06 | 16.2 |
| 136 | 193 | 55 | 5.6 | 142.2 | 204 | 4.96E+05 | 6.6 | 142 | 204 | 3.51E+05 | 1.3 | 132.1 | 179.6 | 2.13E+06 | 9.6 |
| 193 | 272 | 28 | 2.8 | 203.8 | 312 | 1.97E+05 | 2.6 | 204 | 312 | 3.41E+04 | 0.1 | 179.6 | 235.0 | 9.83E+05 | 4.4 |
| | Total | 985 | | | Total | 7.54E+06 | | | Total | 2.80E+07 | | | Total | 2.21E+07 | |

interval of 50.2 – 71.7 nm. For instrument 3, the highest percentage of particles (40.5%) were observed in the size range interval of 41.9 – 74.3 nm. The lowest range of particles (10.5%) were observed in the size range interval of 23.6 – 31.9 nm. 40.5 percent of particles were observed in the size range interval of 41.9 – 74.3 nm. For test 1, instrument 3 identified the highest percentage of particles within the selected NaCl size parameter range.

The distributions from test 1 are presented in figure 3. The lines of fit are roughly parallel; however, the lines of fit for instrument for 3 and the electron microscopy results are the most parallel. The lines of fit for instruments 1 and 2 are similar to each other.

For test 1, the distribution obtained by EM had a CMD of 54.9 nm and a GSD of 1.68, shown in Table 3. The distribution obtained by Instrument 1 had a CMD of 39.8 nm and a GSD of 1.65. The distribution obtained by Instrument 2 had a CMD of 45.6 nm and a GSD of 1.58. The distribution obtained by Instrument 3 had a CMD of 58.5 nm and a GSD of 1.63. The

difference between the CMDs of the EM and instrument 1 is 15 nm. The percent difference between the CMDs of these two techniques is 31.9%. The difference between the two distributions at -1 GSD and + 1 GSD are 7.6 nm and 23 nm, respectively. The difference between the CMDs of the EM and instrument 2 is 9.3 nm. The percent difference between the CMDs of these two techniques is 18.5%. The difference between the two distributions at -1 GSD and + 1 GSD are 3.4 nm and 19 nm, respectively. The difference between the CMDs of the EM and instrument 3 is 3.6 nm. The percent difference between the CMDs of these two techniques is 6.3%. The difference between the two distributions at -1 GSD and + 1 GSD are 3.9 nm and 5.4 nm, respectively. The difference between the CMDs of instrument 1 and instrument 2 is 5.8 nm. The percent difference between the CMDs of these two instruments is 13.6%. The difference between the two distributions at -1 GSD and + 1 GSD are 4.2 nm and 4.2 nm, respectively. The difference between the CMDs of instrument 1 and instrument 3 is 19 nm. The percent difference between the CMDs of these two instruments is 38%. The difference between the two distributions at -1 GSD and + 1 GSD are 12 nm and 29 nm, respectively. The difference between the CMDs of instrument 2 and instrument 3 is 13 nm. The percent difference between the CMDs of these two instruments is 24.8%. The difference between the two distributions at -1 GSD and + 1 GSD are 7.3 nm and 24 nm, respectively. In this test, the CMD of instrument 3 was closer to the selected NaCl size parameter than the other instruments. The difference between the CMDs of instruments 1 and 2 was smaller than the difference between the CMDs of instruments 1 and 2 with instrument 3.

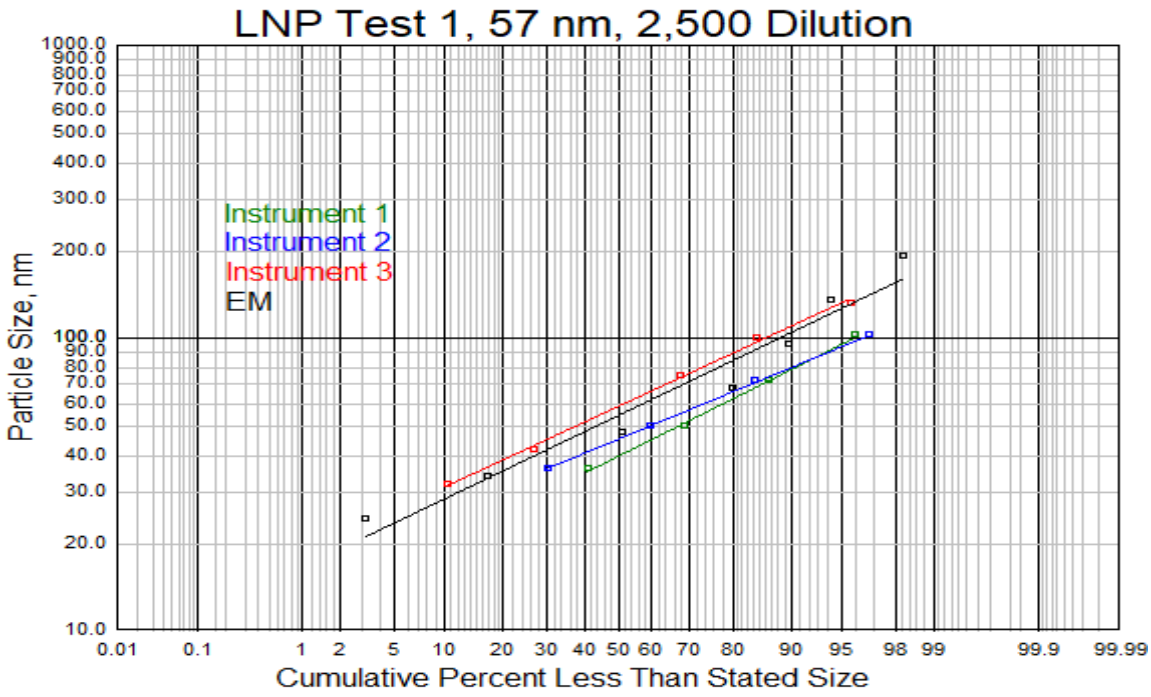


Figure 3: Distribution of NaCl nanoparticle generated aerosol for Test 1, 57 nm generated aerosol, 2,500 dilution

For test 2, the designated sodium chloride aerosol concentration of 57 nm was conducted using a dilution of 2,500. From the EM images, the highest percentage of particles (30%) were observed in the size range interval of 34.1 – 48.1 nm. The lowest range of particles (5.3%) were observed in the size range interval of 96.4 – 136.1 nm. 29.9 percent of particles were observed in the size range interval of 48.2 – 68.1. For instrument 1, the highest percentage of particles (40.7%) were observed in the size range interval of 25.4 – 36.2 nm. The lowest range of particles (4.1%) were observed in the size range interval of 102.9 – 142.1 nm. 17.3 percent of particles were observed in the size range interval of 50.2 – 71.7 nm. For instrument 2, the highest percentage of particles (23.3%) were observed in the size range interval of 25.4 – 36.2 nm. The lowest range of particles (3.6%) were observed in the size range interval of 102.9 – 142.1 nm. 19.6 percent of particles were observed in the size range interval of 50.2 – 71.7 nm. For instrument 3, the highest percentage of particles (35.1%) were observed in the size range interval of 41.9 – 74.3 nm. The lowest range of particles (9.6%)

were observed in the size range interval of 101.0 – 132.1 nm. 35.1 percent of particles were observed in the size range interval of 41.9 – 74.3 nm. For test 2, instrument 3 identified the highest percentage of particles within the selected NaCl size parameter range.

The distributions from test 2 are presented in figure 4. The lines of fit are roughly parallel; however, the lines of fit for instrument for 3 and the electron microscopy results are the most parallel. The lines of fit for instruments 1 and 2 are similar to each other.

For test 2, the distribution obtained by EM had a CMD of 50.1 nm and a GSD of 1.72, shown in Table 3. The distribution obtained by Instrument 1 had a CMD of 39.9 nm and a GSD of 1.84. The distribution obtained by Instrument 2 had a CMD of 47.1 nm and a GSD of 1.64. The distribution obtained by Instrument 3 had a CMD of 56.8 nm and a GSD of 1.67. The difference between the CMDs of the EM and instrument 1 is 10 nm. The percent difference between the CMDs of these two techniques is 22.7%. The difference between the two distributions at -1 GSD and + 1 GSD are 7.6 nm and 13 nm, respectively. The difference between the CMDs of the EM and instrument 2 is 3 nm. The percent difference between the CMDs of these two techniques is 6.2%. The difference between the two distributions at -1 GSD and + 1 GSD are 0.9 nm and 9.8 nm, respectively. The difference between the CMDs of the EM and instrument 3 is 6.7 nm. The percent difference between the CMDs of these two techniques is 12.5%. The difference between the two distributions at -1 GSD and + 1 GSD are 4.7 nm and 8.1 nm, respectively. The difference between the CMDs of instrument 1 and instrument 2 is 7.2 nm. The percent difference between the CMDs of these two instruments is 16.6%. The difference between the two distributions at -1 GSD and + 1 GSD are 6.7 nm and 3.2 nm, respectively. The difference between the CMDs of instrument 1 and instrument 3 is 17 nm. The percent difference between the CMDs of these two instruments is 35%. The difference between the two distributions at -1 GSD and + 1 GSD are 12 nm and 21 nm, respectively. The difference between the CMDs of instrument 2 and instrument 3 is 9.7 nm. The percent difference between the CMDs of these two instruments is 18.7%. The difference

between the two distributions at -1 GSD and + 1 GSD are 5.6 nm and 18 nm, respectively. In this test, the CMD of instrument 3 was closer to the selected NaCl size parameter than the other instruments. The difference between the CMDs of instruments 1 and 2 was smaller than the difference between the CMDs of instruments 1 and 2 with instrument 3.

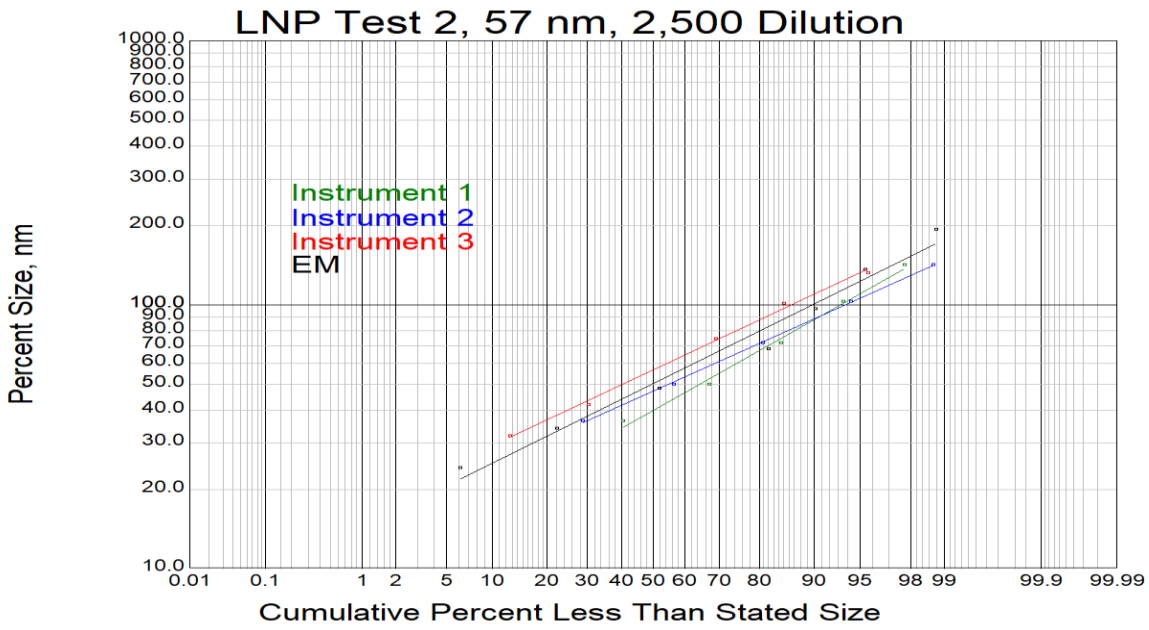


Figure 4: Distribution of NaCl nanoparticle generated aerosol for Test 2, 57 nm generated aerosol, 2,500 dilution

For test 3, the designated sodium chloride aerosol concentration of 92 nm was conducted using a dilution of 1,250. From the EM images, the highest percentage of particles (30.7%) were observed in the size range interval of 34.1 – 48.1 nm. The lowest range of particles (4%) were observed in the size range interval of 136.2 – 192.5 nm. 9.1 percent of particles were observed in the size range interval of 68.2 – 96.3. For instrument 1, the highest percentage of particles (45.3%) were observed in the size range interval of 36.3 – 50.1 nm. The lowest range of particles (3.7%) were observed in the size range interval of 142.2 – 203.7 nm. 15.4 percent of particles were observed in the size range interval of 71.8 – 102.8 nm. For instrument 2, the highest percentage of particles (28.7%) were observed in the size range interval of 36.3 – 50.1 nm. The lowest range of particles (0.8%) were observed in the size

range interval of 142.2 – 203.7 nm. 13.6 percent of particles were observed in the size range interval of 71.8 – 102.8 nm. For instrument 3, the highest percentage of particles (43.1%) were observed in the size range interval of 41.9 – 74.3 nm. The lowest range of particles (4.6%) were observed in the size range interval of 132.1 – 179.6 nm. 16.7 percent of particles were observed in the size range interval of 74.3 – 101 nm. For test 3, instrument 3 identified the highest percentage of particles within the selected NaCl size parameter range.

The distributions from test 3 are presented in figure 5. The lines of fit for instrument 1 and the electron microscopy results are roughly parallel. None of the other lines are parallel. Comparisons of the distributions for 16%, 50%, and 84% are presented in Table 3.

The distribution obtained by EM had a CMD of 54.9 nm and a GSD of 1.89, shown in Table 3. The distribution obtained by Instrument 1 had a CMD of 52.5 nm and a GSD of 1.68. The distribution obtained by Instrument 2 had a CMD of 78.3 nm and a GSD of 3.17. The distribution obtained by Instrument 3 had a CMD of 60 nm and a GSD of 1.55. The difference between the CMDs of the EM and instrument 1 is 2.4 nm. The percent difference between the CMDs of these two techniques is 4.5%. The difference between the two distributions at -1 GSD and + 1 GSD are 2.7 nm and 14 nm, respectively. The difference between the CMDs of the EM and instrument 2 is 23 nm. The percent difference between the CMDs of these two techniques is 35.1%. The difference between the two distributions at -1 GSD and + 1 GSD are 4.8 nm and 142 nm, respectively. The difference between the CMDs of the EM and instrument 3 is 5.1 nm. The percent difference between the CMDs of these two techniques is 8.9%. The difference between the two distributions at -1 GSD and + 1 GSD are 9.8 nm and 10 nm, respectively. The difference between the CMDs of instrument 1 and instrument 2 is 26 nm. The percent difference between the CMDs of these two instruments is 39.4%. The difference between the two distributions at -1 GSD and + 1 GSD are 7.5 nm and 157 nm, respectively. The difference between the CMDs of instrument 1 and instrument 3 is 7.5 nm. The percent difference between the CMDs of these two instruments is 13.3%. The difference between the

two distributions at -1 GSD and + 1 GSD are 7.1 nm and 4.1 nm, respectively. The difference between the CMDs of instrument 2 and instrument 3 is 18 nm. The percent difference between the CMDs of these two instruments is 26.5%. The difference between the two distributions at -1 GSD and + 1 GSD are 15 nm and 153 nm, respectively. In this test, the CMD of instrument 2 was closer to the selected NaCl size parameter than the other instruments. The difference between the CMDs of instruments 1 and 3 was smaller than the difference between the CMDs of instruments 1 and 2, and instruments 2 and 3.

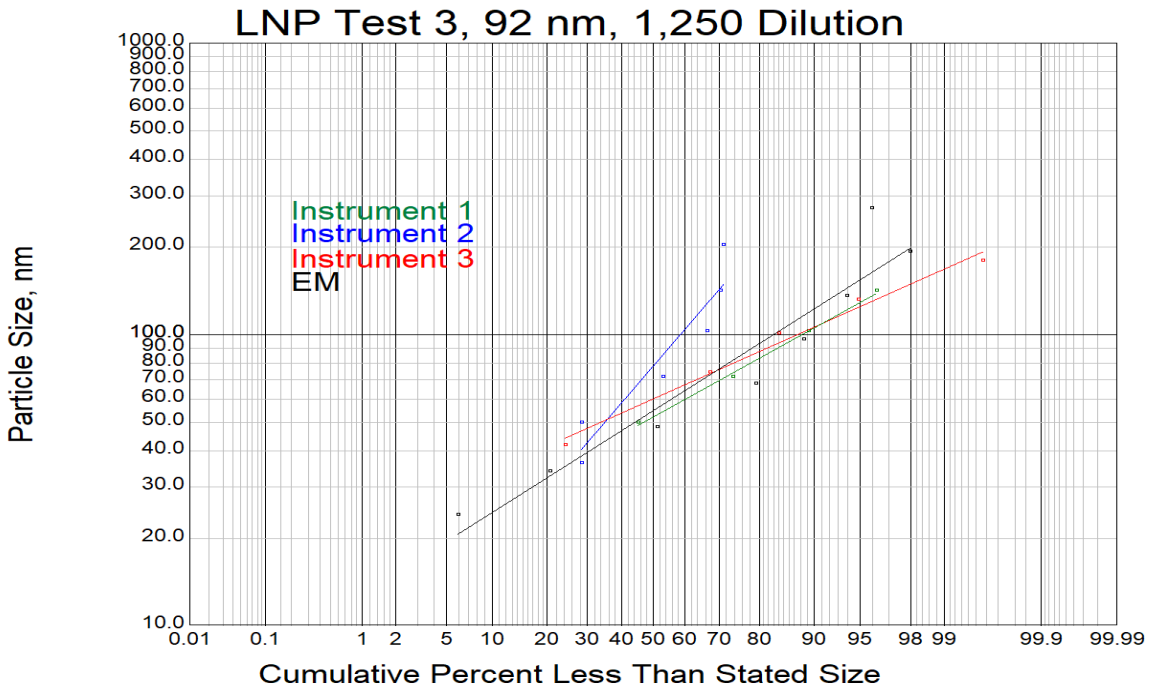


Figure 5: Distribution of NaCl nanoparticle generated aerosol for Test 3, 92 nm generated aerosol, 1,250 dilution.

For test 4, the designated sodium chloride aerosol concentration of 92 nm was conducted using a dilution of 625. From the EM images, the highest percentage of particles (29.8%) were observed in the size range interval of 48.2 – 68.1 nm. The lowest range of particles (4.5%) were observed in the size range interval of 136.2 – 192.5 nm. 8.8 percent of particles were observed in the size range interval of 68.2 – 96.3. For instrument 1, the highest percentage of particles (33.7%) were observed in the size range interval of 50.2 – 71.7 nm. The lowest range of particles (4.6%) were observed in the size range interval of 142.2 – 203.7 nm.

18.9 percent of particles were observed in the size range interval of 71.8 – 102.8 nm. For instrument 2, the highest percentage of particles (39.3%) were observed in the size range interval of 36.3 – 50.1 nm. The lowest range of particles (1.0%) were observed in the size range interval of 142.2 – 203.7 nm. 18.8 percent of particles were observed in the size range interval of 71.8 – 102.8 nm. For instrument 3, the highest percentage of particles (44.1%) were observed in the size range interval of 41.9 – 74.3 nm. The lowest range of particles (4.5%) were observed in the size range interval of 132.1 – 179.6 nm. 18.7 percent of particles were observed in the size range interval of 74.3 – 101 nm. For test 4, instrument 1 identified the highest percentage of particles within the selected NaCl size parameter range, but the observed percentages for instruments 1, 2, and 3 were similar.

The distributions from test 4 are presented in figure 6. The lines of fit are roughly parallel between instrument 1 and the EM data. The lines of fit for instruments 2 and 3 were parallel to each other.

For test 4 the distribution obtained by EM had a CMD of 52.3 nm and a GSD of 1.82, shown in Table 3. The distribution obtained by Instrument 1 had a CMD of 60.6 nm and a GSD of 1.76. The distribution obtained by Instrument 2 had a CMD of 54.8 nm and a GSD of 1.51. The distribution obtained by Instrument 3 had a CMD of 63.2 nm and a GSD of 1.47. The difference between the CMDs of the EM and instrument 1 is 8.3 nm. The percent difference between the CMDs of these two techniques is 14.7%. The difference between the two distributions at -1 GSD and + 1 GSD are 5.6 nm and 10 nm, respectively. The difference between the CMDs of the EM and instrument 2 is 2.5 nm. The percent difference between the CMDs of these two techniques is 4.7%. The difference between the two distributions at -1 GSD and + 1 GSD are 7.3 nm and 13 nm, respectively. The difference between the CMDs of the EM and instrument 3 is 11 nm. The percent difference between the CMDs of these two techniques is 18.9%. The difference between the two distributions at -1 GSD and + 1 GSD are 14 nm and 3.2 nm, respectively. The difference between the CMDs of instrument 1 and

instrument 2 is 5.8 nm. The percent difference between the CMDs of these two instruments is 10.1%. The difference between the two distributions at -1 GSD and + 1 GSD are 1.7 nm and 23 nm, respectively. The difference between the CMDs of instrument 1 and instrument 3 is 2.6 nm. The percent difference between the CMDs of these two instruments is 4.2%. The difference between the two distributions at -1 GSD and + 1 GSD are 8.5 nm and 13 nm, respectively. The difference between the CMDs of instrument 2 and instrument 3 is 8.4 nm. The percent difference between the CMDs of these two instruments is 14.2%. The difference between the two distributions at -1 GSD and + 1 GSD are 6.8 nm and 10 nm, respectively. In this test, the CMD of instrument 3 was closer to the selected NaCl size parameter than the other instruments. The difference between the CMDs of instruments 1 and 3 was smaller than the difference between the CMDs of instruments 1 and 2, and instruments 2 and 3.

For test 5, the designated sodium chloride aerosol concentration of 147 nm was conducted using a dilution of 139. From the EM images, the highest percentage of particles (27.1%) were observed in the size range interval of 48.2 – 68.1 nm. The lowest range of particles (2.2%) were observed in the size range interval of 192.6 – 272.2 nm.

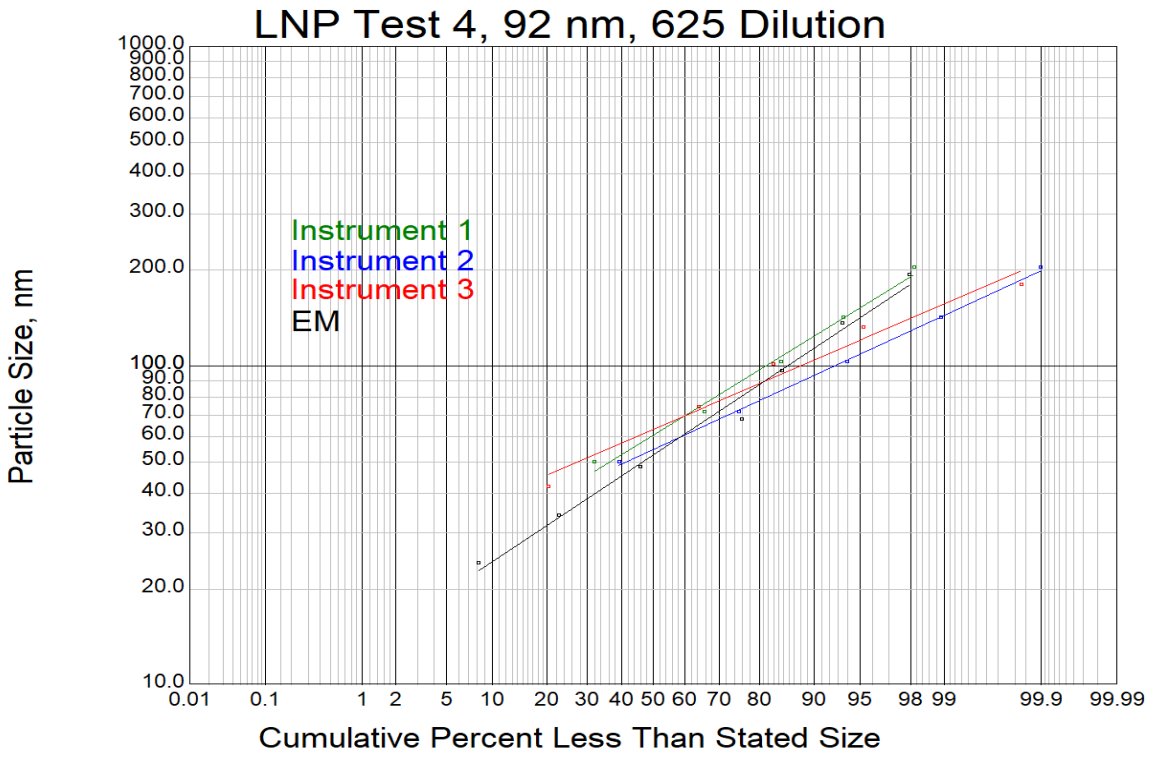


Figure 6: Distribution of NaCl nanoparticle generated aerosol for Test 4, 92 nm generated aerosol, 625 dilution

3.6 percent of particles were observed in the size range interval of 136.2 – 192.5. For instrument 1, the highest percentage of particles (49.2%) were observed in the size range interval of 50.2 – 71.7 nm. The lowest range of particles (3.1%) were observed in the size range interval of 203.8 – 312 nm. 7.1 percent of particles were observed in the size range interval of 142.2 – 203.7 nm. For instrument 2, the highest percentage of particles (64.3%) were observed in the size range interval of 50.2 – 71.7 nm. The lowest range of particles (0.1%) were observed in the size range interval of 203.8 – 312 nm. 0.8 percent of particles were observed in the size range interval of 142.2 – 203.7 nm. For instrument 3, the highest percentage of particles (53.1%) were observed in the size range interval of 41.9 – 74.3 nm. The lowest range of particles (1.6%) were observed in the size range interval of 179.6 – 235 nm. 7.1 percent of particles were observed in the size range interval of 132.1 – 179.6 nm. For test 5, instrument 1 and instrument 3 identified the highest percentage of particles within the selected NaCl size parameter range.

The distributions from test 5 are presented in figure 7. The lines of fit are roughly parallel between instrument 1 and the EM data. The lines of fit for instruments 2 and 3 were parallel to each other.

For test 5, the distribution obtained by EM had a CMD of 55.5 nm and a GSD of 1.71, shown in Table 3. The distribution obtained by Instrument 1 had a CMD of 71.5 nm and a GSD of 1.70. The distribution obtained by Instrument 2 had a CMD of 62.1 nm and a GSD of 1.43. The distribution obtained by Instrument 3 had a CMD of 73.2 nm and a GSD of 1.54. The difference between the CMDs of the EM and instrument 1 is 16 nm. The percent difference between the CMDs of these two techniques is 25.2%. The difference between the two distributions at -1 GSD and + 1 GSD are 10 nm and 29 nm, respectively. The difference between the CMDs of the EM and instrument 2 is 6.6 nm. The percent difference between the CMDs of these two techniques is 11.2%. The difference between the two distributions at -1 GSD and + 1 GSD are 11 nm and 5.9 nm, respectively. The difference between the CMDs of the EM and instrument 3 is 18 nm. The percent difference between the CMDs of these two techniques is 27.5%. The difference between the two distributions at -1 GSD and + 1 GSD are 15 nm and 18 nm, respectively. The difference between the CMDs of instrument 1 and instrument 2 is 9.4 nm. The percent difference between the CMDs of these two instruments is 14.1%. The difference between the two distributions at -1 GSD and + 1 GSD are 1 nm and 35 nm, respectively. The difference between the CMDs of instrument 1 and instrument 3 is 1.7 nm. The percent difference between the CMDs of these two instruments is 2.3%. The difference between the two distributions at -1 GSD and + 1 GSD are 5 nm and 11 nm, respectively. The difference between the CMDs of instrument 2 and instrument 3 is 11 nm. The percent difference between the CMDs of these two instruments is 16.4%. The difference between the two distributions at -1 GSD and + 1 GSD are 4 nm and 24 nm, respectively. In this test, the CMD of instrument 3 was closer to the selected NaCl size parameter than the other instruments.

The difference between the CMDs of instruments 1 and 3 was smaller than the difference between the CMDs of instruments 1 and 2, and instruments 2 and 3.

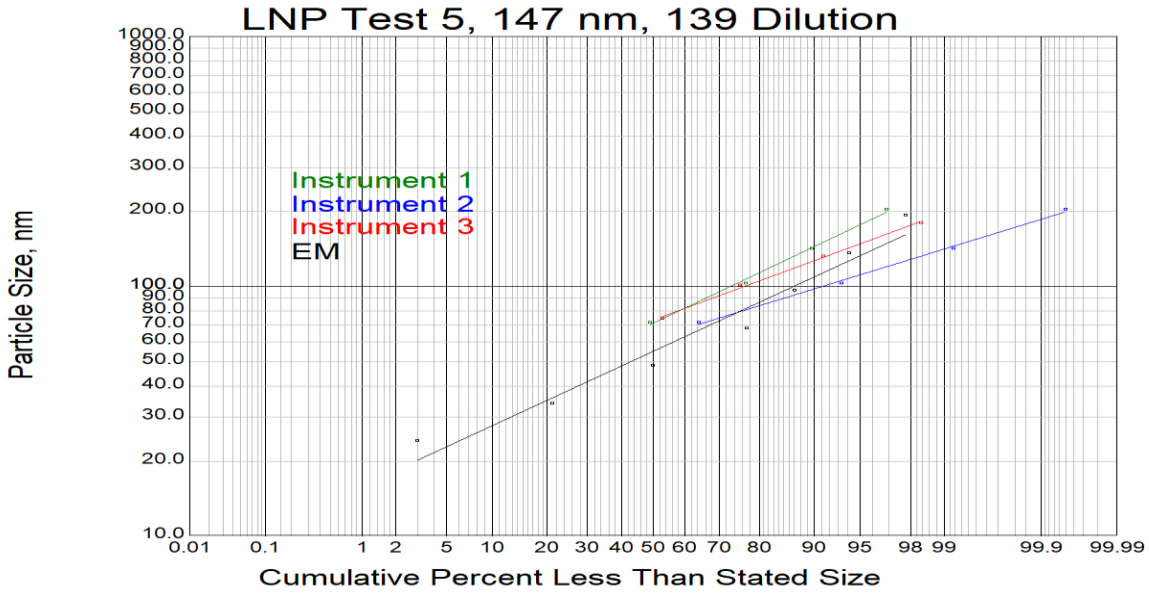


Figure 7: Distribution of NaCl nanoparticle generated aerosol for Test 5, 147 nm generated aerosol, 139 dilution

For test 6, the designated sodium chloride aerosol concentration of 147 nm was conducted using a dilution of 139. From the EM images, the highest percentage of particles (29.7%) were observed in the size range interval of 48.2 – 68.1 nm. The lowest range of particles (4.0%) were observed in the size range interval of 192.6 – 272.2 nm. 4.6 percent of particles were observed in the size range interval of 136.2 – 192.5. For instrument 1, the highest percentage of particles (49.9%) were observed in the size range interval of 50.2 – 71.7 nm. The lowest range of particles (3.0%) were observed in the size range interval of 203.8 – 312 nm. 6.7 percent of particles were observed in the size range interval of 142.2 – 203.7 nm. For instrument 2, the highest percentage of particles (62.6%) were observed in the size range interval of 50.2 – 71.7 nm. The lowest range of particles (0.1%) were observed in the size range interval of 203.8 – 312 nm. 1.1 percent of particles were observed in the size range

interval of 142.2 – 203.7 nm. For instrument 3, the highest percentage of particles (52.8%) were observed in the size range interval of 41.9 – 74.3 nm. The lowest range of particles (4.1%) were observed in the size range interval of 179.6 – 235 nm. 9.1 percent of particles were observed in the size range interval of 132.1 – 179.6 nm. For test 6, instrument 3 identified the highest percentage of particles within the selected NaCl size parameter range.

The distributions from test 6 are presented in figure 8. The lines of fit are roughly parallel between instruments 1, 2 and 3; however, the lines of fit for instruments 1 and 3 and the electron microscopy results are the most parallel. The lines of fit for instruments 1 and 3 are very similar to each other.

For test 6, the distribution obtained by EM had a CMD of 56.1 nm and a GSD of 1.83, shown in Table 3. The distribution obtained by Instrument 1 had a CMD of 69.5 nm and a GSD of 1.72. The distribution obtained by Instrument 2 had a CMD of 61.7 nm and a GSD of 1.44. The distribution obtained by Instrument 3 had a CMD of 73.3 nm and a GSD of 1.68. The difference between the CMDs of the EM and instrument 1 is 13 nm. The percent difference between the CMDs of these two techniques is 21.3%. The difference between the two distributions at -1 GSD and + 1 GSD are 11 nm and 19 nm, respectively. The difference between the CMDs of the EM and instrument 2 is 5.6 nm. The percent difference between the CMDs of these two techniques is 9.5%. The difference between the two distributions at -1 GSD and + 1 GSD are 13 nm and 13 nm, respectively. The difference between the CMDs of the EM and instrument 3 is 17 nm. The percent difference between the CMDs of these two techniques is 26.6%. The difference between the two distributions at -1 GSD and + 1 GSD are 13 nm and 21 nm, respectively. The difference between the CMDs of instrument 1 and instrument 2 is 7.8 nm. The percent difference between the CMDs of these two instruments is 11.9%. The difference between the two distributions at -1 GSD and + 1 GSD are 2.3 nm and 32 nm, respectively. The difference between the CMDs of instrument 1 and instrument 3 is 3.8 nm. The percent difference between the CMDs of these two instruments is 5.3%. The

difference between the two distributions at -1 GSD and + 1 GSD are 2.8 nm and 2.2 nm, respectively. The difference between the CMDs of instrument 2 and instrument 3 is 12 nm. The percent difference between the CMDs of these two instruments is 17.2%. The difference between the two distributions at -1 GSD and + 1 GSD are 0.5 nm and 34 nm, respectively. In this test, the CMD of instrument 3 was closer to the selected NaCl size parameter than the other instruments. The difference between the CMDs of instruments 1 and 3 was smaller than the difference between the CMDs of instruments 1 and 2, and instruments 2 and 3.

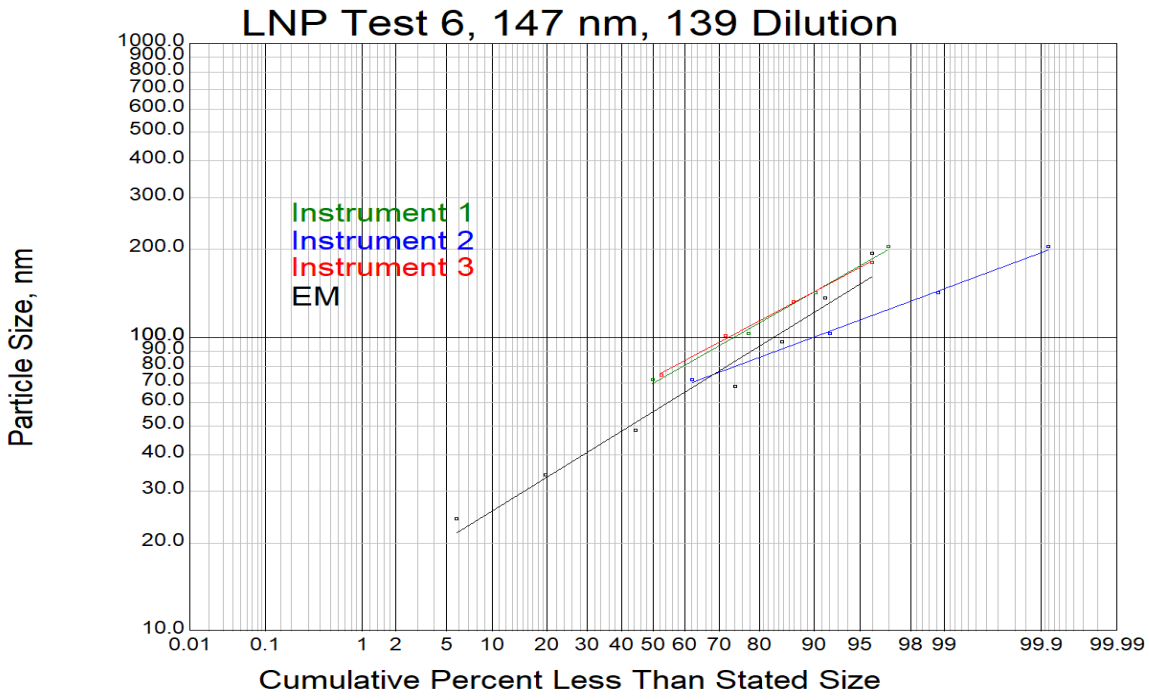


Figure 8: Distribution of NaCl nanoparticle generated aerosol for Test 6, 147 nm generated aerosol, 139 dilution

For test 7, the designated sodium chloride aerosol concentration of 220 nm was conducted using a dilution of 104. From the EM images, the highest percentage of particles (28%) were observed in the size range interval of 48.2 – 68.1 nm. The lowest range of particles (1.6%) were observed in the size range interval of 192.6 – 272.2 nm. 1.6 percent of particles were observed in the size range interval of 192.6 – 272.2. For instrument 1, the highest percentage of particles (53.5%) were observed in the size range interval of 50.2 – 71.7 nm. The

lowest range of particles (2.4%) were observed in the size range interval of 203.8 – 312 nm. 2.4 percent of particles were observed in the size range interval of 203.8 – 312 nm. For instrument 2, the highest percentage of particles (54.8%) were observed in the size range interval of 50.2 – 71.7 nm. The lowest range of particles (0.7%) were observed in the size range interval of 203.8 – 312 nm. 0.7 percent of particles were observed in the size range interval of 203.8 – 312 nm. For instrument 3, the highest percentage of particles (54.6%) were observed in the size range interval of 41.9 – 74.3 nm. The lowest range of particles (0.9%) were observed in the size range interval of 179.6 – 235 nm. 0.9 percent of particles were observed in the size range interval of 179.6 – 235 nm. For test 7, instrument 1 identified the highest percentage of particles within the selected NaCl size parameter range.

The distributions from test 7 are presented in figure 9. The lines of fit of instruments 1, 3, and the EM are roughly parallel; however, the lines of fit for instrument for 1 and the electron microscopy results are the most parallel.

For test 7, the distribution obtained by EM had a CMD of 49.8 nm and a GSD of 1.80, shown in Table 3. The distribution obtained by Instrument 1 had a CMD of 67.8 nm and a GSD of 1.74. The distribution obtained by Instrument 2 had a CMD of 66.6 nm and a GSD of 1.56. The distribution obtained by Instrument 3 had a CMD of 197.7 nm and a GSD of 2.08. The difference between the CMDs of the EM and instrument 1 is 18 nm. The percent difference between the CMDs of these two techniques is 30.6%. The difference between the two distributions at -1 GSD and + 1 GSD are 11 nm and 27 nm, respectively. The difference between the CMDs of the EM and instrument 2 is 17 nm. The percent difference between the CMDs of these two techniques is 28.9%. The difference between the two distributions at -1 GSD and + 1 GSD are 16 nm and 15 nm, respectively. The difference between the CMDs of the EM and instrument 3 is 148 nm. The percent difference between the CMDs of these two techniques is 119.5%. The difference between the two distributions at -1 GSD and + 1 GSD are 66 nm and 319 nm, respectively. The difference between the CMDs of instrument 1 and

instrument 2 is 1.2 nm. The percent difference between the CMDs of these two instruments is 1.8%. The difference between the two distributions at -1 GSD and + 1 GSD are 4.6 nm and 12 nm, respectively. The difference between the CMDs of instrument 1 and instrument 3 is 130 nm. The percent difference between the CMDs of these two instruments is 97.9%. The difference between the two distributions at -1 GSD and + 1 GSD are 55 nm and 292 nm, respectively. The difference between the CMDs of instrument 2 and instrument 3 is 131 nm. The percent difference between the CMDs of these two instruments is 99.2%. The difference between the two distributions at -1 GSD and + 1 GSD are 51 nm and 304 nm, respectively. In this test, the CMD of instrument 3 was closer to the selected NaCl size parameter than the other instruments. The difference between the CMDs of instruments 1 and 2 was smaller than the difference between the CMDs of instruments 1 and 2 with instrument 3.

For test 8, the designated sodium chloride aerosol concentration of 220 nm was conducted using a dilution of 104. From the EM images, the highest percentage of particles (32%) were observed in the size range interval of 48.2 – 68.1 nm. The lowest range of particles (2.8%) were observed in the size range interval of 192.6 – 272.2 nm. 2.8 percent of particles were observed in the size range interval of 192.6 – 272.2.

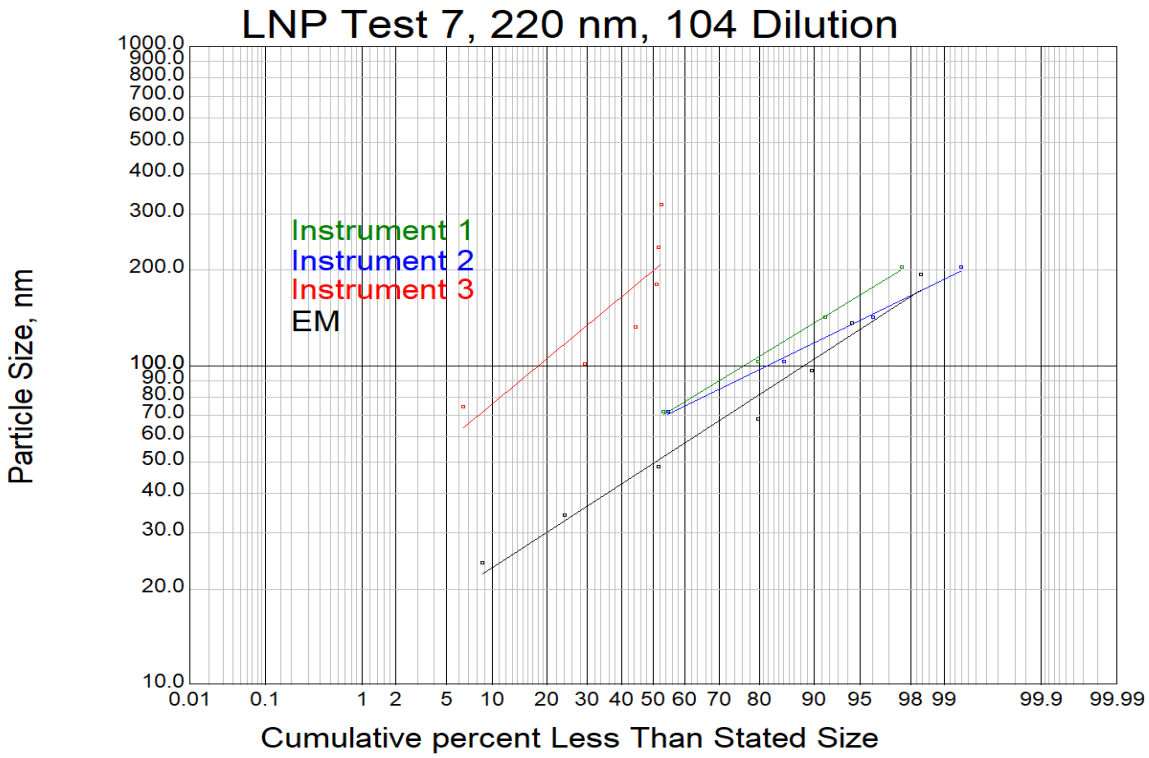


Figure 9: Distribution of NaCl nanoparticle generated aerosol for Test 7, 220 nm generated aerosol, 104 dilution

For instrument 1, the highest percentage of particles (50.7%) were observed in the size range interval of 50.2 – 71.7 nm. The lowest range of particles (2.6%) were observed in the size range interval of 203.8 – 312 nm. 2.6 percent of particles were observed in the size range interval of 203.8 – 312 nm. For instrument 2, the highest percentage of particles (61.3%) were observed in the size range interval of 50.2 – 71.7 nm. The lowest range of particles (0.1%) were observed in the size range interval of 203.8 – 312 nm. 0.1 percent of particles were observed in the size range interval of 203.8 – 312 nm. For instrument 3, the highest percentage of particles (48.0%) were observed in the size range interval of 41.9 – 74.3 nm. The lowest range of particles (4.4%) were observed in the size range interval of 179.6 – 235.0 nm. 4.4 percent of particles were observed in the size range interval of 179.6 – 235.0 nm. For test 8, instrument 3 identified the highest percentage of particles within the selected NaCl size parameter range.

The distributions from test 8 are presented in Figure 10. The lines of fit are roughly parallel; however, the lines of fit for instruments 1, 3, and the electron microscopy results are the most parallel. The lines of fit for instruments 1 and 3 are very similar to each other.

For test 8, the distribution obtained by EM had a CMD of 62.4 nm and a GSD of 1.67, shown in Table 3. The distribution obtained by Instrument 1 had a CMD of 70.7 nm and a GSD of 1.68. The distribution obtained by Instrument 2 had a CMD of 63.2 nm and a GSD of 1.46. The distribution obtained by Instrument 3 had a CMD of 77.3 nm and a GSD of 1.64. The difference between the CMDs of the EM and instrument 1 is 8.3 nm. The percent difference between the CMDs of these two techniques is 12.5%. The difference between the two distributions at -1 GSD and + 1 GSD are 5 nm and 16 nm, respectively. The difference between the CMDs of the EM and instrument 2 is 0.8 nm. The percent difference between the CMDs of these two techniques is 1.3%. The difference between the two distributions at -1 GSD and + 1 GSD are 5.7 nm and 12 nm, respectively. The difference between the CMDs of the EM and instrument 3 is 15 nm. The percent difference between the CMDs of these two techniques is 21.3%. The difference between the two distributions at -1 GSD and + 1 GSD are 9.5 nm and 23 nm, respectively. The difference between the CMDs of instrument 1 and instrument 2 is 7.5 nm. The percent difference between the CMDs of these two instruments is 11.2%. The difference between the two distributions at -1 GSD and + 1 GSD are 0.7 nm and 28 nm, respectively. The difference between the CMDs of instrument 1 and instrument 3 is 6.6 nm. The percent difference between the CMDs of these two instruments is 8.9%. The difference between the two distributions at -1 GSD and + 1 GSD are 4.5 nm and 6.6 nm, respectively. The difference between the CMDs of instrument 2 and instrument 3 is 14 nm. The percent difference between the CMDs of these two instruments is 20.1%. The difference between the two distributions at -1 GSD and + 1 GSD are 3.8 nm and 35 nm, respectively. In this test, the CMD of instrument 3 was closer to the selected NaCl size parameter than the other instruments.

The difference between the CMDs of instruments 1 and 3 was smaller than the difference between the CMDs of instruments 1 and 2, and instruments 2 and 3.

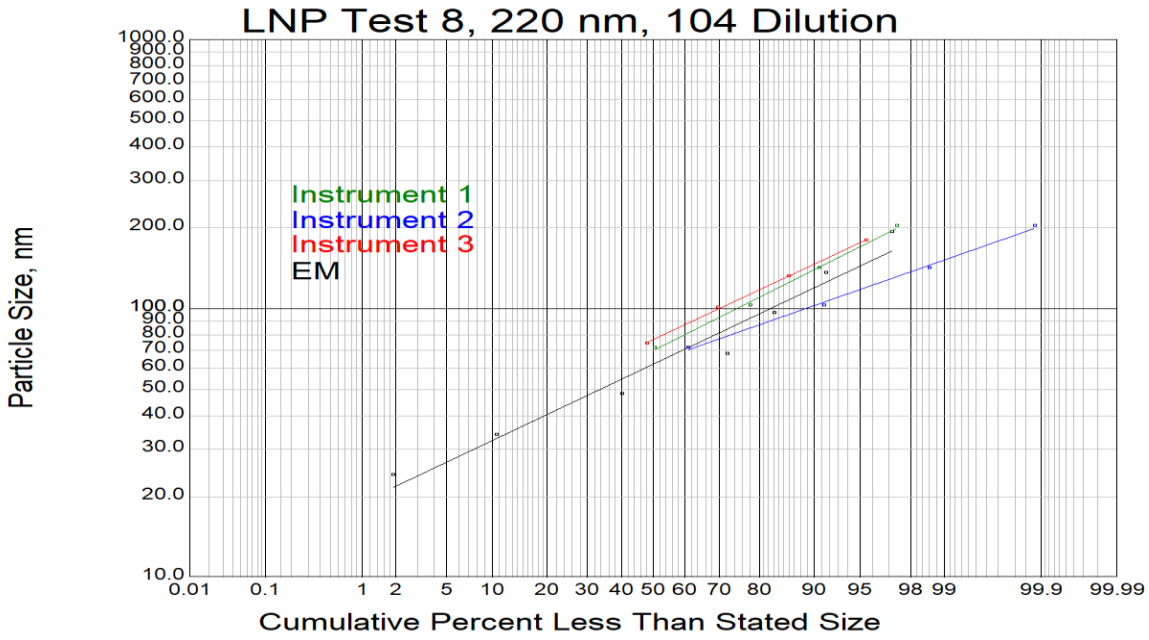


Figure 10: Distribution of NaCl nanoparticle generated aerosol for Test 8, 220 nm generated aerosol, 104 dilution

*Regression Analysis*

For Trial 1 with NaCl, the main effects and interaction were statistically significant with a $p<0.0001$. The instruments and log bucket main effects, and the interaction with the instrument and log bucket were statistically significant. The post-hoc Tukey HSD test identified a significant difference between the instrument 3 dataset and the datasets for instruments 1 and 2. No significant difference was identified between instrument 1 and instrument 2.

Table 3: Data points derived from figures 1-8 and their distributional differences with respect to the analytical technique

| Trial | Analytic Technique | Diameters (nm) at | | | GSD | Differences between EM and Instruments 1, 2, and 3, nm | | | Differences between Instrument 1 and Instrument 2, nm | | | Differences between Instrument 1 and Instrument 3, nm | | | Differences between Instrument 2 and Instrument 3, nm | | |
|---|---|---|---|---|---|---|---|---|---|---|---|---|---|---|---|---|---|
| | | 16% | 50% | 84% | | 16% | 50% | 84% | 16% | 50% | 84% | 16% | 50% | 84% | 16% | 50% | 84% |
| 1 | EM | 32.5 | 54.9 | 91.4 | 1.68 | | | | | | | | | | | | |
| | Instrument 1 | 24.9 | 39.8 | 68.2 | 1.65 | 7.6 | 15.1 | 23.2 | | | | | | | | | |
| | Instrument 2 | 29.1 | 45.6 | 72.4 | 1.58 | 3.4 | 9.3 | 19 | 4.2 | 5.8 | 4.2 | 12 | 18.7 | 28.6 | 7.3 | 12.9 | 24.4 |
| | Instrument 3 | 36.4 | 58.5 | 96.8 | 1.63 | 3.9 | 3.6 | 5.4 | | | | | | | | | |
| 2 | EM | 29.4 | 50.1 | 86.9 | 1.72 | | | | | | | | | | | | |
| | Instrument 1 | 21.8 | 39.9 | 73.9 | 1.84 | 7.6 | 10.2 | 13 | | | | | | | | | |
| | Instrument 2 | 28.5 | 47.1 | 77.1 | 1.64 | 0.9 | 3 | 9.8 | 6.7 | 7.2 | 3.2 | 12 | 16.9 | 21.1 | 5.6 | 9.7 | 17.9 |
| | Instrument 3 | 34.1 | 56.8 | 95 | 1.67 | 4.7 | 6.7 | 8.1 | | | | | | | | | |
| 3 | EM | 29.3 | 54.9 | 105 | 1.89 | | | | | | | | | | | | |
| | Instrument 1 | 32.0 | 52.5 | 90.2 | 1.68 | 2.7 | 2.4 | 14.3 | | | | | | | | | |
| | Instrument 2 | 24.5 | 78.3 | 247 | 3.17 | 4.8 | 23.4 | 142 | 7.5 | 26 | 157 | 7.1 | 7.5 | 4.1 | 15 | 18.3 | 153 |
| | Instrument 3 | 39.1 | 60 | 94.3 | 1.55 | 9.8 | 5.1 | 10.2 | | | | | | | | | |
| 4 | EM | 28.9 | 52.3 | 96.2 | 1.82 | | | | | | | | | | | | |
| | Instrument 1 | 34.5 | 60.6 | 106 | 1.76 | 5.6 | 8.3 | 10.2 | | | | | | | | | |
| | Instrument 2 | 36.2 | 54.8 | 83 | 1.51 | 7.3 | 2.5 | 13.2 | 1.7 | 5.8 | 23.4 | 8.5 | 2.6 | 13.4 | 6.8 | 8.4 | 10 |
| | Instrument 3 | 43 | 63.2 | 93 | 1.47 | 14.1 | 10.9 | 3.2 | | | | | | | | | |
| 5 | EM | 32.5 | 55.5 | 94.5 | 1.71 | | | | | | | | | | | | |
| | Instrument 1 | 42.5 | 71.5 | 123 | 1.70 | 10 | 16 | 28.9 | | | | | | | | | |
| | Instrument 2 | 43.5 | 62.1 | 88.6 | 1.43 | 11 | 6.6 | 5.9 | 1 | 9.4 | 34.8 | 5 | 1.7 | 10.5 | 4 | 11.1 | 24.3 |
| | Instrument 3 | 47.5 | 73.2 | 113 | 1.54 | 15 | 17.7 | 18.4 | | | | | | | | | |
| 6 | EM | 30.7 | 56.1 | 103 | 1.83 | | | | | | | | | | | | |
| | Instrument 1 | 41.2 | 69.5 | 122 | 1.72 | 10.5 | 13.4 | 18.7 | | | | | | | | | |
| | Instrument 2 | 43.5 | 61.7 | 90.1 | 1.44 | 12.8 | 5.6 | 13.2 | 2.3 | 7.8 | 31.9 | 2.8 | 3.8 | 2.2 | 0.5 | 11.6 | 34.1 |
| | Instrument 3 | 44 | 73.3 | 124 | 1.68 | 13.3 | 17.2 | 20.9 | | | | | | | | | |
| 7 | EM | 27.6 | 49.8 | 89.6 | 1.80 | | | | | | | | | | | | |
| | Instrument 1 | 38.6 | 67.8 | 117 | 1.74 | 11 | 18 | 27.4 | | | | | | | | | |
| | Instrument 2 | 43.2 | 66.6 | 105 | 1.56 | 15.6 | 16.8 | 15 | 4.6 | 1.2 | 12.4 | 55 | 130 | 292 | 51 | 131 | 304 |
| | Instrument 3 | 94 | 198 | 409 | 2.08 | 66.4 | 148 | 319 | | | | | | | | | |
| 8 | EM | 37.5 | 62.4 | 105 | 1.67 | | | | | | | | | | | | |
| | Instrument 1 | 42.5 | 70.7 | 121 | 1.68 | 5 | 8.3 | 15.9 | | | | | | | | | |
| | Instrument 2 | 43.2 | 63.2 | 92.3 | 1.46 | 5.7 | 0.8 | 12.3 | 0.7 | 7.5 | 28.2 | 4.5 | 6.6 | 6.6 | 3.8 | 14.1 | 34.8 |
| | Instrument 3 | 47 | 77.3 | 127 | 1.64 | 9.5 | 14.9 | 22.5 | | | | | | | | | |

*Instrument Measurements of Polystyrene Latex Nanoparticle Aerosol - Trial 2 Test Runs*

Tests were conducted using a suspensions of selected polystyrene latex (PSL) nanoparticles, ethyl alcohol, and purified water to generate a nanoaerosol of known particle size while maintaining a high concentration of singlets. Singlets refer to single nanoparticles that are not aggregated or agglomerated. The four sizes of PSL nanoparticles used for the experiments were 57 nm, 92 nm, 147 nm, and 220 nm. Concentration dilutions ranged from 139 to 12,500. The specific particle diameter sizes and dilution concentrations for each of the twelve test runs are presented in Table 4. Instrument 1 refers to the Nano-ID, Instrument 2 refers to the Loaner Nano-ID, and Instrument 3 refers to the TSI Nanoscan. Instruments 1, 2, and 3 were used to obtain measurements during each test run.

Table 5 presents the frequency and percent within each size interval for instruments 1, 2, and 3. Figures 11-22 present the comparison between the upper size intervals of the distributions and the cumulative percent for each test. Table 6 presents the diameters at 16%, 50%, and 84%. These diameters, as well as the geometric standard deviations (GSD), were calculated from the lines of fit presented in Figures 11-22. A comparison of the count median diameters (CMDs) for instruments 1, 2, and 3 are also included in Table 6.

Table 4: Trial Group 2 Target Particle Sizes and Dilutions

| Trial 2 | Particle Size, nm | Dilution |
|---|---|---|
| 1 | 57 | 1,250 |
| 2 | 57 | 1,250 |
| 3 | 57 | 12,500 |
| 4 | 92 | 2,778 |
| 5 | 92 | 312 |
| 6 | 147 | 234 |
| 7 | 147 | 347 |
| 8 | 147 | 694 |
| 9 | 220 | 208 |
| 10 | 220 | 208 |
| 11 | 220 | 139 |
| 12 | 220 | 139 |

Table 5: Frequency and Percent of Polystyrene Latex (PSL) nanoparticles Observed by Instruments 1-3, Based on Size Interval

| Trial 2, Test 1, 57 nm | | | | | | | | | | | |
|---|---|---|---|---|---|---|---|---|---|---|---|
| Instrument 1 | | | | Instrument 2 | | | | Instrument 3 | | | |
| Size Interval, nm | | Frequency | % | Size Interval, nm | | Frequency | % | Size Interval, nm | | Frequency | % |
| 48.4 | 85.9 | 1.21E+08 | 70.0 | 48.4 | 85.9 | 5.48E+06 | 82.0 | 48.8 | 86.6 | 3.39E+06 | 52.5 |
| 86.0 | 114.5 | 3.08E+07 | 17.8 | 86.0 | 114.5 | 9.28E+05 | 13.9 | 86.7 | 115.5 | 1.68E+06 | 25.9 |
| 114.6 | 152.7 | 1.41E+07 | 8.2 | 114.6 | 152.7 | 2.28E+05 | 3.4 | 115.6 | 154.0 | 1.03E+06 | 15.9 |
| 152.8 | 203.7 | 5.10E+06 | 3.0 | 152.8 | 203.7 | 4.11E+04 | 0.6 | 154.1 | 205.4 | 3.67E+05 | 5.7 |
| 203.8 | 349.4 | 1.80E+06 | 1.0 | 203.8 | 349.4 | 5.42E+03 | 0.1 | 205.5 | 365.2 | 0.00E+00 | 0.0 |
| | Total | 1.73E+08 | | | Total | 6.69E+06 | | | Total | 6.46E+06 | |
| Trial 2, Test 2, 57 nm | | | | | | | | | | | |
| Instrument 1 | | | | Instrument 2 | | | | Instrument 3 | | | |
| Size Interval, nm | | Frequency | % | Size Interval, nm | | Frequency | % | Size Interval, nm | | Frequency | % |
| 48.4 | 85.9 | 9.69E+04 | 61.5 | 48.4 | 85.9 | 5.01E+05 | 71.2 | 48.8 | 86.6 | 5.87E+04 | 54.6 |
| 86.0 | 114.5 | 4.28E+04 | 27.1 | 86.0 | 114.5 | 1.45E+05 | 20.5 | 86.7 | 115.5 | 1.52E+04 | 14.2 |
| 114.6 | 152.7 | 1.59E+04 | 10.1 | 114.6 | 152.7 | 5.28E+04 | 7.5 | 115.6 | 154.0 | 1.82E+04 | 16.9 |
| 152.8 | 203.7 | 1.70E+03 | 1.1 | 152.8 | 203.7 | 5.20E+03 | 0.7 | 154.1 | 205.4 | 1.30E+04 | 12.1 |
| 203.8 | 349.4 | 3.61E+02 | 0.2 | 203.8 | 349.4 | 3.63E+02 | 0.1 | 205.5 | 365.2 | 2.41E+03 | 2.2 |
| | Total | 1.58E+05 | | | Total | 7.04E+05 | | | Total | 1.07E+05 | |
| Trial 2, Test 3, 57 nm | | | | | | | | | | | |
| Instrument 1 | | | | Instrument 2 | | | | Instrument 3 | | | |
| Size Interval, nm | | Frequency | % | Size Interval, nm | | Frequency | % | Size Interval, nm | | Frequency | % |
| 48.4 | 85.9 | 1.30E+06 | 81.6 | 48.4 | 85.9 | 2.39E+06 | 79.3 | 48.8 | 86.6 | 2.31E+06 | 51.3 |
| 86.0 | 114.5 | 2.02E+05 | 12.7 | 86.0 | 114.5 | 4.39E+05 | 14.6 | 86.7 | 115.5 | 1.15E+06 | 25.6 |
| 114.6 | 152.7 | 6.75E+04 | 4.2 | 114.6 | 152.7 | 1.45E+05 | 4.8 | 115.6 | 154.0 | 7.42E+05 | 16.5 |
| 152.8 | 203.7 | 1.73E+04 | 1.1 | 152.8 | 203.7 | 3.30E+04 | 1.1 | 154.1 | 205.4 | 2.94E+05 | 6.5 |
| 203.8 | 349.4 | 6.60E+03 | 0.4 | 203.8 | 349.4 | 7.47E+03 | 0.2 | 205.5 | 365.2 | 5.14E+02 | 0.0 |
| | Total | 1.59E+06 | 100 | | Total | 3.01E+06 | | | Total | 4.50E+06 | |
| Trial 2, Test 4, 92 nm | | | | | | | | | | | |
| Instrument 1 | | | | Instrument 2 | | | | Instrument 3 | | | |
| Size Interval, nm | | Frequency | % | Size Interval, nm | | Frequency | % | Size Interval, nm | | Frequency | %t |
| 86.0 | 114.5 | 3.05E+04 | 55.4 | 86.0 | 114.5 | 1.34E+05 | 67.2 | 86.7 | 115.5 | 0.00E+00 | 0.0 |
| 114.6 | 152.7 | 1.96E+04 | 35.7 | 114.6 | 152.7 | 5.54E+04 | 27.8 | 115.6 | 154.0 | 1.75E+05 | 30.7 |
| 152.8 | 203.7 | 2.54E+03 | 4.6 | 152.8 | 203.7 | 9.12E+03 | 4.6 | 154.1 | 205.4 | 2.65E+05 | 46.2 |
| 203.8 | 349.4 | 2.39E+03 | 4.3 | 203.8 | 349.4 | 9.78E+02 | 0.5 | 205.5 | 365.2 | 1.32E+05 | 23.1 |
| | Total | 5.50E+04 | | | Total | 2.00E+05 | | | Total | 5.72E+05 | 100 |

Table 5: Frequency and Percent Based on Size Interval (continued)

| Trial 2, Test 5, 92 nm | | | | | | | | | | | |
|---|---|---|---|---|---|---|---|---|---|---|---|
| Instrument 1 | | | | Instrument 2 | | | | Instrument 3 | | | |
| Size Interval, nm | | Frequency | % | Size Interval, nm | | Frequency | % | Size Interval, nm | | Frequency | % |
| 86.0 | 114.5 | 1.26E+06 | 67.7 | 86.0 | 114.5 | 2.58E+06 | 73.3 | 86.7 | 115.5 | 2.03E+06 | 38.3 |
| 114.6 | 152.7 | 4.54E+05 | 24.4 | 114.6 | 152.7 | 7.52E+05 | 21.4 | 115.6 | 154.0 | 2.07E+06 | 39.1 |
| 152.8 | 203.7 | 1.06E+05 | 5.7 | 152.8 | 203.7 | 1.55E+05 | 4.4 | 154.1 | 205.4 | 1.16E+06 | 21.9 |
| 203.8 | 349.4 | 3.92E+04 | 2.1 | 203.8 | 349.4 | 3.22E+04 | 0.9 | 205.5 | 365.2 | 3.67E+04 | 0.7 |
| | Total | 1.86E+06 | | | Total | 3.52E+06 | | | Total | 5.29E+06 | |
| Trial 2, Test 6, 147 nm | | | | | | | | | | | |
| Instrument 1 | | | | Instrument 2 | | | | Instrument 3 | | | |
| Size Interval, nm | | Frequency | % | Size Interval, nm | | Frequency | % | Size Interval, nm | | Frequency | % |
| 114.6 | 152.7 | 1.38E+06 | 75.4 | 114.6 | 152.7 | 1.14E+06 | 64.5 | 115.6 | 154.0 | 1.04E+06 | 36.1 |
| 152.8 | 203.7 | 2.88E+05 | 15.7 | 152.8 | 203.7 | 5.03E+05 | 28.4 | 154.1 | 205.4 | 1.11E+06 | 38.7 |
| 203.8 | 349.4 | 1.64E+05 | 8.9 | 203.8 | 349.4 | 1.27E+05 | 7.2 | 205.5 | 365.2 | 7.22E+05 | 25.2 |
| | Total | 1.83E+06 | | | Total | 1.77E+06 | | | Total | 2.87E+06 | |
| Trial 2, Test 7, 147 nm | | | | | | | | | | | |
| Instrument 1 | | | | Instrument 2 | | | | Instrument 3 | | | |
| Size Interval, nm | | Frequency | % | Size Interval, nm | | Frequency | % | Size Interval, nm | | Frequency | % |
| 114.6 | 152.7 | 7.06E+05 | 74.2 | 114.6 | 152.7 | 6.85E+05 | 65.3 | 115.6 | 154.0 | 5.81E+05 | 35.7 |
| 152.8 | 203.7 | 1.61E+05 | 16.9 | 152.8 | 203.7 | 2.71E+05 | 25.8 | 154.1 | 205.4 | 6.38E+05 | 39.2 |
| 203.8 | 349.4 | 8.46E+04 | 8.9 | 203.8 | 349.4 | 9.31E+04 | 8.9 | 205.5 | 365.2 | 4.07E+05 | 25.1 |
| | Total | 9.52E+05 | | | Total | 1.05E+06 | | | Total | 1.63E+06 | |
| Trial 2, Test 8, 147 nm | | | | | | | | | | | |
| Instrument 1 | | | | Instrument 2 | | | | Instrument 3 | | | |
| Size Interval, nm | | Frequency | %t | Size Interval, nm | | Frequency | % | Size Interval, nm | | Frequency | % |
| 114.6 | 152.7 | 2.09E+05 | 65.9 | 114.6 | 152.7 | 3.04E+05 | 68.5 | 115.6 | 154.0 | 1.84E+05 | 28.1 |
| 152.8 | 203.7 | 7.56E+04 | 23.8 | 152.8 | 203.7 | 1.31E+05 | 29.5 | 154.1 | 205.4 | 2.71E+05 | 41.4 |
| 203.8 | 349.4 | 3.29E+04 | 10.3 | 203.8 | 349.4 | 9.24E+03 | 2.1 | 205.5 | 365.2 | 2.00E+05 | 30.5 |
| | Total | 3.18E+05 | | | Total | 4.45E+05 | | | Total | 6.54E+05 | |
| Trial 2, Test 9, 220 nm | | | | | | | | | | | |
| Instrument 1 | | | | Instrument 2 | | | | Instrument 3 | | | |
| Size Interval, nm | | Frequency | % | Size Interval, nm | | Frequency | % | Size Interval, nm | | Frequency | % |
| 152.8 | 203.7 | 3.11E+01 | 8.2 | 152.8 | 203.7 | 3.22E+02 | 88.8 | 154.1 | 205.4 | 5.82E+04 | 72.2 |
| 203.8 | 349.4 | 3.50E+02 | 91.8 | 203.8 | 349.4 | 4.04E+01 | 11.2 | 205.5 | 365.2 | 2.24E+04 | 27.8 |
| | Total | 3.81E+02 | | | Total | 3.62E+02 | | | Total | 8.06E+04 | |

Table 5: Frequency and Percent Based on Size Interval (continued)

| Trial 2, Test 10, 220 nm | | | | | | | | | | | |
|---|---|---|---|---|---|---|---|---|---|---|---|
| Instrument 1 | | | | Instrument 2 | | | | Instrument 3 | | | |
| Size Interval, nm | | Frequency | % | Size Interval, nm | | Frequency | % | Size Interval, nm | | Frequency | % |
| 152.8 | 203.7 | 3.37E+05 | 33.5 | 152.8 | 203.7 | 1.20E+05 | 36.3 | 154.1 | 205.4 | 4.47E+05 | 37.3 |
| 203.8 | 349.4 | 6.69E+05 | 66.5 | 203.8 | 349.4 | 2.11E+05 | 63.7 | 205.5 | 365.2 | 7.52E+05 | 62.7 |
| | Total | 1.01E+06 | | | Total | 3.32E+05 | | | Total | 1.20E+06 | |
| Trial 2, Test 11, 220 nm | | | | | | | | | | | |
| Instrument 1 | | | | Instrument 2 | | | | Instrument 3 | | | |
| Size Interval, nm | | Frequency | % | Size Interval, nm | | Frequency | % | Size Interval, nm | | Frequency | % |
| 152.8 | 203.7 | 3.41E+05 | 32.2 | 152.8 | 203.7 | 1.04E+05 | 39.3 | 154.1 | 205.4 | 4.76E+05 | 36.4 |
| 203.8 | 349.4 | 7.18E+05 | 67.8 | 203.8 | 349.4 | 1.60E+05 | 60.7 | 205.5 | 365.2 | 8.31E+05 | 63.6 |
| | Total | 1.06E+06 | | | Total | 2.64E+05 | | | Total | 1.31E+06 | |
| Trial 2, Test 12, 220 nm | | | | | | | | | | | |
| Instrument 1 | | | | Instrument 2 | | | | Instrument 3 | | | |
| Size Interval, nm | | Frequency | % | Size Interval, nm | | Frequency | % | Size Interval, nm | | Frequency | % |
| 152.8 | 203.7 | 3.01E+05 | 22.2 | 152.8 | 203.7 | 1.25E+05 | 42.3 | 154.1 | 205.4 | 5.94E+05 | 37.7 |
| 203.8 | 349.4 | 1.06E+06 | 77.8 | 203.8 | 349.4 | 1.70E+05 | 57.7 | 205.5 | 365.2 | 9.83E+05 | 62.3 |
| | Total | 1.36E+06 | | | Total | 2.95E+05 | | | Total | 1.58E+06 | |

The distributions from test 2-1 are presented in Figure 11. The lines of fit are roughly parallel; however, the lines of fit for instruments 1 for 2 results are the most parallel. Comparisons of the distributions for 16%, 50%, and 84% are presented in Table 6.

For test 2-1, the distribution obtained by Instrument 1 had a CMD of 67.8 nm and a GSD of 1.56, shown in Table 6. The distribution obtained by Instrument 2 had a CMD of 59.9 nm and a GSD of 1.49. The distribution obtained by Instrument 3 had a CMD of 85.0 nm and a GSD of 1.38. The difference between the CMDs of instrument 1 and instrument 2 is 7.9 nm. The percent difference between the CMDs of these two instruments is 12.4%. The difference between the two distributions at -1 GSD and + 1 GSD are 3.7 nm and 17.8 nm, respectively. The difference between the CMDs of instrument 1 and instrument 3 is 17.2 nm. The percent difference between the CMDs of these two instruments is 22.5%. The difference between the two distributions at -1 GSD and + 1 GSD are 17.8 nm and 11.2 nm, respectively. The difference between the CMDs of instrument 2 and instrument 3 is 25.1 nm. The percent difference between the CMDs of these two instruments is 34.6%. The difference between the two distributions at -1 GSD and + 1 GSD are 21.5 nm and 29 nm, respectively. In this test, the CMD

of instrument 2 was closer to the selected PSL size parameter than the other instruments. The difference between the CMDs of instruments 1 and 2 was smaller than the difference between the CMDs of instruments 1 and 2 with instrument 3.

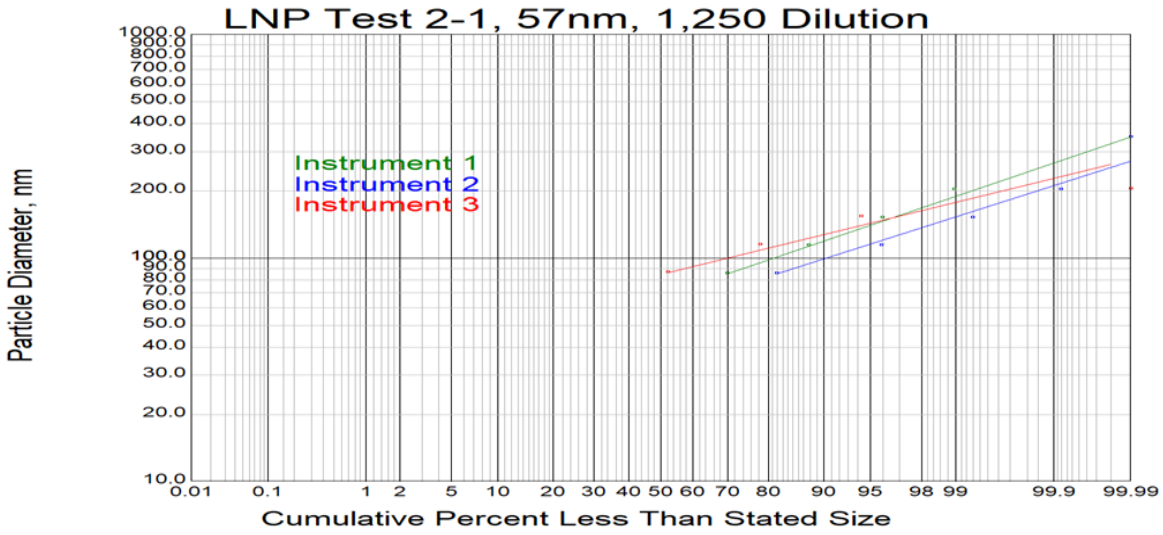


Figure 11: Distribution of PSL nanoparticle generated aerosol for Test 2-1, 57 nm generated aerosol, 1,250 dilution

For test 2-2, the designated PSL nanoparticle of 57 nm was used at a dilution of 1,250 to prepare a lower concentration of PSL particles as a comparison with test 2-1 results. For instrument 1, the highest percentage of particles (61.5%) were observed in the size range interval of 48.4-85.9 nm. The lowest range of particles (0.2%) were observed in the size range interval of 203.8-349.4 nm. 61.5 percent of particles were observed in the size range interval of 48.4-85.9 nm. For instrument 2, the highest percentage of particles (71.2%) were observed in the size range interval of 48.4-85.9 nm. The lowest range of particles (0.1%) were observed in the size range interval of 203.8 – 349.4 nm. 71.2 percent of particles were observed in the size range interval of 48.4 – 85.9 nm. For instrument 3, the highest percentage of particles (54.6%) were observed in the size range interval of 48.8-86.6 nm. The lowest range of particles (2.2%) were observed in the size range interval of 205.5 – 365.2 nm. 54.6 percent of particles were

observed in the size range interval of 48.8 – 86.6 nm. For this test, instrument 2 identified the highest percentage of particles within the selected PSL size parameter range.

The distributions from test 2-2 are presented in Figure 12. The lines of fit are roughly parallel. Comparisons of the distributions for 16%, 50%, and 84% are presented in Table 6.

For test 2-2, the distribution obtained by Instrument 1 had a CMD of 74.1 nm and a GSD of 1.51, shown in Table 6. The distribution obtained by Instrument 2 had a CMD of 65.8 nm and a GSD of 1.47. The distribution obtained by Instrument 3 had a CMD of 87.5 nm and a GSD of 1.50. The difference between the CMDs of instrument 1 and instrument 2 is 8.3 nm. The percent difference between the CMDs of these two instruments is 11.9%. The difference between the two distributions at -1 GSD and + 1 GSD are 4.2 nm and 14.4 nm, respectively. The difference between the CMDs of instrument 1 and instrument 3 is 13.4 nm. The percent difference between the CMDs of these two instruments is 16.6%. The difference between the two distributions at -1 GSD and + 1 GSD are 9.5 nm and 19.4 nm, respectively. The difference between the CMDs of instrument 2 and instrument 3 is 21.7 nm. The percent difference between the CMDs of these two instruments is 28.3%. The difference between the two distributions at -1 GSD and + 1 GSD are 13.7 nm and 33.8 nm, respectively. In this test, the CMD of instrument 2 was closer to the selected PSL size parameter than the other instruments. The difference between the CMDs of instruments 1 and 2 was smaller than the difference between the CMDs of instruments 1 and 2 with instrument 3.

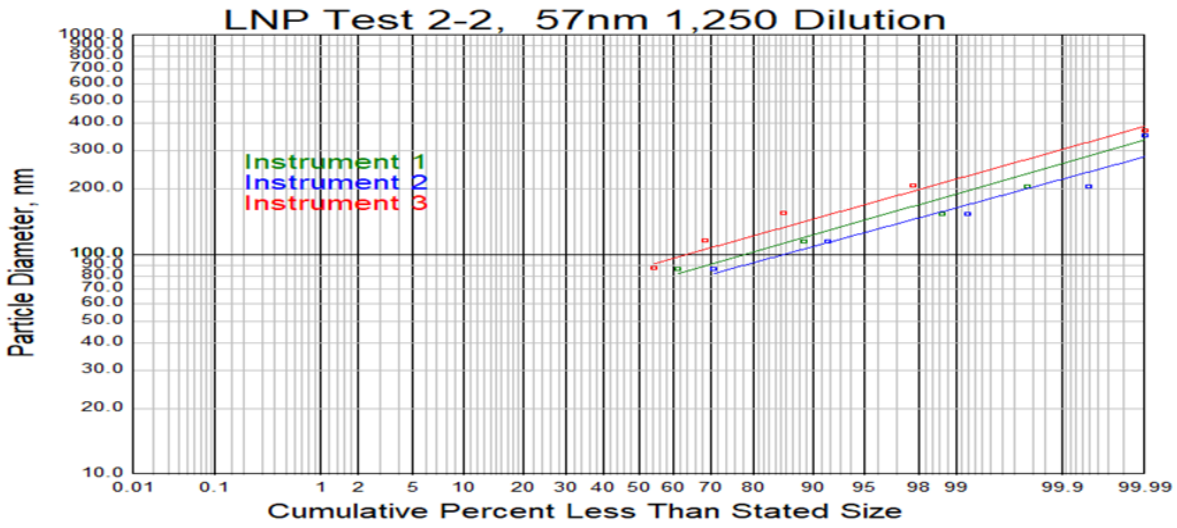


Figure 12: Distribution of PSL nanoparticle generated aerosol for Test 2-2, 57 nm generated aerosol, 1,250 dilution

For test 2-3, the designated PSL nanoparticle of 57 nm was used at a dilution of 12,500 to prepare a very low concentration of PSL particles to evaluate the measurement instrument responses compared with test 2-1 and test 2-1. For instrument 1, the highest percentage of particles (81.6%) were observed in the size range interval of 48.4-85.9 nm. The lowest range of particles (0.4%) were observed in the size range intervals of 203.8-349.4 nm. 81.6 percent of particles were observed in the size range interval of 48.4-85.9 nm. For instrument 2, the highest percentage of particles (79.3%) were observed in the size range interval of 48.4-85.9 nm. The lowest range of particles (0.2%) were observed in the size range interval of 203.8 – 349.4 nm. 79.3 percent of particles were observed in the size range interval of 48.4 – 85.9 nm. For instrument 3, the highest percentage of particles (51.3%) were observed in the size range interval of 48.8 – 86.6 nm. The lowest range of particles (0.0%) were observed in the size range interval of 205.5 – 365.2 nm. 51.3 percent of particles were observed in the size range interval of 48.8 – 86.6 nm. For this test, instrument 1 identified the highest percentage of particles within the selected PSL size parameter range.

The distributions from test 2-3 are presented in Figure 13. The lines of fit for instruments 1 and 2 are roughly parallel. Comparisons of the distributions for 16%, 50%, and 84% are presented in Table 6.

For test 2-3, the distribution obtained by Instrument 1 had a CMD of 55.1 nm and a GSD of 1.64, shown in Table 6. The distribution obtained by Instrument 2 had a CMD of 56.4 nm and a GSD of 1.59. The distribution obtained by Instrument 3 had a CMD of 94.5 nm and a GSD of 1.28. The difference between the CMDs of instrument 1 and instrument 2 is 1.3 nm. The percent difference between the CMDs of these two instruments is 2.3%. The difference between the two distributions at -1 GSD and + 1 GSD are 1.8 nm and 0 nm, respectively. The difference between the CMDs of instrument 1 and instrument 3 is 39.4 nm. The percent difference between the CMDs of these two instruments is 52.7%. The difference between the two distributions at -1 GSD and + 1 GSD are 40.6 nm and 30.9 nm, respectively. The difference between the CMDs of instrument 2 and instrument 3 is 38.1 nm. The percent difference between the CMDs of these two instruments is 50.5%. The difference between the two distributions at -1 GSD and + 1 GSD are 38.8 nm and 30.9 nm, respectively. For this test, the CMD of instruments 1 and 2 were closer to the selected PSL size parameter than instrument 3. The difference between the CMDs of instruments 1 and 2 was smaller than the difference between the CMDs of instruments 1 and 2 with instrument 3.

For test 2-4, the designated PSL nanoparticle of 92 nm was used at a dilution of 2,778 to prepare a lower concentration of PSL particles. For instrument 1, the highest percentage of particles (55.4%) were observed in the size range interval of 86.0-114.5 nm. The lowest range of particles (4.3%) were observed in the size range intervals of 203.8-349.4 nm. 55.4 percent of particles were observed in the size range interval of 86.0-114.5 nm.

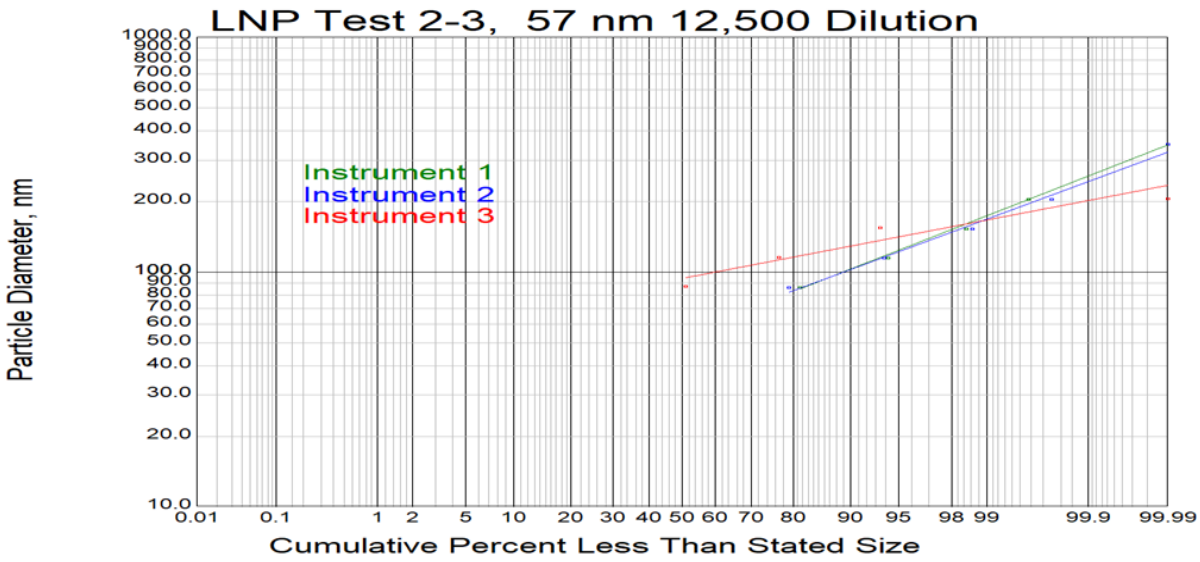


Figure 13: Distribution of PSL nanoparticle generated aerosol for Test 2-3, 57 nm generated aerosol, 12,500 dilution.

For instrument 2, the highest percentage of particles (67.2%) were observed in the size range interval of 86.0-114.5 nm. The lowest range of particles (0.5%) were observed in the size range interval of 203.8 – 349.4 nm. 67.2 percent of particles were observed in the size range interval of 86.0 – 114.5 nm. For instrument 3, the highest percentage of particles (46.2%) were observed in the size range interval of 154.1 – 205.4 nm. The lowest range of particles (0.0%) were observed in the size range interval of 86.7 – 115.5 nm. Zero percent of particles were observed in the size range interval of 86.7 – 115.5 nm. For this test, instrument 2 identified the highest percentage of particles within the selected PSL size parameter range.

The distributions from test 2-4 are presented in Figure 14. The lines of fit are roughly parallel between instruments 1, 2, and 3. The lines of fit for instruments 1 and 2 were more parallel to each other. Comparisons of the distributions for 16%, 50%, and 84% are presented in Table 6.

For test 2-4, the distribution obtained by Instrument 1 had a CMD of 107.6 nm and a GSD of 1.37, shown in Table 6. The distribution obtained by Instrument 2 had a CMD of 88.6 nm and a GSD of 1.45. The distribution obtained by Instrument 3 had a CMD of 192.5 nm and a GSD

of 1.18. The difference between the CMDs of instrument 1 and instrument 2 is 19 nm. The percent difference between the CMDs of these two instruments is 19.4%. The difference between the two distributions at -1 GSD and + 1 GSD are 18.8 nm and 22.3 nm, respectively. The difference between the CMDs of instrument 1 and instrument 3 is 84.9 nm. The percent difference between the CMDs of these two instruments is 56.6%. The difference between the two distributions at -1 GSD and + 1 GSD are 82.0 nm and 73.7 nm, respectively. The difference between the CMDs of instrument 2 and instrument 3 is 104 nm. The percent difference between the CMDs of these two instruments is 73.9%. The difference between the two distributions at -1 GSD and + 1 GSD are 101 nm and 96 nm, respectively. For this test, the CMD of instrument 2 was closer to the selected PSL size parameter. The difference between the CMDs of instruments 1 and 2 was smaller than the difference between the CMDs of instruments 1 and 2 with instrument 3.

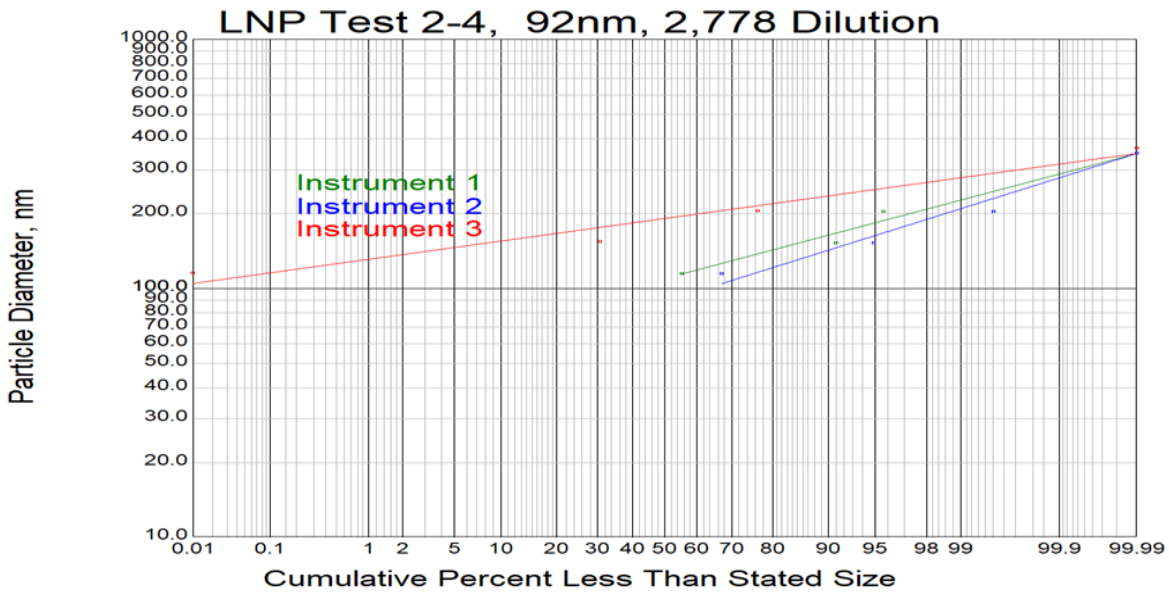


Figure 14: Distribution of PSL nanoparticle generated aerosol for Test 2-4, 92 nm generated aerosol, 2,778 dilution

For test 2-5, the designated PSL nanoparticle of 92 nm was used at a dilution of 312 to prepare a higher concentration of PSL particles than test 2-4. For instrument 1, the highest percentage of particles (67.7%) were observed in the size range interval of 86.0-114.5 nm. The lowest range of particles (2.1%) were observed in the size range intervals of 203.8-349.4 nm.

67.7 percent of particles were observed in the size range interval of 86.0-114.5 nm. For instrument 2, the highest percentage of particles (73.3%) were observed in the size range interval of 86.0-114.5 nm. The lowest range of particles (0.9%) were observed in the size range interval of 203.8 – 349.4 nm. 73.3 percent of particles were observed in the size range interval of 86.0-114.5 nm. For instrument 3, the highest percentage of particles (39.1%) were observed in the size range interval of 115.6-154.0 nm. The lowest range of particles (0.7%) were observed in the size range interval of 205.5 – 365.2 nm. 38.3 percent of particles were observed in the size range interval of 86.7-115.5 nm. For this test, instrument 2 identified the highest percentage of particles within the selected PSL size parameter range.

The distributions from test 2-5 are presented in Figure 15. The lines of fit for instruments 1, 2, and 3 were similar to each other. Comparisons of the distributions for 16%, 50%, and 84% are presented in Table 6.

For test 2-5, the distribution obtained by Instrument 1 had a CMD of 100.9 nm and a GSD of 1.39, shown in Table 6. The distribution obtained by Instrument 2 had a CMD of 88.6 nm and a GSD of 1.44. The distribution obtained by Instrument 3 had a CMD of 112.2 nm and a GSD of 1.35. The difference between the CMDs of instrument 1 and instrument 2 is 12.3 nm. The percent difference between the CMDs of these two instruments is 13.0%. The difference between the two distributions at -1 GSD and + 1 GSD are 10.0 nm and 12.0 nm, respectively. The difference between the CMDs of instrument 1 and instrument 3 is 11.3 nm. The percent difference between the CMDs of these two instruments is 10.6%. The difference between the two distributions at -1 GSD and + 1 GSD are 10.5 nm and 11.3 nm, respectively. The difference between the CMDs of instrument 2 and instrument 3 is 23.6 nm. The percent difference between the CMDs of these two instruments is 23.5%. The difference between the two distributions at -1 GSD and + 1 GSD are 20.5 nm and 23.3 nm, respectively. For this test, the CMD of instrument 2 was closer to the selected PSL size parameter. The difference between

the CMDs of instruments 1 and 3 was smaller than the difference between the CMD of instruments 1 and 2, and the difference between the CMD of instruments 2 and 3.

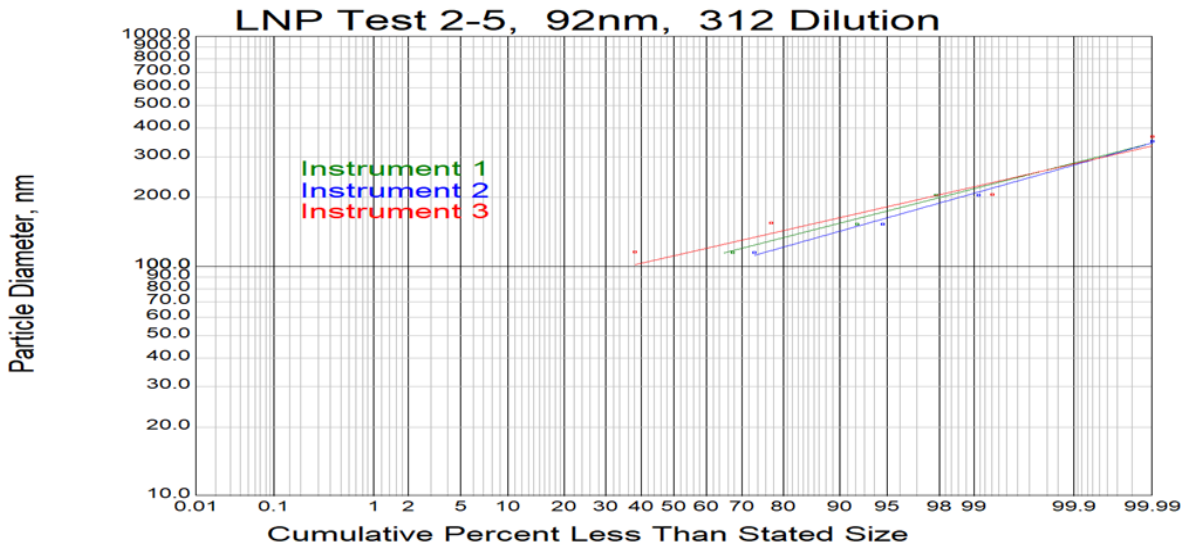


Figure 15: Distribution of PSL nanoparticle generated aerosol for Test 2-5, 92 nm generated aerosol, 312 dilution

For test 2-6, the designated PSL nanoparticle of 147 nm was used at a dilution of 234 to prepare a higher concentration of PSL particles. For instrument 1, the highest percentage of particles (75.4%) were observed in the size range interval of 114.6-152.7 nm. The lowest range of particles (8.9%) were observed in the size range intervals of 203.8-349.4 nm. 75.4 percent of particles were observed in the size range interval of 114.6-152.7 nm. For instrument 2, the highest percentage of particles (64.5%) were observed in the size range interval of 114.6-152.7 nm. The lowest range of particles (7.2%) were observed in the size range interval of 203.8 – 349.4 nm. 64.5 percent of particles were observed in the size range interval of 114.6-152.7 nm. For instrument 3, the highest percentage of particles (38.7%) were observed in the size range interval of 154.1-205.4 nm. The lowest range of particles (25.2%) were observed in the size range interval of 205.5-365.2 nm. 36.1 percent of particles were observed in the size range

interval of 115.6-154.0 nm. For this test, instrument 1 identified the highest percentage of particles within the selected PSL size parameter range.

The distributions from test 2-6 are presented in Figure 16. The lines of fit are roughly parallel between instruments 1, 2 and 3. The lines of fit for instruments 1 and 2 are similar to each other. Comparisons of the distributions for 16%, 50%, and 84% are presented in Table 6.

For test 2-6, the distribution obtained by Instrument 1 had a CMD of 135.7 nm and a GSD of 1.30, shown in Table 6. The distribution obtained by Instrument 2 had a CMD of 141.4 nm and a GSD of 1.28. The distribution obtained by Instrument 3 had a CMD of 172.0 nm and a GSD of 1.24. The difference between the CMDs of instrument 1 and instrument 2 is 5.7 nm. The percent difference between the CMDs of these two instruments is 4.1%. The difference between the two distributions at -1 GSD and + 1 GSD are 5.8 nm and 4.3 nm, respectively. The difference between the CMDs of instrument 1 and instrument 3 is 36.3 nm. The percent difference between the CMDs of these two instruments is 23.6%. The difference between the two distributions at -1 GSD and + 1 GSD are 35.3 nm and 37.1 nm, respectively. The difference between the CMDs of instrument 2 and instrument 3 is 30.6 nm. The percent difference between the CMDs of these two instruments is 19.5%. The difference between the two distributions at -1 GSD and + 1 GSD are 29.5 nm and 32.8 nm, respectively. For this test, the CMD of instrument 2 was closer to the selected PSL size parameter. The difference between the CMDs of instruments 1 and 2 was smaller than the difference between the CMDs of instruments 1 and 2 with instrument 3.

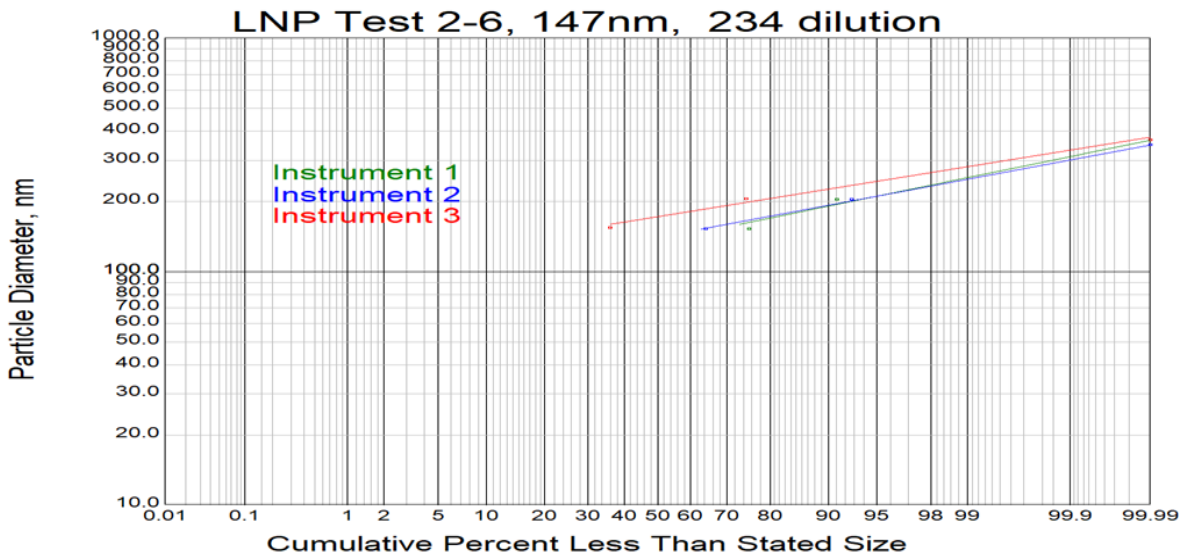


Figure 16: Distribution of PSL nanoparticle generated aerosol for Test 2-6, 147 nm generated aerosol, 234 dilution

For test 2-7, the designated PSL nanoparticle of 147 nm was used at a dilution of 347 to prepare a lower concentration of PSL particles than test 2-6. For Instrument 1, the highest percentage of particles (74.2%) were observed in the size range interval of 114.6-152.7 nm. The lowest range of particles (8.9%) were observed in the size range intervals of 203.8-349.4 nm. 74.2 percent of particles were observed in the size range interval of 114.6-152.7 nm. For instrument 2, the highest percentage of particles (65.3%) were observed in the size range interval of 114.6-152.7 nm. The lowest range of particles (8.9%) were observed in the size range interval of 203.8 – 349.4 nm. 65.3 percent of particles were observed in the size range interval of 114.6-152.7 nm. For instrument 3, the highest percentage of particles (39.2%) were observed in the size range interval of 154.1-205.4 nm. The lowest range of particles (25.1%) were observed in the size range interval of 205.5-365.2 nm. 35.7 percent of particles were observed in the size range interval of 115.6-154.0 nm. For this test, instrument 1 identified the highest percentage of particles within the selected PSL size parameter range.

The distributions from test 2-7 are presented in Figure 17. The lines of fit of instruments 1, 2, and 3 are roughly parallel. The lines of fit for instruments for 1 and 2 are similar to each other. Comparisons of the distributions for 16%, 50%, and 84% are presented in Table 6.

For test 2-7, the distribution obtained by Instrument 1 had a CMD of 144 nm and a GSD of 1.29, shown in Table 6. The distribution obtained by Instrument 2 had a CMD of 144.8 nm and a GSD of 1.26. The distribution obtained by Instrument 3 had a CMD of 174.1 nm and a GSD of 1.24. The difference between the CMDs of instrument 1 and instrument 2 is 0.8 nm. The percent difference between the CMDs of these two instruments is 0.6%. The difference between the two distributions at -1 GSD and + 1 GSD are 9.8 nm and 6.4 nm, respectively. The difference between the CMDs of instrument 1 and instrument 3 is 30.1 nm. The percent difference between the CMDs of these two instruments is 18.9%. The difference between the two distributions at -1 GSD and + 1 GSD are 34.8 nm and 38.2 nm, respectively. The difference between the CMDs of instrument 2 and instrument 3 is 29.3 nm. The percent difference between the CMDs of these two instruments is 18.4%. The difference between the two distributions at -1 GSD and + 1 GSD are 25.0 nm and 31.8 nm, respectively. For this test, the CMD of instruments 1 and 2 were closer to the selected PSL size parameter than instrument 3. The difference between the CMDs of instruments 1 and 2 was smaller than the difference between the CMDs of instruments 1 and 2 with instrument 3.

For test 2-8, the designated PSL nanoparticle of 147 nm was used at a dilution of 694 to prepare a lower concentration of PSL particles than test 2-6 or test 2-7. For instrument 1, the highest percentage of particles (65.9%) were observed in the size range interval of 114.6-152.7 nm. The lowest range of particles (10.3%) were observed in the size range intervals of 203.8-349.4 nm. 65.9 percent of particles were observed in the size range interval of 114.6-152.7 nm. For instrument 2, the highest percentage of particles (68.5%) were observed in the size range interval of 114.6-152.7 nm.

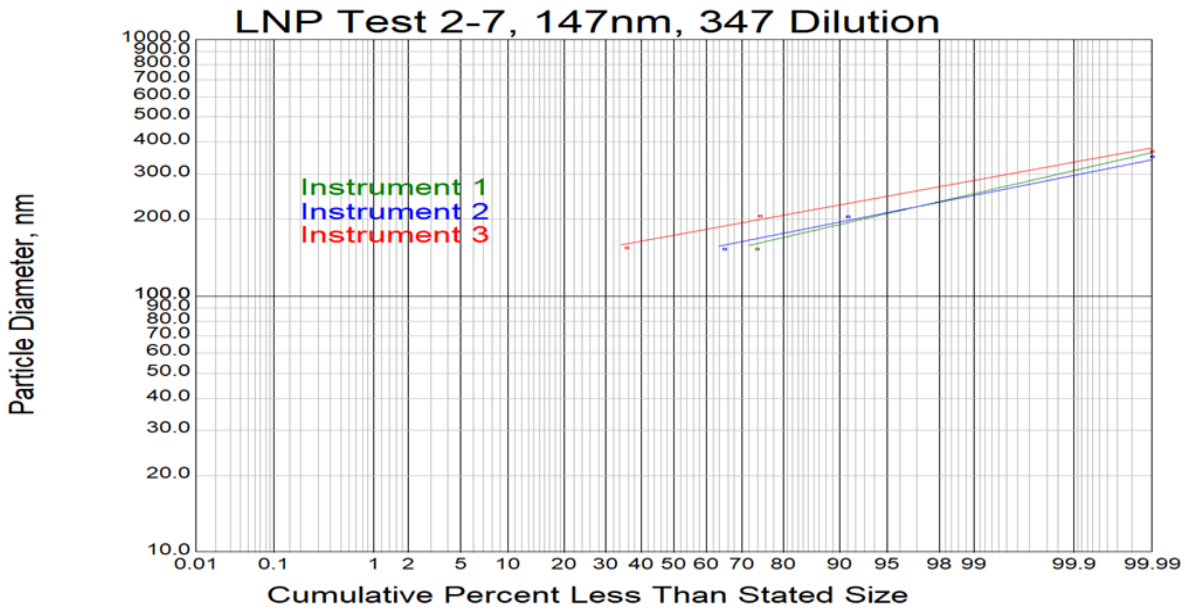

Figure 17: Distribution of PSL nanoparticle generated aerosol for Test 2-7, 147 nm generated aerosol, 347 dilution

The lowest range of particles (2.1%) were observed in the size range interval of 203.8 – 349.4 nm. 68.5 percent of particles were observed in the size range interval of 114.6 – 152.7 nm. For instrument 3, the highest percentage of particles (41.4%) were observed in the size range interval of 154.1-205.4 nm. The lowest range of particles (28.1%) were observed in the size range interval of 115.6-154.0 nm. 28.1 percent of particles were observed in the size range interval of 115.6-154.0 nm. For this test, instrument 2 identified the highest percentage of particles within the selected PSL size parameter range.

The distributions from test 2-8 are presented in Figure 18. The lines of fit are roughly parallel; however, the lines of fit for instruments 1 and 2 are more similar to each other. Comparisons of the distributions for 16%, 50%, and 84% are presented in Table 6.

For test 2-8, the distribution obtained by Instrument 1 had a CMD of 148.3 nm and a GSD of 1.23, shown in Table 6. The distribution obtained by Instrument 2 had a CMD of 134.9 nm and a GSD of 1.29. The distribution obtained by Instrument 3 had a CMD of 180.3 nm and a GSD of 1.23. The difference between the CMDs of instrument 1 and instrument 2 is 13.4 nm.

The percent difference between the CMDs of these two instruments is 9.5%. The difference between the two distributions at -1 GSD and + 1 GSD are 21.4 nm and 18.6 nm, respectively. The difference between the CMDs of instrument 1 and instrument 3 is 32.0 nm. The percent difference between the CMDs of these two instruments is 19.5%. The difference between the two distributions at -1 GSD and + 1 GSD are 27.8 nm and 39.6 nm, respectively. The difference between the CMDs of instrument 2 and instrument 3 is 45.4 nm. The percent difference between the CMDs of these two instruments is 28.8%. The difference between the two distributions at -1 GSD and + 1 GSD are 49.2 nm and 58.2 nm, respectively. For this test, the CMD of instrument 1 was closer to the selected PSL size parameter. The difference between the CMDs of instruments 1 and 2 was smaller than the difference between the CMDs of instruments 1 and 2 with instrument 3.

For test 2-9, the designated PSL nanoparticle of 220 nm was used at a dilution of 208 to prepare a higher concentration of PSL particles. For instrument 1, the highest percentage of particles (91.8%) were observed in the size range interval of 203.8-349.4 nm. The lowest range of particles (8.2%) were observed in the size range intervals of 152.8-203.7 nm. 91.8 percent of particles were observed in the size range interval of 203.8-349.4 nm.

For instrument 2, the highest percentage of particles (88.8%) were observed in the size range interval of 152.8-203.7 nm. The lowest range of particles (11.2%) were observed in the size range interval of 203.8-349.4 nm. 11.2 percent of particles were observed in the size range interval of 203.8-349.4 nm. For instrument 3, the highest percentage of particles (72.2%) were observed in the size range interval of 154.1-205.4 nm. The lowest range of particles (27.8%) were observed in the size range interval of 205.5-365.2 nm. 27.8 percent of particles were observed in the size range interval of 205.5-365.2 nm. For this test, instrument 2 identified the highest percentage of particles within the selected PSL size parameter range.

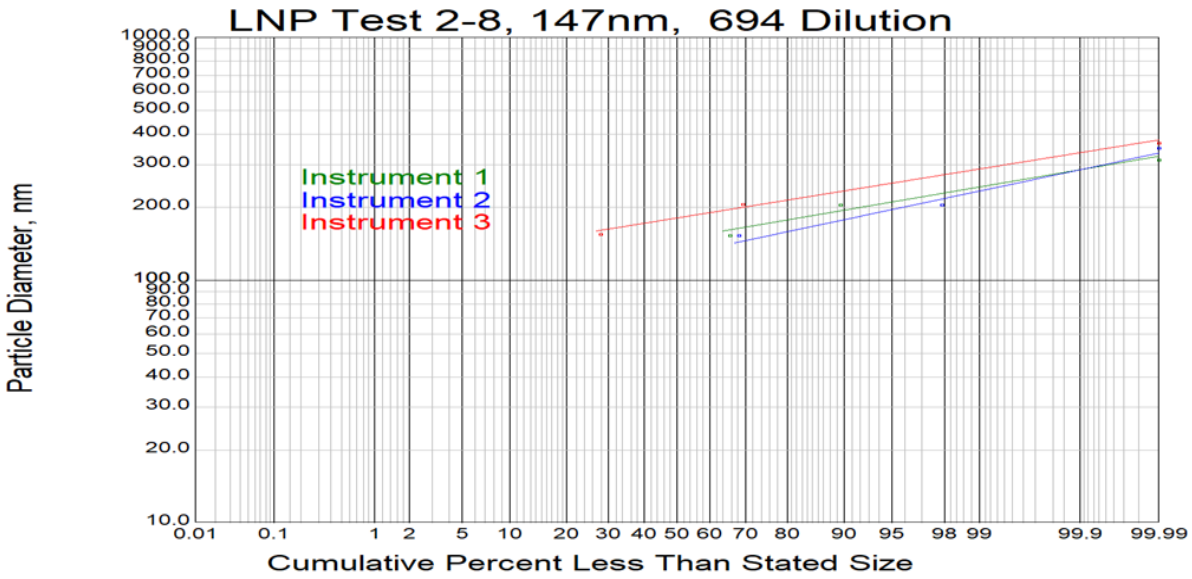


Figure 18: Distribution of PSL nanoparticle generated aerosol for Test 2-8, 147 nm generated aerosol, 694 dilution

The distributions from test 2-9 are presented in Figure 19. The lines of fit are roughly parallel to each other. Comparisons of the distributions for 16%, 50%, and 84% are presented in Table 6.

For test 2-9, the distribution obtained by Instrument 1 had a CMD of 236.9 nm and a GSD of 1.11, shown in Table 6. The distribution obtained by Instrument 2 had a CMD of 155.5 nm and a GSD of 1.25. The distribution obtained by Instrument 3 had a CMD of 185.8 nm and a GSD of 1.20. The difference between the CMDs of instrument 1 and instrument 2 is 81.4 nm. The percent difference between the CMDs of these two instruments is 41.5%. The difference between the two distributions at -1 GSD and + 1 GSD are 87.8 nm and 63.8 nm, respectively. The difference between the CMDs of instrument 1 and instrument 3 is 51.1 nm. The percent difference between the CMDs of these two instruments is 24.2%. The difference between the two distributions at -1 GSD and + 1 GSD are 59.6 nm and 40.1 nm, respectively. The difference between the CMDs of instrument 2 and instrument 3 is 30.3 nm. The percent difference between the CMDs of these two instruments is 17.8%. The difference between the two distributions at -1 GSD and + 1 GSD are 28.2 nm and 23.7 nm, respectively. For this test, the

CMD of instrument 1 was closer to the selected PSL size parameter. The difference between the CMDs of instruments 2 and 3 was smaller than the difference between the CMD of instruments 1 and 2, and the difference between the CMD of instruments 1 and 3.

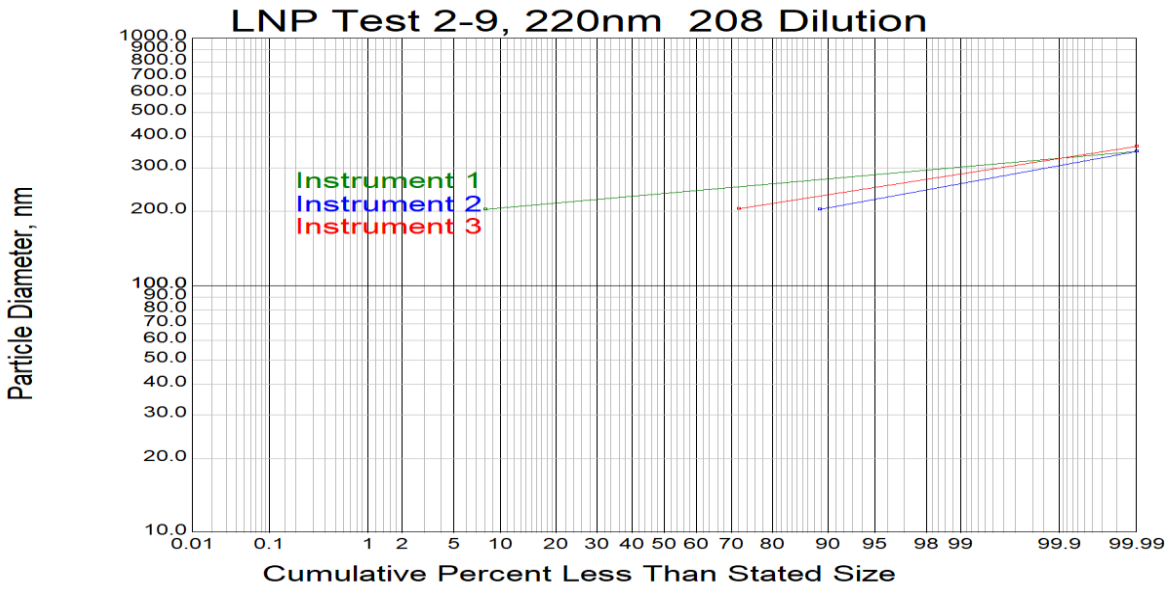


Figure 19: Distribution of PSL nanoparticle generated aerosol for Test 2-9, 220 nm generated aerosol, 208 dilution

For test 2-10, the designated PSL nanoparticle of 220 nm was used at a dilution of 208 to prepare a higher concentration of PSL particles as a comparison with test 2-9. For instrument 1, the highest percentage of particles (66.5%) were observed in the size range interval of 203.8-349.4 nm. The lowest range of particles (33.5%) were observed in the size range intervals of 152.8-203.7 nm. 66.5 percent of particles were observed in the size range interval of 203.8-349.4 nm. For instrument 2, the highest percentage of particles (63.7%) were observed in the size range interval of 203.8-349.4 nm. The lowest range of particles (36.3%) were observed in the size range interval of 152.8-203.7 nm. 63.7 percent of particles were observed in the size range interval of 203.8-349.4 nm. For instrument 3, the highest percentage of particles (62.7%) were observed in the size range interval of 205.5-365.2 nm. The lowest range of particles (37.3%) were observed in the size range interval of 154.1-205.4 nm. 62.7

percent of particles were observed in the size range interval of 203.8-349.4 nm. For this test, instrument 3 identified the highest percentage of particles within the selected PSL size parameter range.

The distributions from test 2-10 are presented in Figure 20. The lines of fit for instruments 1, 2, and 3 are parallel and similar to each other. Comparisons of the distributions for 16%, 50%, and 84% are presented in Table 6.

For test 2-10, the distribution obtained by Instrument 1 had a CMD of 214.2 nm and a GSD of 1.14, shown in Table 6. The distribution obtained by Instrument 2 had a CMD of 214.2 nm and a GSD of 1.14. The distribution obtained by Instrument 3 had a CMD of 216.7 nm and a GSD of 1.16. The difference between the CMDs of instrument 1 and instrument 2 is 0 nm. The percent difference between the CMDs of these two instruments is 0%. The difference between the two distributions at -1 GSD and + 1 GSD are 0 nm and 0 nm, respectively. The difference between the CMDs of instrument 1 and instrument 3 is 2.5 nm. The percent difference between the CMDs of these two instruments is 1.2%. The difference between the two distributions at -1 GSD and + 1 GSD are 2.2 nm and 3.09 nm, respectively. The difference between the CMDs of instrument 2 and instrument 3 is 2.5 nm. The percent difference between the CMDs of these two instruments is 1.2%. The difference between the two distributions at -1 GSD and + 1 GSD are 2.2 nm and 3.0 nm, respectively. For this test, the CMD of instrument 3 was closer to the selected PSL size parameter. The difference between the CMDs of instruments 1 and 2 was smaller than the difference between the CMDs of instruments 1 and 2 with instrument 3, however the difference between the CMDs of all of the instruments was small.

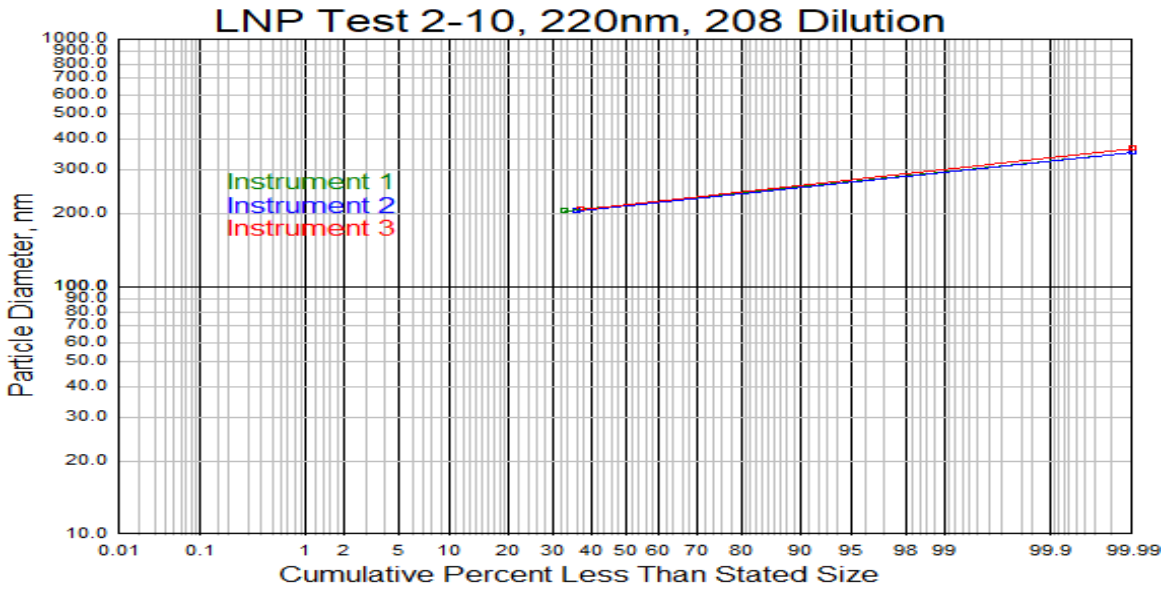


Figure 20: Distribution of PSL nanoparticle generated aerosol for Test 2-10, 220 nm generated aerosol, 208 dilution

For test 2-11, the designated PSL nanoparticle of 220 nm was used at a dilution of 139 to prepare a higher concentration of PSL particles than test 2-9 and test 2-10. For instrument 1, the highest percentage of particles (67.8%) were observed in the size range interval of 203.8-349.4 nm. The lowest range of particles (32.2%) were observed in the size range intervals of 152.8-203.7 nm. 67.8 percent of particles were observed in the size range interval of 203.8-349.4 nm. For instrument 2, the highest percentage of particles (60.7%) were observed in the size range interval of 203.8-349.4 nm. The lowest range of particles (39.3%) were observed in the size range interval of 152.8-203.7 nm. 60.7 percent of particles were observed in the size range interval of 203.8-349.4 nm. For instrument 3, the highest percentage of particles (63.6%) were observed in the size range interval of 205.5-365.2 nm. The lowest range of particles (36.4%) were observed in the size range interval of 154.1-205.4 nm. 63.6 percent of particles were observed in the size range interval of 205.5-365.2 nm. For this test, instrument 2 identified the highest percentage of particles within the selected PSL size parameter range.

The distributions from test 2-11 are presented in Figure 21. The lines of fit for instruments 1, 2, and 3 are parallel and similar to each other. Comparisons of the distributions for 16%, 50%, and 84% are presented in Table 6.

For test 2-11, the distribution obtained by Instrument 1 had a CMD of 219.3 nm and a GSD of 1.17, shown in Table 6. The distribution obtained by Instrument 2 had a CMD of 209.2 nm and a GSD of 1.14. The distribution obtained by Instrument 3 had a CMD of 214.2 nm and a GSD of 1.15. The difference between the CMDs of instrument 1 and instrument 2 is 10.1 nm. The percent difference between the CMDs of these two instruments is 4.7%. The difference between the two distributions at -1 GSD and + 1 GSD are 2.2 nm and 16.1 nm, respectively. The difference between the CMDs of instrument 1 and instrument 3 is 5.1 nm. The percent difference between the CMDs of these two instruments is 2.4%. The difference between the two distributions at -1 GSD and + 1 GSD are 0 nm and 8.8 nm, respectively. The difference between the CMDs of instrument 2 and instrument 3 is 5 nm. The percent difference between the CMDs of these two instruments is 2.4%. The difference between the two distributions at -1 GSD and + 1 GSD are 2.2 nm and 7.3 nm, respectively. For this test, the CMD of instrument 1 was closer to the selected PSL size parameter. The difference between the CMDs of instruments 2 and 3 was smaller than the difference between the CMD of instruments 1 and 2, and the difference between the CMD of instruments 1 and 3. The difference between the CMD of instrument 1 and 3, and the difference between the CMD instrument 2 and 3 were similar.

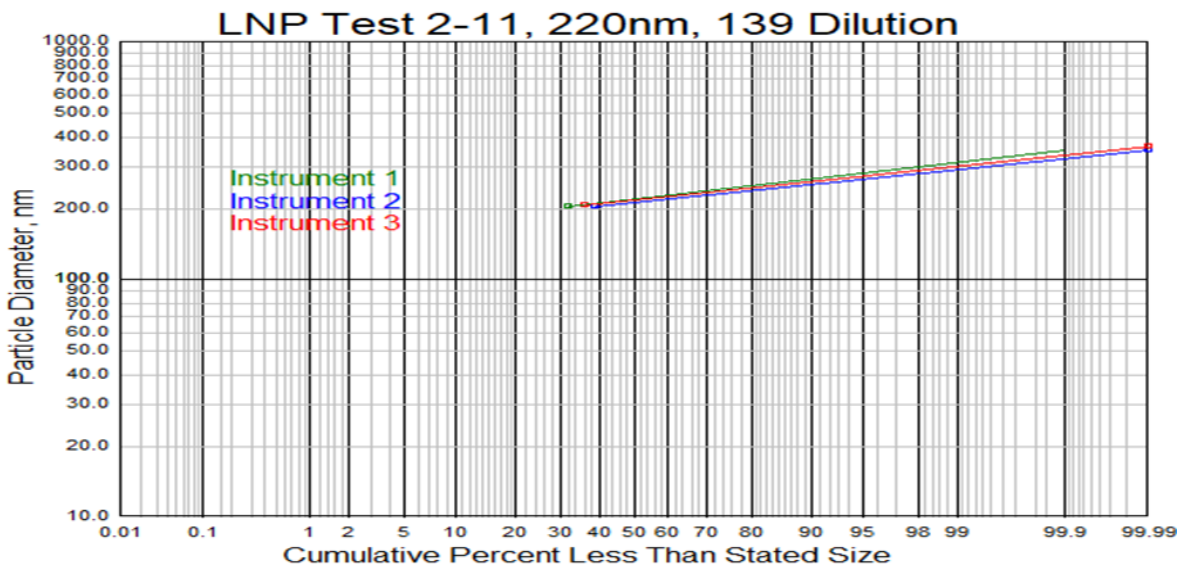


Figure 21: Distribution of PSL nanoparticle generated aerosol for Test 2-11, 220 nm generated aerosol, 139 dilution

For test 2-12, the designated PSL nanoparticle of 220 nm was used at a dilution of 139 to prepare a higher concentration of PSL particles as a comparison with test 2-11. For instrument 1, the highest percentage of particles (77.8%) were observed in the size range interval of 203.8-349.4 nm. The lowest range of particles (22.2%) were observed in the size range intervals of 152.8-203.7nm. 77.8 percent of particles were observed in the size range interval of 203.8-349.4 nm. For instrument 2, the highest percentage of particles (57.7%) were observed in the size range interval of 203.8-349.4 nm. The lowest range of particles (42.3%) were observed in the size range interval of 152.8-203.7 nm. 57.7 percent of particles were observed in the size range interval of 203.8-349.4 nm. For instrument 3, the highest percentage of particles (62.3%) were observed in the size range interval of 205.5-365.2 nm. The lowest range of particles (37.7%) were observed in the size range interval of 154.1-205.4 nm. 62.3 percent of particles were observed in the size range interval of 205.5-365.2 nm. For this test, instrument 2 identified the highest percentage of particles within the selected PSL size parameter range.

The distributions from test 2-12 are presented in Figure 22. The lines of fit for instruments 1, 2, and 3 are parallel and similar to each other. Comparisons of the distributions for 16%, 50%, and 84% are presented in Table 6.

For test 2-12, the distribution obtained by Instrument 1 had a CMD of 224.6 nm and a GSD of 1.13 shown in Table 6. The distribution obtained by Instrument 2 had a CMD of 209.2 nm and a GSD of 1.15. The distribution obtained by Instrument 3 had a CMD of 214.2 nm and a GSD of 1.15. The difference between the CMDs of instrument 1 and instrument 2 is 15.4 nm. The percent difference between the CMDs of these two instruments is 7.1%. The difference between the two distributions at -1 GSD and + 1 GSD are 18.1 nm and 14.5 nm, respectively. The difference between the CMDs of instrument 1 and instrument 3 is 10.4 nm. The percent difference between the CMDs of these two instruments is 4.7%. The difference between the two distributions at -1 GSD and + 1 GSD are 13.7 nm and 5.9 nm, respectively. The difference between the CMDs of instrument 2 and instrument 3 is 5.0 nm. The percent difference between the CMDs of these two instruments is 2.4%. The difference between the two distributions at -1 GSD and + 1 GSD are 4.4 nm and 8.6 nm, respectively. For this test, the CMD of instrument 1 was closer to the selected PSL size parameter. The difference between the CMDs of instruments 2 and 3 was smaller than the difference between the CMD of instruments 1 and 2, and the difference between the CMD of instruments 1 and 3.

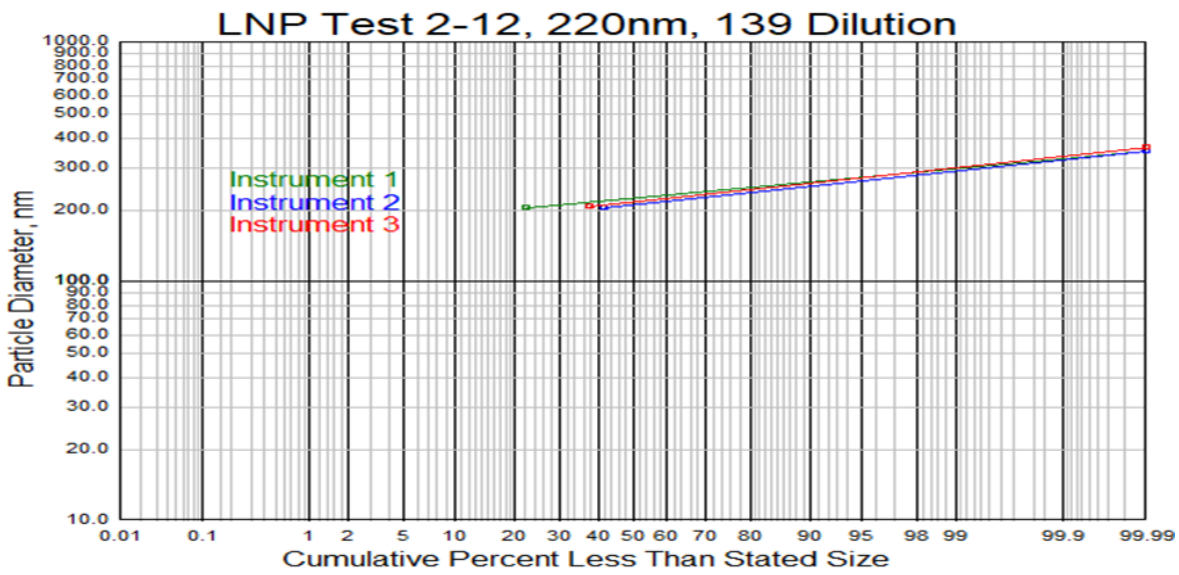


Figure 22: Distribution of PSL nanoparticle generated aerosol for Test 2-12, 220 nm generated aerosol, 139 dilution

*Regression Analysis*

For Trial 2 with PSL, the main effects and interaction were significant with $p<0.01$. The instrument and log bucket main effects, and the interaction with the instrument and the log bucket were statistically significant. The post-hoc Tukey HSD identified a significant difference between the instrument 3 dataset and the instrument 1 dataset. No significant difference was identified between instrument 2 and the other instruments.

Table 6: Data points derived from figures 11-22 and their distributional differences with respect to the analytical technique

| Trial | PSL Bead Diameter, nm | Sample Dilution | Analytic Technique | Diameters (nm) at | | | GSD | Differences between Instrument 1 & 2, nm | | | Differences between Instrument 1 & 3, nm | | | Differences between Instrument 2 & 3, nm | | |
|---|---|---|---|---|---|---|---|---|---|---|---|---|---|---|---|---|
| | | | | 16% | 50% | 84% | | 16% | 50% | 84% | 16% | 50% | 84% | 16% | 50% | 84% |
| 2-1 | 57 | 1,250 | Instrument 1 | 43.5 | 67.8 | 105.8 | 1.56 | 3.7 | 7.9 | 18 | 18 | 17 | 11.2 | 22 | 25 | 29 |
| | | | Instrument 2 | 39.8 | 59.9 | 88.0 | 1.49 | | | | | | | | | |
| | | | Instrument 3 | 61.3 | 85.0 | 117.0 | 1.38 | | | | | | | | | |
| 2-2 | 57 | 1,250 | Instrument 1 | 49.3 | 74.1 | 112.3 | 1.51 | 4.2 | 8.3 | 14 | 9.5 | 13 | 19.4 | 14 | 22 | 33.8 |
| | | | Instrument 2 | 45.1 | 65.8 | 97.9 | 1.47 | | | | | | | | | |
| | | | Instrument 3 | 58.8 | 87.5 | 131.7 | 1.50 | | | | | | | | | |
| 2-3 | 57 | 12,500 | Instrument 1 | 33.5 | 55.1 | 89.6 | 1.64 | 1.8 | 1.3 | 0 | 41 | 39 | 30.9 | 39 | 38 | 30.9 |
| | | | Instrument 2 | 35.3 | 56.4 | 89.6 | 1.59 | | | | | | | | | |
| | | | Instrument 3 | 74.1 | 94.5 | 120.5 | 1.28 | | | | | | | | | |
| 2-4 | 92 | 2,778 | Instrument 1 | 80.1 | 107.6 | 150.9 | 1.37 | 19 | 19 | 22 | 82 | 85 | 73.7 | 101 | 104 | 96 |
| | | | Instrument 2 | 61.3 | 88.6 | 128.6 | 1.45 | | | | | | | | | |
| | | | Instrument 3 | 162.1 | 192.5 | 224.6 | 1.18 | | | | | | | | | |
| 2-5 | 92 | 312 | Instrument 1 | 72.4 | 100.9 | 140.6 | 1.39 | 10 | 12 | 12 | 11 | 11 | 11.3 | 21 | 24 | 23.3 |
| | | | Instrument 2 | 62.4 | 88.6 | 128.6 | 1.44 | | | | | | | | | |
| | | | Instrument 3 | 82.9 | 112.2 | 151.9 | 1.35 | | | | | | | | | |
| 2-6 | 147 | 234 | Instrument 1 | 104.5 | 135.7 | 177.1 | 1.30 | 5.8 | 5.7 | 4.3 | 35 | 36 | 37.1 | 30 | 31 | 32.8 |
| | | | Instrument 2 | 110.3 | 141.4 | 181.4 | 1.28 | | | | | | | | | |
| | | | Instrument 3 | 139.8 | 172.0 | 214.2 | 1.24 | | | | | | | | | |
| 2-7 | 147 | 347 | Instrument 1 | 105.8 | 144.0 | 177.2 | 1.29 | 9.8 | 0.8 | 6.4 | 35 | 30 | 38.2 | 25 | 29 | 31.8 |
| | | | Instrument 2 | 115.6 | 144.8 | 183.6 | 1.26 | | | | | | | | | |
| | | | Instrument 3 | 140.6 | 174.1 | 215.4 | 1.24 | | | | | | | | | |
| 2-8 | 147 | 694 | Instrument 1 | 120.5 | 148.3 | 183.6 | 1.23 | 21 | 13 | 19 | 28 | 32 | 39.6 | 49 | 45 | 58.2 |
| | | | Instrument 2 | 99.1 | 134.9 | 165.0 | 1.29 | | | | | | | | | |
| | | | Instrument 3 | 148.3 | 180.3 | 223.2 | 1.23 | | | | | | | | | |
| 2-9 | 220 | 208 | Instrument 1 | 214.2 | 236.9 | 262.0 | 1.11 | 88 | 81 | 64 | 60 | 51 | 40.1 | 28 | 30 | 23.7 |
| | | | Instrument 2 | 126.4 | 155.5 | 198.2 | 1.25 | | | | | | | | | |
| | | | Instrument 3 | 154.6 | 185.8 | 221.9 | 1.20 | | | | | | | | | |
| 2-10 | 220 | 208 | Instrument 1 | 188.0 | 214.2 | 245.4 | 1.14 | 0 | 0 | 0 | 2.2 | 2.5 | 3 | 2.2 | 2.5 | 3 |
| | | | Instrument 2 | 188.0 | 214.2 | 245.4 | 1.14 | | | | | | | | | |
| | | | Instrument 3 | 185.8 | 216.7 | 248.4 | 1.16 | | | | | | | | | |
| 2-11 | 220 | 139 | Instrument 1 | 188.0 | 219.3 | 255.8 | 1.17 | 2.2 | 10 | 16 | 0 | 5.1 | 8.8 | 2.2 | 5 | 7.3 |
| | | | Instrument 2 | 185.8 | 209.2 | 239.7 | 1.14 | | | | | | | | | |
| | | | Instrument 3 | 188.0 | 214.2 | 247.0 | 1.15 | | | | | | | | | |
| 2-12 | 220 | 139 | Instrument 1 | 199.5 | 224.6 | 252.8 | 1.13 | 18 | 15 | 15 | 13.7 | 10.4 | 5.9 | 4.4 | 5.0 | 8.6 |
| | | | Instrument 2 | 181.4 | 209.2 | 238.3 | 1.15 | | | | | | | | | |
| | | | Instrument 3 | 185.8 | 214.2 | 246.9 | 1.15 | | | | | | | | | |

# Chapter Five

# Discussion and Conclusions

## *Instrument Response to Sodium Chloride Aerosols*

The performance of the scanning mobility particle sizers compared in these experiments was acceptable. For the NaCl nanoaerosol suspensions, the SMPS lines of fit presented in figures 1-8 are predominantly parallel, which suggests that the log-normal distributions are similar. The GSD of these distributions was approximately 1.7, which confirms that the distributions were approximately the same. In these experiments, instrument 3 identified a higher percentage of NaCl particles within the size range intervals of the selected NaCl size parameter. This higher percentage of detection suggests that instrument 3 is more responsive than the other instruments to the selected size range. Additionally, the CMDs for the instrument 3 measurements were closer to the selected NaCl size parameter more often than the other instruments. However, the difference between the CMD of instrument 3 and the CMD of at least one of the other instruments was less than 8 nm. Instrument 3 may have been more responsive to the selected NaCl size parameter, however, the other instruments were also fairly responsive.

The EM lines of fit for the NaCl experiments presented in figures 1-8 are predominantly parallel with the SMPS lines of fit, suggesting that the log-normal distributions have similar GSD. The GSD of EM distributions was approximately 1.8, which confirms that the distributions were approximately the same as the SMPS distributions. The EM CMDs were similar to the selected NaCl size parameter at the lower particle diameters, but were less than the larger selected particle sizes. The reduction in size correlation may have been related to dilution. The

diameters of the selected NaCl particle sizes were calculated using the $d/d_o = (100p_o/W_2P)^{1/3}$ equation. To prevent overloading of the instrument detection capabilities and EM sample filters, the NaCl suspensions were diluted with additional water. The diluted suspensions were used to generate aerosols with lower concentrations of NaCl, resulted in a lower detection of the generated particles. This may not have been observed at the lower particles sizes due to background particle concentrations in the solution water.

The water used to create the NaCl suspensions was a potential cause of additional, unwanted particles in the generated aerosol. For NaCl solutions, filtered water was added to NaCl and stirred until the NaCl was dissolved. Early pre-test runs identified a bimodal response in the SMPS data. Based on these results, the first peak was believed to be the result of particles in the filtered water. In response to these initial pre-test results, environmental grade water was used for the following tests. While this reduced the magnitude of bimodal observations, elevated concentrations of nanoparticles less than 50 nm were observed. After evaporation, environmental grade water has a residual maximum of 1 ppm (Water (Environmental Grade)-Fisher Chemical, MFCD00011332). This background level of contaminants in the water can be a contributing factor. For future experiments, the use of environmental grade purified water with the lowest background contamination is recommended.

Results from the regression plots demonstrated that the main effects and interaction were statistically significant with a $p<0.0001$. This indicates a rejection of the null hypothesis, and suggests that at least one of the instrument measured particle group mean counts differently than another instrument. The post-hoc Tukey HSD results identified a significant difference between the instrument 3 dataset, and the datasets for instruments 1 and 2. These results are in agreement with the CMD and percent data presented in Table 2 and 3. The coefficient of determination, $R^2$, for the regression lines was 0.87.

*Instrument Response to Polystyrene Latex Aerosols*

The performance of the scanning mobility particle sizers compared in these experiments was acceptable. For the PSL nanoaerosol suspensions, the SMPS lines of fit presented in figures 9-20 are predominantly parallel, which suggests that the log-normally distributions are similar. The GSD of these distributions was approximately 1.3, which confirms that the distributions were approximately the same. In these experiments, instrument 2 identified a higher percentage of PSL particles within the size range intervals of the selected PSL size parameter. This higher percentage of detection suggests that instrument 2 is more responsive than the other instruments to the selected size range. Additionally, instrument 2 CMDs were closer to the selected PSL size parameter more often than the other instruments. This indicates that Instrument 2 was more responsive to the selected PSL size parameter for the generated PSL aerosols.

Results from the regression plots demonstrated that the main effects and interaction were statistically significant with a $p<0.01$. The coefficient of determination, $R^2$, for the regression lines was 0.44. This indicates a rejection of the null hypothesis. The low P values and lower $R^2$ combination, suggests a higher variability in the data results, but indicates that at least one of the instrument measured particle group mean counts differently than another instrument. The post-hoc Tukey HSD identified a significant difference between the instrument 3 dataset and the instrument 1 dataset. This suggests that 56% of the variance in the particle counts is not explained by the measurement instruments or geometric mean of the selected PSL particle collection groups. Potential sources of variability include solution water background contamination, surfactants in the PSL solution, and agglomeration.

Similar to the background contamination of the NaCl suspensions noted above, the water used to create the PSL suspensions was a potential cause of additional, unwanted particles in the generated aerosol. In addition to the environmental grade water, PSL solutions were prepared with 95% ethyl alcohol and PSL stock material. The 95% alcohol contained 5%

water and had a residual of less than 1 ppm (AAPER Alcohol and Chemical Co., Product Code: 111000190). This residual, though minimal in most applications, would contribute to the background level of aerosol particles produced by the nebulizer. The PSL solutions contained an additive that has a trace amount of surfactant. The additive (surfactant) inhibits agglomeration and promotes stability (Polysciences, Inc Technical Data Sheet 238). This surfactant provided an additional background contamination that may have contributed to observed particles sizes.

In addition to the contribution to background contamination from the PSL additives, the PSL spheres may have left residual contamination on the nebulizer components which resulted in unwanted particle generation during the nebulization process. The methodology for the experiments included cleaning of the aerosol generation system prior to each test run. The Collison Nebulizer glassware, lid, and "T" stem were cleaned with deionized water and solvents, sonicated, and then rinsed with deionized and high grade pure water. Due to the natural solubility of NaCl in the water, the cleaning procedures should have resulted in minimal NaCl residual on the nebulizer components. However, cleaning of the components used with PSL solutions may have left residual spheres or fragments of particles adhered to the nebulizer components. These PSL spheres/fragments may have been released from the nebulizer components during the next experiment, resulting in aerosolization and production of particles outside of the desire size range. Although the nebulizer components were rinsed and partially submerged in a solvent, ultrasonic cleaning of the nebulizer components in a solvent bath may be more effective in removing residual PSL components.

### *Comparison of SMPS for NaCl and PSL Monitoring*

The performance of all the scanning mobility particle sizers compared in these experiments was acceptable. For the NaCl experiments, instrument 3 was more responsive than the other instruments to the selected size range and size parameter, but the other

instruments were also fairly responsive. For the PSL experiments, instrument 2 was more responsive than the other instruments to the selected size range and size parameter.

Instruments 1 and 2 could measure particle size distributions over a range of 5 nm to 500 nm with up to 128 user selectable channels, Particle Measuring systems (2011). For this study, they were set up to measure 15 nm – 300 nm spread out over 84 channels (size intervals), with a 2 minute scan and a 50 second reverse scan. Instrument 3 could measure particle size distributions over a range of 10 nm to 420 nm, TSI (2011). For this study, it was set up to measure 10 nm – 420 nm spread out over 13 channels (size intervals), with a 45 second scan and a 15 second downscan. Instruments 1 and 2 collect one sample approximately every three minutes, and that sample is separated into 84 channels. This provided less samples over each experiment sampling period, but provided greater detail on the sample particle sizes collected over the sampling period. Instrument 3 collects one sample every minute, and that sample is separated into 13 channels. This provided more samples over each experiment sampling period, but provided less detail on the sample particle sizes collected over the sampling period.

In this study, differences were observed in the measurements between SMPS from the same manufacturer, but the difference between these instruments were smaller than the differences observed between SMPS from different manufacturers. Caution should be used when comparing measurement readings between SMPS, especially SMPS from different manufacturers, as noted by Ham et al (2016).

### *Sampling Chamber and Aerosol Performance*

After the sampling chamber was tested and the penetrations sources were corrected, the chamber was effective for the experiments. The Collison nebulizer was effective at providing a consistent concentration over several hours, which was in agreement with Schmoll

et al. (2009) evaluation of this device. During the initial development, testing, and operations of the chamber, potential items of concern were observed.

One item of concern is chamber design and manufacturing. For this study, the design specifications for the chamber were submitted to a manufacturer, without providing requested leakage allowances or performance testing requirements. As a result, the test chamber required extensive penetration testing, and minor modifications, once it was installed in the laboratory. The chamber manufacturer had previously assembled test chambers, however the particle size requirements for previous projects were larger than the nanometer size parameters of this experiment. To prevent these type of delays in the future, design specification should include performance requirements, including testing prior to delivery. Although this will increase the proposal estimate, the manufacturer is better equipped to modify the chamber to address structural leaks, including repairing leaking welds. These repairs, conducted at the manufacturing facility, will provide a more permanent correction to the leaks than the corrective steps conducted in the laboratory. Although minor modifications and corrections to the chamber are expected with any new assembly, correcting the larger chamber issues at the manufacturing facility is recommended.

Another item of concern in the use of an aerosol sampling chamber is supplemental lighting. During the initial evaluation of the chamber, a light mounted adjacent to the test chamber affected the air flow pattern of the smoke aerosol test. Energy from the light may have warmed up the side of the test chamber adjacent to it, impacting the flow of gas around it. This impact was confirmed through multiple tests. The mechanism that affected the smoke aerosol may have been an effect of thermophoresis or photophoresis. Based on these findings, the use of external lighting located close to the aerosol test chambers should be limited during experiments.

A final item of concern involves the preparation of the aerosol generation system. Prior to conducting each test, an evaluation of the nitrogen compressed gas volume and Collison

Nebulizer solution should be conducted to ensure that there is adequate gas and solution available to complete the scheduled test. Some of the test runs may run longer than expected, requiring larger quantities of compressed gas and solution to maintain the generation of a steady aerosol volume. Because the aerosol solution is custom made for each test run, additional nebulizer solution should be made for each run to maintain the proper nebulizer solution concentrations during an extended test run. The additional solution can be used to refill the nebulizer during the test run, as needed, without impacting the aerosol concentration. If a test run is delayed or extends beyond the expected time limit, then depletion of the base materials below acceptable parameters of operation may result in a loss of the data obtained during the affected test.

### *Conclusions*

The purpose of this study was to evaluate the performance of scanning mobility particle sizers in the characterization of nanoaerosols. The performance of the SMPS instruments evaluated in this study were acceptable. For the NaCl and PSL nanoaerosol suspensions, the SMPS lines of fit were log-normally distributed and predominantly parallel. The geometric standard deviation (GSD) of these distributions was approximately 1.7 and 1.3, respectively. Results from the regression plots for the NaCl and PSL experiments demonstrated that the main effects and interaction were statistically significant. For the NaCl experiments, instrument 3 was more accurate than the other instruments to the selected size range and the selected NaCl size parameters. For the PSL experiments, instrument 2 was more accurate than the other instruments to the selected size range and the selected PSL size parameters. Based on these results and an understanding of the instrument's limitations, these instruments are suitable for field use. In the practice of industrial hygiene, quantifying contaminant air concentrations is required to determine the need for controls or evaluate the effectiveness of previously implemented controls. In the ENM manufacturing and service industry, the potential for

nanoparticle exposures often occurs during short, task-driven manufacturing or cleaning activities (McGarry et al. 2013). Field-operated SMPS instruments are currently being used to obtain nanoparticle measurements during these activities. Real-world tests of these instruments could provide a solid baseline that professionals may use to ascertain ENM contaminant concentration levels, develop controls, and ascertain the effectiveness of the controls in providing a safe working environment for employees. There is a need for additional tests that are well-designed, and appropriately analyze, that are published in the peer-reviewed literature.

References

Abbott, L. C. & Maynard, A. D. (2010). Exposure assessment approaches for engineered nanomaterials. *Risk Analysis*, 30: 1634–1644.

Amaral, S. S., de Carvalho, J. A., Jr, Costa, M., & Pinheiro, C. (2015). An overview of particulate matter measurement instruments. *Atmosphere*, 6(9):1327-1345.

Beck-Broichsitter, M., Knuedeler, M. C., Schmehl, T., & Seeger, W. (2013). Following the concentration of polymeric nanoparticles during nebulization, *Pharm Res*, 30: 16.

Berlo, D., Clift, M., Albrecht, C., & Schins, R. (2012). Carbon nanotubes: An insight into the mechanisms of their potential genotoxicity. *Swiss Medical Weekly,* 142; w13698.

BGI, Inc. (2001). Collison Nebulizer Instructions, NSF Model CN 311.

Chen, D. R., Pui, D. Y. H., Hummes, D., Fissan, H., Quant, F. R., & Sem, G. J. (1998). Design and evaluation of a nanometer aerosol differential mobility analyzer (Nano-DMA). *Journal of Aerosol Science*, *29*(5-6), 497-509.

Dailey, L. A., Schmehl, T., Gessler, T., Wittmar, M., Grimminger, F., Seeger, W., & Kissel, T. (2003). Nebulization of biodegradable nanoparticles: Impact of nebulizer technology and nanoparticle characteristics on aerosol features. *Journal of Controlled Release*, 86(1), 131-144

Department of Human and Health Services (2009). Approaches to safe nanotechnology: Managing the health and safety concerns associated with engineered nanomaterials. DHHS (NIOSH) Publication No. 2009-125, 25-27.

Donaldson, K., Poland, C. A., Murphy, F. A., MacFarlane, M., Chernova, T., & Schinwald, A. (2013). Pulmonary toxicity of carbon nanotubes and asbestos - Similarities and differences. *Advanced Drug Delivery Reviews*, 65(15), 2078-2086.

Engeman, C. D., Baumgartner, L., Carr, B. M., Fish, A.M., Meyerhofer, J. D., Satterfield, T. A., Holden, P. A., & Harthorn, B. H. (2013). The hierarchy of environmental health and safety practices in the U.S. nanotechnology workplace. *Journal of Occupational and Environmental Hygiene*, 10: 487-495.

Evans, D., Ku, B., Birch, M.E., & Dunn, K. (2010). Aerosol monitoring during carbon nanofiber production: mobile direct-reading sampling. *Annals of Occupational Hygiene*, 54:5 514-531.

Giechaskiel, B., Maricq, M., Ntziachristos, L., Dardiots, C., Wang, X., Azmann, H., Bergmann, A., Achindler, W. (2014) Review of motor vehicle particle emissions sampling and measurement: From smoke and filter mass to particle number, *Journal of Aerosol Science*, 67, 48-86.

Gojova, A., Guo, B., Kota, R. S., Rutledge, J. C., Kennedy, I. M., & Barakat, A. I. (2007). Induction of inflammation in vascular endothelial cells by metal oxide nanoparticles: Effect of particle composition. *Environmental Health Perspectives*, *115*(3), 403-409.

Grassian, V. H., O'Shaughnessy, P. T., Adamcakova-Dodd, A., Pettibone, J. M., & Thorne, P. S. (2007). Inhalation exposure study of titanium dioxide nanoparticles with a primary particle size of 2 to 5 nm. *Environmental Health Perspectives*, 115(3):397-402.

Ham, S., Lee, N., Eom, I., Lee, B., Tsai, P. J., Lee, K., & Yoon, C. (2016). Comparison of real time nanoparticle monitoring instruments in the workplaces. *Safety and Health at Work*, *7*(4), 381-388.

Kumar, P., Garmory, A., Ketzel, M., Berkowicz, M., & Britter, R. (2009). Comparative study of measured and modelled number concentration of nanoparticles in an urban street canyon. *Atmospheric Environment,* 43 (4), 949-958.

Lagos, M. J., da Silva, P. C., & Ugarte, D. (2015). High-throughput nanoparticle analysis in a FEG-SEM using an inexpensive multi-sample STEM-ADF system. Eprint arXiv: 1510.02690.

Liu, J. (2005). Scanning transmission electron microscopy and its application to the study of nanoparticles and nanoparticle systems. *Journal of Electron Microscopy*, *54*(3), 251-278.

McGarry, P., Morawska, L., & Knibbs, L. (2013). Excursion guidance criteria to guide control of peak emission and exposure to airborne engineered particles. *Journal of Occupational and Environmental Hygiene*, 10: 11, 640-651.

Methner, M., Crawford, C., & Geraci, C. (2012). Evaluation of potential airborne release of carbon nanofibers during the preparation, grinding, and cutting of epoxy-based nanocomposite material. *Journals of Occupational and Environmental Hygiene*, 9:5 308-318.

Murashov, V., & Howard, J. (2013). Protecting nanotechnology workers while waiting for Godot. *Journal of Occupational and Environmental Hygiene*, 10 (8):D111-5

Murphy, F. A., Poland, C. A., Duffin, R., & Donaldson, K. (2013). Length-dependent pleural inflammation and parietal pleural responses after deposition of carbon nanotubes in the pulmonary airspaces of mice. *Nanotoxicology*, 7(6), 1157-1167.

Noel, A., Cloutier, Y., Wilkinson, K., Dion, C., Hallé, S., Maghni, K., Tardif, R., & Truchon, G. (2012). Generating nano-aerosols from $TiO_2$ (5 nm) nanoparticles showing different agglomeration states. Application to toxicological studies. *Journal of Occupational and Environmental Hygiene*, 10(2), 86-96.

Olishifski, J. B. (1988). Overview of Industrial Hygiene. In B. A. Plog (Ed.), Fundamentals of Industrial Hygiene Third edition (pp. 3-27), Itasca, IL; National Safety Council.

Particle Measuring Systems Nano-ID NPS500 Nanoparticle Spectrometer Operations Manual (2011). P/N 1000015990 Rev 5.

Peters, T. M., Heitbrink, W. A., Evans, D. E., Slavin, T. J., & Maynard, A. D. (2005).The mapping of fine and ultrafine particle concentrations in an engine machining and assembly facility. *Annals of Occupational Hygiene*, 50(3), 249-257.

Polk, W. W., Sharma, M., Sayes, C. M., Hotchkiss, J. A., & Clippinger, A. J. (2016). Aerosol generation and characterization of multi-walled carbon nanotubes exposed to cells cultured at the air-liquid interface. *Part Fibre Toxicol*. 13:20.

Polysciences, Inc. (2013) Technical Data Sheet 238, Revision 11, Polybead Polystyrene Microspheres

Rengasamy, S., & Eimer, B. (2011) Total inward leakage of nanoparticles through filtering facepiece respirators. *Annals of Occupational Hygiene*, 55(3), 253-263.

Rengasamy, S., BerryAnn, R., & Szalajda, J. (2013). Nanoparticle filtration performance of filtering facepiece respirators, and canister/cartridge filters, *Journal of Occupational and Environmental Hygiene*, 10(9), 519-525.

Schmoll, L., Elzey, S., Grassian, V., & O'Shaughnessy, P. (2009). Nanoparticle aerosol generation methods from bulk powders for inhalation exposure studies. *Nanotoxicology*, 3(4), 265-275.

Seipenbusch, M (2008). Temporal evolution of nanoparticle aerosols in workplace exposure, *Annals of Occupational Hygiene*, 52(8), 707-716

Shimada, M., Wang, W., Okuyama, K., Myojo, T., Oyabu, T., Morimoto, Y., … & Nakanishi, J. (2009). Development and evaluation of an aerosol generation and supplying system for inhalation experiments of manufactured nanoparticles. *Environmental Science & Technology*, 43(14), 5529-34.

Shin, W.G, Pui, D.Y.H., Fissan, H., Neumann, S., & Trampe, A. (2007). Calibration and numerical simulation of nanoparticle surface area monitor (TSI Model 3550 NSAM), *Journal of Nanoparticle Research*, 9:61-69

Solomon, P. (2012). An overview of ultrafine particles in ambient air. *EM: Air and Waste Management Association's Magazine for Environmental Managers*, (May, 2012) 18-27.

Toyokuni, S. (2013) Genotoxicity and carcinogenicity risk of carbon nanotubes. *Advanced Drug Delivery Reviews*, 65(15), 2098-2110.

TSI Particle Instruments NanoScan SMPS (2011).P/N5001282, Rev B.

Wiedensohler, A., Birmili, W., Nowak, A., Sonntag, A., Weinhold, K., Merkel, M., …Bastian, S. (2012). Mobility particle size spectrometers: Harmonization of technical standards and data structure to facilitate high quality long-term observations of atmospheric particle number size distributions. *Atmospheric Measurement Techniques*, 5, 657-685.

Williams, R. A., Kulinowski, K. M., White, R., & Louis, G. (2010). Risk Characterization for Nanotechnology. *Risk Analysis*, *30*(11), 1671-1679.

Williams, R. O., Carvalho, T. C., & Peters, J. I. (2011). Influence of particle size on regional lung deposition - What evidence is there? *International Journal of Pharmaceutics*, *406*(1-2), 1-10.

Yokel, R., & MacPhail, R. (2011). Engineered nanomaterials: Exposures, hazards, and risk prevention. *Journal of Occupational Medicine and Toxicology*, 6:7.